# Systems metabolic engineering of electrogenic-anaerobic *Pseudomonas putida* for enhanced 2-ketogluconate production

**Dissertation**

zur Erlangung des Grades

des Doktors der Naturwissenschaften

der Naturwissenschaftlich-Technischen Fakultät

der Universität des Saarlandes

von

**Anna Lea Auguste Weimer**

Saarbrücken

2024

| | |
|---|---|
| Tag des Kolloquiums: | 10.12.2024 |
| Dekan: | Prof. Dr.-Ing. Dirk Bähre |
| Berichterstatter: | Prof. Dr. Christoph Wittmann |
| | Prof. Dr. Andriy Luzhetskyy |
| Akad. Mitarbeiter: | Dr. Mark Lommel |
| Vorsitz: | Priv.-Doz. Dr. Frank Breinig |

## Publications

Portions of this work have been published with prior authorization from the Institute of Systems Biotechnology (Universität des Saarlandes), as represented by Prof. Dr. Christoph Wittmann.

Figures 2-1 and 2-2 in the introduction are derived from a previously published review article (Weimer, Kohlstedt, Volke, Nikel, & Wittmann, 2020). Results from Chapters 4-1 and 4-2 were previously published in (Weimer et al., 2024). Both articles are licensed under a Creative Commons Attribution 4.0 International License (https://creativecommons.org/licenses/by/4.0/). Figures in these chapters are reproduced with permission from Springer Nature.

### Peer-reviewed articles:

**Weimer A**, Kohlstedt M, Volke DC, Nikel PI, Wittmann C (2020) Industrial biotechnology of *Pseudomonas putida*: advances and prospects. *Applied Microbiology and Biotechnology*, *104*(18), 7745–7766.

Pause L, **Weimer A**, Wirth NT, Nguyen AV, Lenz C, Kohlstedt M, Wittmann C, Nikel PI, Lai B, Krömer JO (2024) Anaerobic glucose uptake in *Pseudomonas putida* KT2440 in a bioelectrochemical system. *Microbial Biotechnology*, 17, e14375.

**Weimer A**, Pause L, Ries F, Kohlstedt M, Adrian L, Krömer JO, Lai B, Wittmann C (2024) Systems biology of electrogenic *Pseudomonas putida* - multi-omics insights and metabolic engineering for enhanced 2-ketogluconate production. *Microbial Cell Factories*, 23, 246.

**The following peer-reviewed article was co-authored during this work, but is not part of the dissertation:**

Kohlstedt M, **Weimer A**, Weiland F, Stolzenberger J, Selzer M, Sanz M, Kramps L, Wittmann C (2022) Biobased PET from lignin using an engineered *cis*, *cis*-muconate-producing *Pseudomonas putida* strain with superior robustness, energy and redox properties. *Metabolic engineering*, *72*, 337–352.

## Conference contributions

### Oral presentations

**Weimer A**, Pause L, Krömer JO, Lai B, Wittmann C. e*Pseudomonas* – Understanding the Electrogenic Lifestyle of *Pseudomonas putida*. Joint SPP Conference of eBiotech and Interzell, November 6-8, 2023, Jena, Germany

**Weimer A**, Pause L, Ries F, Kohlstedt M, Krömer JO, Lai B, Wittmann C. Electro-Powered *Pseudomonas putida* for Anaerobic Bio-electrochemical Production. *Pseudomonas* Grassroots Meeting (PGM4), October 28-29, 2024, Leipzig, Germany

### Poster presentations

**Weimer A**, Pause L, Wirth N, Nikel P, Lai B, Kohlstedt M, Wittmann C, Krömer JO. e*Pseudomonas* – What the $e^-$ is going on? Understanding the Electrogenic Lifestyle of *P. putida*. SPP2240 Summer School, September 1-3, 2022, Hamburg, Germany

**Weimer A**, Pause L, Kohlstedt M, Krömer JO, Lai B, Wittmann C. e*Pseudomonas* - Understanding the Electrogenic Lifestyle of *Pseudomonas putida.* 6$^{th}$ European Meeting of the International Society for Microbial Electrochemistry and Technology (EU-ISMET), September 6-8, 2023, Wageningen, The Netherlands

## Acknowledgement

I would like to express my deepest gratitude to all those who have supported and helped me in various ways throughout this phase of my career and life. The journey to completing this dissertation has been filled with both professional challenges and personal adversity, as well as great learning experiences. I am especially thankful for the unwavering support of my supervisor, Prof. Dr. Christoph Wittmann, who not only provided me with the opportunity but also guided me through this work. I greatly appreciate his willingness to listen, his valuable advice, and the empathy and compassion he consistently showed along the way.

I would also like to extend my sincere thanks to Prof. Dr. Andriy Luzhetskyy and the entire Actinobacteria Metabolic Engineering (AMEG) team for warmly welcoming me into their group and accommodating my bio-electrochemical reactor setup.

I am deeply grateful to my colleagues at the Institute of Systems Biotechnology (iSBio) for cultivating such an enjoyable working environment. I would like to extend my heartfelt thanks to Michel Fritz for his incredible patience in resolving technical issues, and his invaluable assistance with analytical measurements. Thanks to Dr. Michael Kohlstedt for his support during the set-up phase of the bio-electrochemical reactors. Special thanks also go to Izabook Gutiérrez-Urrutia and Muzi Tangyu, whose warm and caring nature consistently lifted my spirits. I am thankful for my coffee and office companion, Dr. Fabian Ries, whose engaging scientific discussions were immensely helpful. Additionally, I want to express my gratitude to Kyoyoung Seo, my long-term office partner and friend, for all the moments and conversations we shared, both the highs and the lows. You have truly been my rock. To all my colleagues whose names I may not be able to mention individually, your support has been invaluable.

I would also like to thank our project partners from the Helmholtz Centre for Environmental Research (UFZ) in Leipzig, Laura Pause, Dr. Bin Lai, and Prof. Dr. Jens Krömer, for their excellent collaboration and fruitful exchanges.

I would like to express my deepest gratitude to my family, my friends and my partner Hannes Hofmann for their relentless support during my journey.

I dedicate this work to my mother, Rosi Weimer, the greatest woman I knew, my role model.

# Table of Contents

## Summary

*P. putida* KT2440 is as a promising host for industrial bioproduction. However, its strictly aerobic nature limits the range of potential applications. Interestingly, when cultured in an anoxic bio-electrochemical system (BES) supplemented with redox mediators, where the anode replaces oxygen as the terminal electron acceptor, this microbe exhibits high bioconversion efficiency. This environment supports the production of valuable chemicals, such as 2-ketogluconate (2KG). To further investigate this electrogenic phenotype, a systems-level analysis through integration of transcriptomic, proteomic, and metabolomic analyses was conducted.

*P. putida* did not grow in the anaerobic BES but produced significant amounts of 2KG, along with smaller amounts of gluconate, acetate, pyruvate, succinate, and lactate. Through $^{13}C$ tracer studies, it was shown that these products were partially derived from biomass carbon. Over time, the cells underwent global transcriptomic and proteomic changes, mainly related to energy metabolism. These adaptations allowed the cells to sustain significant metabolic activity. Based on the obtained insights, novel mutants were constructed with enhanced 2KG production in terms of titer, yield, and productivity.

Additionally, components involved in the transport of redox mediators across the outer membrane were identified. These insights advance our understanding of extracellular electron transfer processes between the cell, mediator, and electrode.

## Zusammenfassung

*P. putida* KT2440 hat sich als vielversprechender Wirt für die industrielle Bioproduktion erwiesen, jedoch schränkt seine strikt aerobe Natur die Einsatzmöglichkeiten ein. Interessanterweise zeigt die Mikrobe in einem anoxischen bio-elektrochemischen System (BES) mit Redox-Mediatoren eine hohe Biokonversionseffizienz, wobei die Anode als Ersatz für Sauerstoff als terminaler Elektronenakzeptor dient. In dieser Umgebung produziert *P. putida* wertvolle Chemikalien wie z.B. 2-Ketogluconat (2KG). Um den elektrogenen Phänotyp zu verstehen, wurden Transkriptom-, Proteom- und Metabolomanalysen integriert.

Zwar wuchs *P. putida* im anaeroben BES nicht, produzierte aber erhebliche Mengen an 2KG, sowie kleinere Mengen an Gluconat, Acetat, Pyruvat, Succinat und Laktat. $^{13}$C-Tracer-Studien zeigten, dass diese Produkte teilweise aus Biomasse-Kohlenstoff stammen. Über die Zeit traten globale transkriptomische und proteomische Veränderungen auf, vor allem im Energiestoffwechsel, wodurch die Zellen eine signifikante metabolische Aktivität beibehielten. Basierend auf diesen Erkenntnissen wurden Mutanten entwickelt, die eine verbesserte 2KG-Produktion hinsichtlich Titer, Ertrag und Produktivität aufweisen.

Zudem wurden Komponenten identifiziert, die am Transport von Redox-Mediatoren durch die äußere Membran beteiligt sind, was das Verständnis des extrazellulären Elektronentransfers zwischen Zelle, Mediator und Elektrode verbessert.

# 1 Introduction

## 1.1 General introduction

A major challenge to optimize bio-based production processes is their suboptimal efficiency, with yields, rates, and titers often falling far below their theoretical limits (G. Wu et al., 2016). This shortfall is primarily due to imbalances in cellular redox metabolism, where oxidative and reductive reactions must be precisely regulated to balance the differences in reduction between substrates and final products. When external electron donors or acceptors become limited, cells are compelled to produce by-products, which reduces carbon efficiency and complicates downstream processing. Attempts to genetically block these by-product formation pathways generally prove ineffective, as cells reroute metabolic fluxes to alternative pathways. In some instances, the elimination of multiple by-product pathways can lead to cells secreting intermediates from their core metabolic processes (Becker et al., 2013).

In this context, microbial electrochemical technology presents a promising approach to enhance the efficiency of bio-based production (Kracke & Krömer, 2014; Kracke, Lai, Yu, & Krömer, 2018). This technology utilizes systems equipped with electrodes that function as electron source (cathode) or electron sink (anode). These bio-electrochemical systems effectively decouple redox metabolism from carbon metabolism, thereby significantly improving product yields (Kracke & Krömer, 2014). In these systems, the interaction between microbes and electrodes can occur either directly, e.g. through conductive pili or outer membrane c-type cytochromes, or indirectly via redox-active compounds (Scott & Yu, 2015).

*Pseudomonas putida* can colonize diverse environments. Its versatile metabolism enables it to utilize a broad spectrum of substrates, allowing the organism to adapt and thrive in challenging ecological niches. This robust metabolic network makes *P. putida* particularly well-suited for applications in biotechnology and bioremediation, where its

ability to degrade pollutants and produce valuable compounds is of significant interest (Weimer, et al., 2020). Among its strains, *P. putida* KT2440 is widely recognized as a safe and dependable microbial cell factory for industrial biotechnology. Although *P. putida* possesses numerous advantageous traits that make it a promising industrial workhorse, there are specific characteristics that may be considered limitations (de Lorenzo, Pérez-Pantoja, & Nikel, 2024). Among these, its strictly aerobic lifestyle is particularly constraining, as it restricts its applicability in anaerobic or low-oxygen environments. Several efforts have aimed to establish fermentative pathways, such as ethanol and acetate production (Nikel & de Lorenzo, 2013), as well as anaerobic nitrate respiration (Steen et al., 2013). However, these attempts achieved only limited success, highlighting the challenges of modifying its native metabolic processes for anaerobic functionality.

More recently, *P. putida* KT2440 and related strains have emerged as promising candidates for electrochemically supported bioconversions (Lai et al., 2016; Schmitz, Nies, Wierckx, Blank, & Rosenbaum, 2015; Yu et al., 2018). When cultivated in a bio-electrochemical system, these naturally obligate aerobes can use the anode as an electron acceptor instead of molecular oxygen, enabling them to generate ATP and redox power under anaerobic conditions. This unique anode-driven, electrogenic phenotype is capable of non-growth production of chemicals with high yield and selectivity. Powered by a continuous electron flow from cells to mediators and the anode, *P. putida* KT2440 efficiently converts glucose into 2-ketogluconate via periplasmic glucose oxidation (Pause et al., 2023), achieving yields of over 90% (Lai, et al., 2016; Weimer, et al., 2024). This approach has proven effective not only with glucose but also with other aldoses and ketoses, resulting in the production of the corresponding sugar acids (Nguyen, Lai, Adrian, & Krömer, 2021).

## 1.2 Main objectives

The main objective of this work is to investigate the industrially relevant obligate aerobic strain *Pseudomonas putida* KT2440 under anaerobic conditions in a bio-electrochemical system, in which the anode acts as the terminal electron acceptor instead of oxygen, with the goal of developing an efficient bio-electrochemical platform for the production of valuable sugar acids.

This research aimed to deepen our understanding of the electrogenic phenotype of *P. putida* and to identify previously uncharacterized metabolic reactions and pathways active under these conditions. To achieve this goal, detailed systems biology insights into this phenotype should be obtained through multi-omics profiling to yield a comprehensive view of the cellular processes involved. This approach should integrate transcriptomic, proteomic, and metabolomic analyses. Building on these findings, novel mutants should be constructed with improved yields, titers, and productivity of the industrial relevant 2-ketogluconate, which is important as a precursor in chemical synthesis and has valuable applications in the food and cosmetic industry.

Notably, *P. putida* cannot directly interact with the anode and instead relies on redox mediators for electron transfer. These mediators must cross the outer membrane to reach their molecular interaction site, a process that remains poorly understood so far but is crucial for optimizing *P. putida*'s bio-electrochemical performance. To address this, the obtained data should be used to identify key targets involved in the transport of mediators across the outer membrane. These insights should then inform the design of mutants, thereby advancing our understanding of extracellular electron transfer between the cell, mediator, and anode.

# 2 Theoretical Background

## 2.1 *Pseudomonas putida* as a host for industrial biotechnology

The genus *Pseudomonas* is a large and highly diverse taxonomic group of gram-negative bacteria. It is found in numerous ecological habitats, such as terrestrial and marine environments and in association with animals and plants, where they are involved in important ecological activities: Biodegradation and bioremediation, nutrient cycling, food spoilage, plant growth promotion and disease suppression, and parasitism of other bacteria, plants and animals (Kiil et al., 2008; Timmis, 2002). This reflects a high degree of genomic diversity and genetic adaptability.

*Pseudomonas putida* is frequently isolated from (polluted) water, plants, and (polluted) soils (Weimer, et al., 2020), and the best characterized strain *P. putida* KT2440 has emerged as a versatile microbial laboratory workhorse and cell factory for industrial biotechnology (Weimer, et al., 2020). This can be traced back to its HV1 certification, which underscores its safety for use in diverse applications (Kampers, Volkers, & Martins Dos Santos, 2019), multifaceted biocatalytic capabilities (Akkaya, Pérez-Pantoja, Calles, Nikel, & de Lorenzo, 2018), and tolerance to a wide range of chemical stressors (Reva et al., 2006). Besides its capability to utilize a wide range of carbon and nitrogen sources (Belda et al., 2016), the strain offers rapid growth and low nutrient requirements, making it an excellent choice as a chassis (Loeschcke & Thies, 2015; Nikel, Martínez-García, & de Lorenzo, 2014). Over the last years, research on *P. putida* has made considerable progress: The genome is fully sequenced, allowing easy access to the genomic repertoire (Belda, et al., 2016; Nelson et al., 2002). The strain is well accessible for genetic modification, and extensive genetic and metabolic knowledge and tools are available (Cook et al., 2018; Nikel & de Lorenzo, 2018; Volke, Martino, Kozaeva, Smania, & Nikel, 2022). Moreover, the construction of genome-scale metabolic models for in silico simulations and data mapping (Nogales et al., 2020;

Puchałka et al., 2008; Tokic, Hatzimanikatis, & Miskovic, 2020), and high-resolution metabolic flux analysis (Kohlstedt & Wittmann, 2019; Nikel, Chavarria, Fuhrer, Sauer, & de Lorenzo, 2015; Sasnow, Wei, & Aristilde, 2016; Volke, Gurdo, Milanesi, & Nikel, 2023) have further expanded the available toolbox.

### 2.1.1 Central carbon core and energy metabolism

*P. putida* KT2440, a TOL plasmid-free derivative of *P. alloputida* mt-2, was originally isolated from a soil sample in Japan in 1960 (Nakazawa, 2002; Nakazawa & Yokota, 1973). In the challenging soil environment, where bacteria are exposed to various stressors, *P. putida* has evolved opportunistic and versatile nutritional strategies. As a result, it can metabolize a wide array of substrates, including organic acids, sugars, recalcitrant aromatic compounds, and even xenobiotics (chemicals foreign to life) (Nikel, Chavarría, Danchin, & de Lorenzo, 2016). Catabolism of these challenging substrates often involves harsh redox reactions, which are prone to generate reactive oxygen species (ROS) (Akkaya, et al., 2018). In this context, the robustness, flexibility, and adaptability of *P. putida* are largely attributed to its distinctive metabolic architecture (Fig. 2-1).

Like many other Pseudomonads, sugar metabolism in *P. putida* is compartmentalized: After glucose crosses the outer membrane, it follows one of two pathways: it is either directly transported into the cytoplasm and is subsequently phosphorylated, or it is oxidized in the periplasm to gluconate or 2-ketogluconate (2KG) (Lessie & Phibbs, 1984). These (keto)sugar acids can then also be transported into the cytoplasm, where they are likewise phosphorylated. All three entry pathways converge at the level of 6-phosphogluconate (6PG) in the central metabolism (del Castillo et al., 2007), but differ in their ATP demand and redox outcome: The direct cytosolic uptake via an inner membrane ABC transporter, followed by phosphorylation, requires hydrolysis of two ATP molecules, further oxidation of glucose-6-phosphate generates 1/3 NADPH and

2/3 NADH (Olavarria et al., 2015). In contrast, periplasmic oxidation to gluconate or 2KG generates $PQQH_2$ and $PQQH_2$ + $FADH_2$, respectively. The oxidation of these redox cofactors via the electron transport chain leads to ATP production. As a result, this periplasmic pathway enables *P. putida* to partially decouple ATP generation from NADH formation (Ebert, Kurth, Grund, Blank, & Schmid, 2011; Kohlstedt & Wittmann, 2019). The cytosolic uptake of gluconate and 2KG and the conversion to 6PG each require one ATP and, in the case of 2KG, one additional NADPH. During balanced aerobic growth on glucose, the uptake via gluconate is the preferred route (Kohlstedt & Wittmann, 2019; Nikel, et al., 2015). Only a small fraction undergoes further oxidation to 2KG, with approximately 90% of the carbon flux bypassing this node (Kohlstedt & Wittmann, 2019; Nikel, et al., 2015). In contrast, nutrient-starved, stressed, slow-growing, or resting cells produce increased levels of gluconate and 2KG (Sasnow, et al., 2016; Volke, et al., 2023). Under challenging conditions, such as later stages of a demanding fed-batch process on lignin-based aromatics (Kohlstedt et al., 2018) or during anaerobic, electrogenic conditions, *P. putida* can almost exclusively convert glucose into 2KG, achieving yields of up to 96% (Weimer, et al., 2024). A deuterium-based method for flux analysis revealed, that in *P. putida* periplasmic glucose oxidation activity is inversely correlated with growth (Volke, et al., 2023).

Notably, *P. putida* has an incomplete Embden-Meyerhof-Parnas (EMP) pathway due to the absence of the glycolytic enzyme 6-phosphofructo-1-kinase (Pfk). Consequently, the central intermediate 6PG is predominantly catabolized via the Entner-Doudoroff (ED) pathway, generating the two triose intermediates pyruvate (PYR) and glyceraldehyde-3-phosphate (G3P). While a major portion of pyruvate enters lower catabolism, about 10% is recycled back to hexoses through reactions compromising enzymes from the ED, gluconeogenic EMP, and pentose phosphate pathway during growth on glucose, forming an amphibolic cycle known as the EDEMP cycle (Nikel, et al., 2015). The yield of NADPH is closely linked to the reaction catalyzed by

glucose-6-phosphate-1-dehydrogenase, and it varies with the extent of recycling and the proportion of glucose phosphorylated by glucokinase.

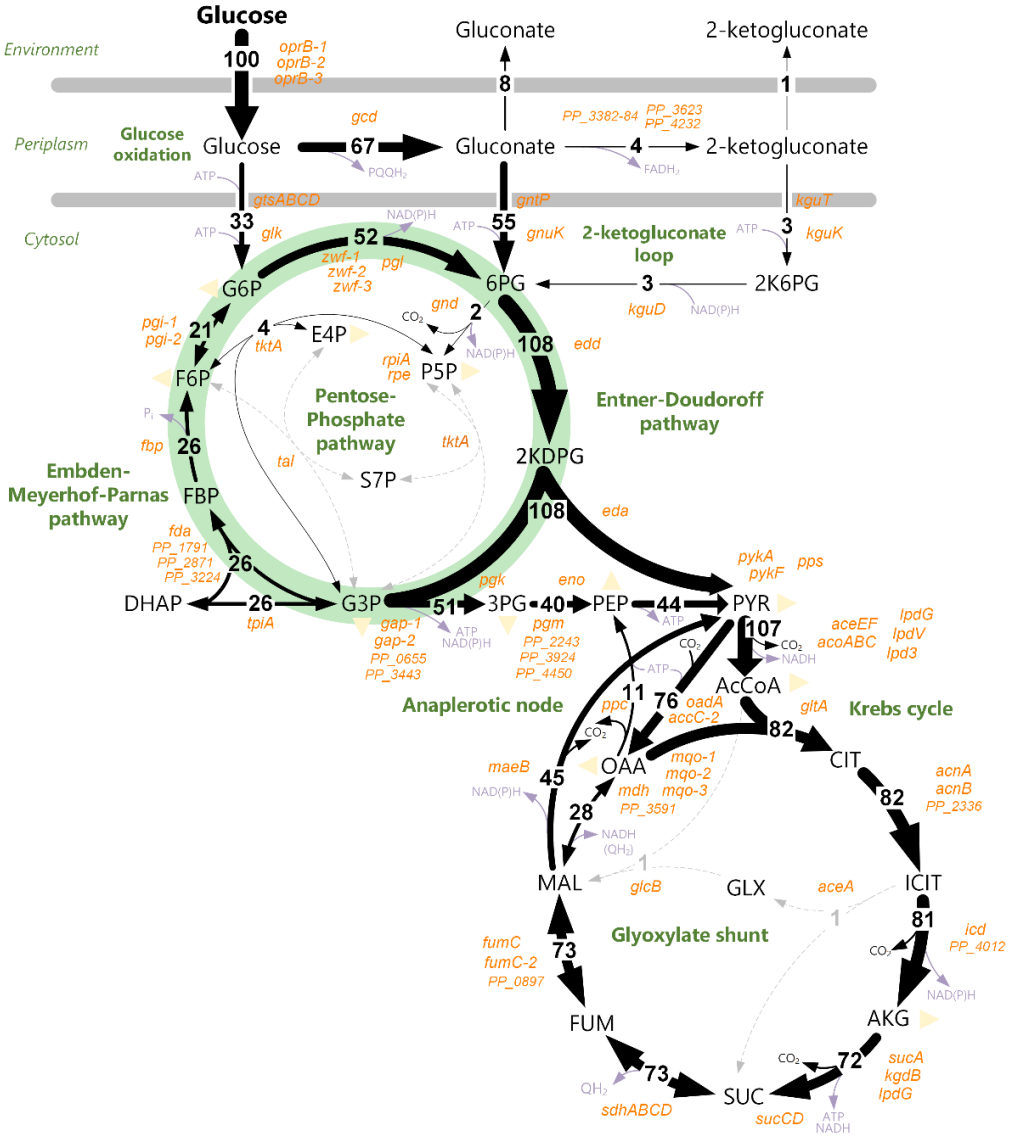


**Fig. 2-1: Typical carbon flux distribution throughout central carbon metabolism of glucose-grown *Pseudomonas putida*.** *P. putida* features a predominant ED pathway, coupled with an incomplete EMP pathway and activities of the PP pathway. The C3 intermediates, pyruvate (PYR) and glyceraldehyde-3-P (G3P), are recycled back via the gluconeogenic operation of the EMP pathway, a network topology called EDEMP cycle (Nikel, et al., 2015). Respective enzyme-coding genes (orange), redox and energy cofactors (light purple). Reproduced with permission from Springer Nature (Weimer, et al., 2020).

This ability to modulate NADPH production, often at the expense of ATP, is crucial for *P. putida*'s endurance to oxidative stress (Nikel et al., 2021). This is especially beneficial in redox-intensive biocatalytic processes. Moreover, the central carbon metabolism of *P. putida* was reengineered to include a phosphoketolase shunt (Bruinsma et al., 2023), and a functional linear glycolysis based on the EMP pathway (Sánchez-Pascuala, Fernández-Cabezón, de Lorenzo, & Nikel, 2019). These modifications highlight the adaptability of this bacterium.

### 2.1.2 Product spectrum and industrial application

An extensive body of literature highlights the use of *Pseudomonas* for bioremediation and plant growth promotion (de Lorenzo, et al., 2024). The frequent isolation of *P. putida* from polluted environments (Weimer, et al., 2020) underscores its remarkable ability to thrive in harsh conditions. Notably, the parental strain of the industrially strain KT2440 was originally isolated from soil during a search for bacteria capable of degrading aromatic compounds (Nakazawa, 2002). It is therefore unsurprising that much of the early research on its biotechnological applications primarily focused on the degradation of complex and challenging compounds such as polychlorinated biphenyls (Dowling, Pipke, & Dwyer, 1993), 2,4-dichlorophenoxyacetic acid (Short, King, Seidler, & Olsen, 1992), and 1,3-dichloroprop-1-ene (Nikel & de Lorenzo, 2013). The capability to deal with harsh reactions is of particular interest for industrial processes that involve crude extracts from raw materials and waste streams (Son et al., 2023), e.g. crude glycerol (Borrero-de Acuña, Rohde, Saldias, & Poblete-Castro, 2021), alkaline pretreated liquor (waste stream from bioethanol production) (Vardon et al., 2015) or lignin hydrolysates (Borrero-de Acuña et al., 2021; Kohlstedt, et al., 2018; He Liu et al., 2024).

In addition, as a soil bacterium, *P. putida* is well adapted to the rhizosphere and excels as a seed and root colonizer. These colonization abilities have been extensively studied

for its use as a biocontrol agent and plant growth promoter (Espinosa-Urgel, Kolter, & Ramos, 2002; Espinosa-Urgel, Salido, & Ramos, 2000; Matilla & Krell, 2018; Matilla et al., 2010). However, in recent years, applications of *P. putida* have expanded beyond these two most obvious applications, now encompassing the production of polymers, bulk chemicals, pharmaceuticals, and high-value specialty products (Loeschcke & Thies, 2015; Poblete-Castro, Becker, Dohnt, dos Santos, & Wittmann, 2012; Weimer, et al., 2020).

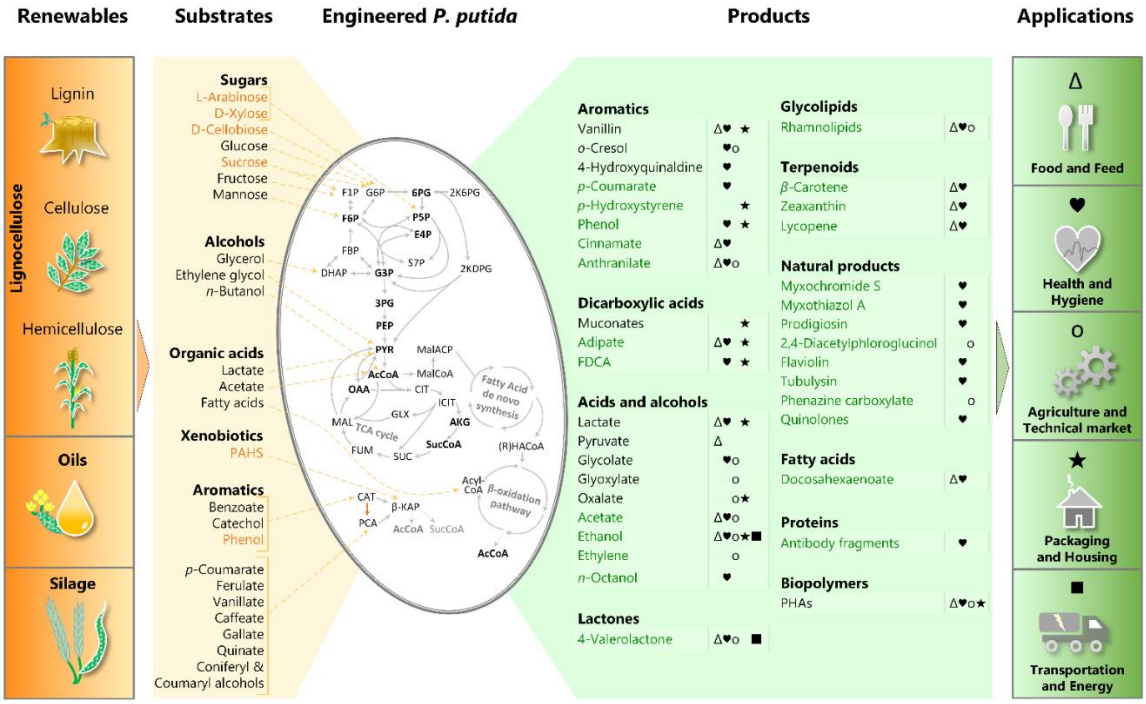


**Fig. 2-2**: **Production using engineered *P. putida* strains.** Substrates generated from renewable feedstocks, such as lignocellulose, oils and silage can be used to produce value added products for application in the food and feed (Δ), health and hygiene (♥), packaging and housing (★), transportation and energy sector (■), and for agriculture and technical application (o). Entry points of the respective substrates in the metabolism (orange), new to *P. putida* substrates and products (green). Reproduced with permission from Springer Nature (Weimer, et al., 2020).

Additionally, the substrate spectrum of *P. putida* has been expanded to include a wider range of compounds e.g. sucrose (Löwe, Schmauder, Hobmeier, Kremling, & Pflüger-Grau, 2017), D-xylose (Dvořák et al., 2024), D-cellobiose (Bujdoš et al., 2023), phenol (Vardon, et al., 2015), terephthalic acid (Brandenberg, Schubert, & Kruglyak, 2022) and ethylene glycol (Franden et al., 2018) (Fig. 2-2). Despite the growing research interest and recent advancements in using *P. putida* as a host, the number of large-scale industrial bioprocesses utilizing this bacterium remains limited, as in the case for the industrial application of other microbes (Wehrs et al., 2019). Notable exceptions include the production of polyhydroxyalkanoates (PHA), 2,5-furandicarboxylic acid (FDCA), and rhamnolipids, which are still relatively rare examples (Weimer, et al., 2020). The need to transition towards a sustainable economy, combined with the increasing availability of rational, predictable design through advanced strain engineering and analytic technologies, has significantly reduced the time and investment required to reach minimal viable products or proof-of-concepts. This progress is expected to drive the market expansion of industrial biotechnology in the near future (Nielsen, Tillegreen, & Petranovic, 2022).

### 2.1.3 Metabolic engineering towards non-natural electron acceptors

Despite the many favorable traits (described above) that make *P. putida* a promising industrial workhorse, there are certain characteristics that could be considered drawbacks (de Lorenzo, et al., 2024):

Firstly, *P. putida* KT2440 exhibits high resistance to some antibiotics. While this is not a concern in terms of pathogenicity - since this strain is non-pathogenic, unlike other members of the *Pseudomonas* genus - it can pose challenges for episomal expression. The resistance may interfere with the use of antibiotic selection markers. However, integrative expression is often preferred for large-scale processes, since these systems

offer several advantages over episomal expression, such as lower costs, improved regulatory compliance, and greater stability. Another challenge is the strain's complex surface structure and the presence of multiple prophages in its genome. These challenges have been effectively addressed through the development of streamlined strains like EM42, in which genes encoding flagella, prophages, transposons, and deoxyribonucleases I have been deleted (Martínez-García, Nikel, Aparicio, & de Lorenzo, 2014). Another example is strain EM371, in which approximately 5% of the genomic DNA was removed, targeting genes that encode bulky cell surface structures involved in the display of adhesins and multiprotein assemblies. However, under harsh bioprocess conditions, further optimization of the degree of surface exposure may be necessary, as the larger cell surface area of EM371 makes it more susceptible to external stressors (Martinez-Garcia et al., 2020).

Additionally, *P. putida* KT2440 is an obligate aerobe, relying on oxygen as the sole terminal electron acceptor (Nelson, et al., 2002). At large scale aerobic bioprocesses are gas transfer limited, which leads to higher operating costs due to agitation, sparging and cooling requirements. This ultimately restricts the maximum size of such reactors and leads to significant carbon losses due to the formation of $CO_2$, resulting in lower yields compared to anaerobic conditions (Hannon, Bakker, Lynd, & Wyman, 2007).

In contrast to *P. putida* KT2440, other closely related facultative anaerobic members of the genus *Pseudomonas* can grow anaerobically via nitrate or nitrite reduction (Carlson & Ingraham, 1983; Davies, Lloyd, & Boddy, 1989), or via fermentation of arginine (Vander Wauven, Piérard, Kley-Raymann, & Haas, 1984). Although, *P. putida* KT2440 is incapable of anaerobic metabolism, it has acquired functions for metabolism under low oxygen tension. The strains aerobic respiratory chain contains five terminal oxidases: Cyo, CIO, $aa_3$, $cbb_3$-1, and $cbb_3$-2 oxidases, which differ in their redox potential, affinity to oxygen, and their potential to pump protons. Their relative proportion changes depending on the environmental conditions (Ugidos, Morales, Rial, Williams, & Rojo,

2008). Moreover, the genome contains a nitrite reductase complex (*nirB*, *nirD*; *PP_1705-1706*), two oxygen-independent coproporphyrinogen III oxidase genes (*PP_0141, PP_5101*), and gene homologs for fermentation of pyruvate such as arginine deiminase operon (*arcCBAD*; *PP_0999-1002*), D-lactate dehydrogenase (*ldhA*; *PP_1649*), and phosphotransacetylase (*pta*; *PP_0774*) (Dos Santos, Heim, Moore, Strätz, & Timmis, 2004). However, the genome of *P. putida* does not contain the second gene of the Pta-AckA acetate fermentation pathway which encodes acetate kinase (*ackA*), catalyzing the ATP generating reaction from acetyl-phosphate to acetate. The ability to withstand fluctuating oxygen concentrations reflects the strains ability to thrive in diverse, and ecological habitats such as soils, and the rhizosphere, where oxygen depleted zones can occur (Dos Santos, et al., 2004). This property has also shown to be advantageous for large scale industrial bioreactors (Ankenbauer et al., 2020), in which it is difficult to ensure even oxygen distribution throughout the entire reactor volume (Nadal-Rey et al., 2022). However, the strict oxygen dependency of *P. putida* clearly limits its industrial application, and transforming *P. putida* into a strain capable of anaerobic metabolism has therefore been a long-standing goal.

In this context, research efforts have focused on enabling *P. putida* to adopt a true anaerobic lifestyle, with the goal of expanding its potential for anaerobic bioprocess applications. The nitrate/nitrite respiration system from *P. aeruginosa* were transferred into *P. putida*. This enabled the mutant to reduce nitrate and nitrite, which supported anaerobic survival, but no growth (Steen, et al., 2013). Similarly, the introduction of fermentative pathways by expression of acetate kinase (*ackA*) from *E. coli* and pyruvate decarboxylase (*pdc*) and alcohol dehydrogenase II (*adhB*) from *Zymomonas mobilis* enhanced degradation of 1,3-dichloroprop-1-ene and the anaerobic survival but did not promote growth (Nikel & de Lorenzo, 2013). A disadvantage of the latter approach is carbon loss through the production of reduced fermentation by-products. A recent *in-silico* study predicted the necessary genes for enabling anaerobic capabilities in

*P. putida* by comparing its protein domains with those of 1627 other Pseudomonas strains including facultative anaerobic strains. The data-driven approach suggested that 49 genes with known function and 3 external vitamins would need to be added (Kampers et al., 2021). This shows that the establishment of an anoxic regime is more challenging than previously assumed. However, many of the predicted genes are related to alternative electron acceptors (nitrate/nitrate), redox and energy metabolism. Other studies adopted a bio-electrochemical system supplemented with redox mediators in which the anode acts as an alternative terminal electron acceptor instead of oxygen. This enabled *P. putida* non-growth conversion of sugars into their respective (keto)sugar acids (Lai, et al., 2016; Nguyen, et al., 2021) or production of rhamnolipids (Askitosari et al., 2020). By providing an alternative electron acceptor (redox mediator and anode), this approach eliminates the need for most of the predicted genes.

## 2.2 Microbial electrochemical technology

The ability of microorganisms to produce energy has been studied for more than a century (Potter & Waller, 1911). But it was not until the early 2000s that the field of microbial electrochemical technology experienced a true revival with greatly increased research interest (Schröder, 2011), covering among others, the production of energy, $H_2$, and value added chemicals, water treatment, and biosensors. This development is largely attributable to an increased focus on eco-friendly and sustainable applications, and value addition to the whole process, especially for wastewater treatment (De Vrieze, Arends, Verbeeck, Gildemyn, & Rabaey, 2018; Hernandez & Osma, 2020). Bio-electrochemical systems display an innovative convergence of biology and electrochemistry capable of interconverting chemical and electrical energy while employing enzymes or whole microorganisms as biocatalysts. It should be noted that in the following the term ‘Bio-electrochemical system (BES)’ is used exclusively for microbial electrochemical reactions.

Bio-electrochemical systems are generally composed of two compartments with one electrode each, a working and counter electrode, which may be separated by an ion-permeable membrane. Both are hooked externally to complete an electrical circuit. Whereat, oxidation reactions take place at the anode and reduction reactions at the cathode (IUPAC, 1997). Electrons transferred to the anode flow towards the cathode. Thereby, these systems allow recreating microbial interactions with insoluble electron donors and acceptors (Rabaey et al., 2007). With regard to the system configuration, targeted product, and current density requirements, different bio-electrochemical systems can be distinguished (Moscoviz, Toledo-Alarcón, Trably, & Bernet, 2016) (Fig. 2-3): The prototypical microbial fuel cell is operated as a galvanic cell where the overall reaction occurs spontaneously. Microorganisms serve as biocatalysts at the anode, releasing electrons through substrate oxidation. These electrons are transferred to the anode and then flow through an external circuit to the cathode, where they reduce e.g. oxygen, generating current that can be directly harnessed (Fig. 2-3A) (Lovley, 2008). However, because electricity is a relatively low-value product, microbial fuel cells have gained attention as a promising hybrid technology offering multiple benefits beyond power generation. They are now recognized for their potential to enhance wastewater treatment, facilitate the removal or recovery of metals and nutrients, desalinate water, and recover energy simultaneously. Despite these advancements, challenges remain, particularly in boosting power output. Additionally, the use of expensive materials and issues with material stability further complicate the scaling and commercialization of microbial fuel cells (Boas, Oliveira, Simões, & Pinto, 2022). In microbial electrolysis cells, microorganisms oxidize organic matter at the anode, generating $CO_2$, electrons, and protons. The released electrons are then utilized at the cathode to produce hydrogen from the free protons (Fig. 2-3B) (Hong Liu, Grot, & Logan, 2005; Logan et al., 2008; Rozendal, Hamelers, Euverink, Metz, & Buisman, 2006) and, more recently, methane in microbial electrolysis-assisted anaerobic digesters (Zakaria & Dhar, 2019). Hydrogen

production in this systems is not spontaneous and requires an externally applied voltage of more than 0.2 V (pH 7, 30 °C, 1 atm), compared to 1.23 – 1.8 V required for conventional water electrolysis (Kadier et al., 2016).

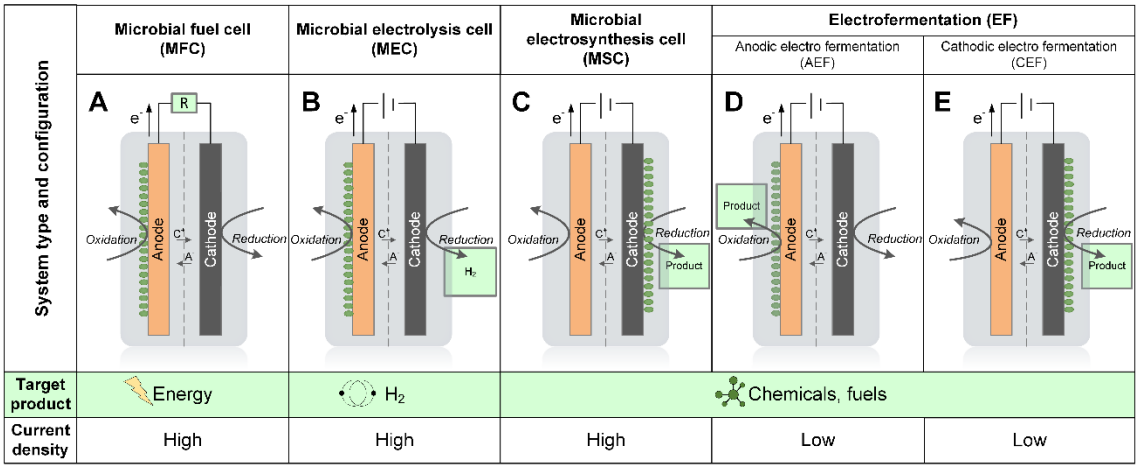


**Figure 2-3: Simplified scheme of different types and configurations of bio-electrochemical systems – Microbial fuel cell, Microbial electrolysis cell, Microbial electrosynthesis cell, and Electrofermentation.** The different types can be distinguished according to their respective target products (marked in green) and current densities (Moscoviz, et al., 2016).

Microbial electrosynthesis cells are used for biotic, cathodic $CO_2$ reduction for the electrochemical driven production of organic acids (Batlle-Vilanova et al., 2017), bioplastics (Sciarria et al., 2018), and biofuels (Vassilev, Hernandez, et al., 2018) (Fig. 2-3C). Up-scaling of the latter is considered a challenge: Achieving high current densities while maintaining acceptable voltage levels can be difficult, and the amount of product generated is directly linked to the number of electrons transferred; thus, higher current densities are essential for increasing product yields (Prévoteau, Carvajal-Arroyo, Ganigué, & Rabaey, 2020). Therefore recently, electro-fermentation, which requires only low energy input, experienced a rise in popularity (Fig. 2-3D). Depending on the electrode that drives biosynthesis, a distinction can be made between cathodic

electro-fermentation towards the production of more reduced products, and anodic electro-fermentation aiming at more oxidized products. Electro-fermentation generally operates at lower current densities compared to other types of bio-electrochemical systems, as the electric current serves a secondary, modulating function in redox reactions rather than acting as the primary energy source or product (Moscoviz, et al., 2016). Providing low electrical currents allows to fine-tune the redox potential (oxidation reduction potential, ORP) of the medium, which in turn influence the internal redox balance of the used microorganisms by modifying their $NAD^+$/NADH ratio. These changes can influence metabolic reactions both directly, and indirectly by affecting gene expression (Pei et al., 2011). In classical fermentation different strategies are employed to manipulate the redox balance. These include gassing, addition of redox active compounds such as sorbitol, sodium sulfate, dithiothreitol or cysteine, and pH control (Chen-Guang, Jin-Cheng, & Yen-Han, 2017; Chen, Jiang, Zheng, Pan, & Luo, 2012; Kastner, Eiteman, & Lee, 2003; J. Li et al., 2010). In contrast, electro-fermentation provides more precise control over the redox environment, offering a dynamic, non-invasive (without the need for chemical additives) modulation of microbial metabolism, surpassing the capabilities of conventional ORP control strategies. Electro-fermentation has shown to hold potential to enhance yields from anaerobic glycerol and sugar fermentation by redirecting carbon flux toward desired products while minimizing by-products (Kracke & Krömer, 2014; Vassilev, Averesch, Ledezma, & Kokko, 2021). For example, electro-fermentation was shown to enhance the anaerobic production of L-lysine using *Corynebacterium glutamicum* from glucose (Vassilev, Gießelmann, et al., 2018), the production of 3-hydroxypropionic acid from glycerol using *Klebsiella pneumonia* (C. Kim et al., 2017), and the production of acetoin under limited aeration conditions using *Bacillus subtilis* (Y. Sun, Kokko, & Vassilev, 2023). A great advantage of electro-fermentation is that it can be applied for already established fermentation processes. Furthermore, anodic electro-fermentation was also used for

anaerobic production of 2-ketogluconate using the obligate aerobic *P. putida* (Lai, et al., 2016).

### 2.2.1 Extracellular electron transfer in the bio-electrochemical system

The coupling of electron donor oxidation with electron acceptor reduction is fundamental to biological processes, including energy production, biosynthesis, and the maintenance of cellular redox balance. While most organisms rely on soluble electron acceptors (e.g. $O_2$, $NO_3^-$, $NO_2^-$, $SO_4^{2-}$) or donors (e.g. $H_2$, $NH_3$, $H_2S$, $S^{2-}$), certain microorganisms have evolved the ability to utilize insoluble or solid-state electron acceptors or donors, particularly metallic ions (e.g. manganese, ferric, uranium, and cupric), expanding the diversity of metabolic strategies that support life in various environments (Lovley, 1993). This process requires the transport of electrons across the non-conductive cell membrane. To enable this exchange, these organisms have developed specialized extracellular electron transfer mechanisms, which can be harnessed in bio-electrochemical systems for electron transfer between microbes and anode or cathode. Broadly, two types of extracellular electron transfer in the bio-electrochemical system can be distinguished: (I) Direct electron transfer, and (II) indirect electron transfer (Fig. 2-4). This section focuses on anodic electron transfer using pure microbial cultures.

The molecular mechanisms, underlying direct electron transfer have been extensively studied in different model organisms, including the metal-reducing bacteria *Geobacter sulfurreducens* and *Shewanella oneidensis*. Most organisms capable of direct electron transfer rely on outer-membrane c-type cytochromes (Butler, Kaufmann, Coppi, Núñez, & Lovley, 2004; H. J. Kim et al., 2002) (Fig. 2-4A). These c-type cytochromes possess a multiheme structure, with each heme exhibiting a distinct redox potential. The arrangement of the heme groups results in overlapping redox potential windows, which facilitate efficient electron transfer across the cell membrane (Firer-Sherwood, Pulcu, & Elliott, 2008). Another mechanism of direct electron transfer involves conductive cell

appendages, pili, commonly known as nanowires (Childers, Ciufo, & Lovley, 2002; Gorby et al., 2006) (Fig. 2-4B). These nanowires enable long-range electron transfer, spanning distances of 50 µm or more within biofilms (Malvankar & Lovley, 2012). In addition, these pilli were reported to play a role in microbial cell attachment, which is essential for the formation of biofilms (Thormann, Saville, Shukla, Pelletier, & Spormann, 2004).

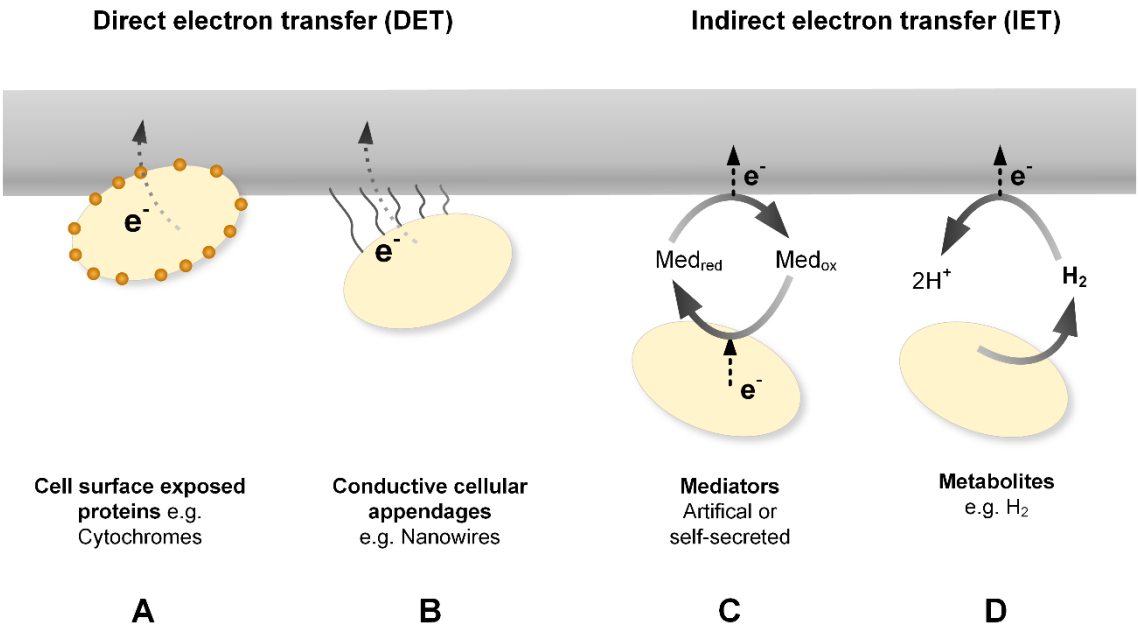


**Fig. 2-4: Extracellular electron transfer mechanisms between electrode and microorganisms.** There are two general types of electron transfer: (I) direct electron transfer, and (II) indirect electron transfer. Direct electron transfer can occur through cell surface exposed proteins (A), or conductive cellular appendages (B). Indirect electron transfer can occur through mediators (C) or metabolites (D).

On the other hand, non-electroactive microbes, which lack the ability for direct electron transfer, can still transfer electrons across the cell membrane through indirect electron transfer. This process occurs via redox-active compounds, known as mediators, which act as electron shuttles between the microbe and the electrode (Fig. 2-4C). These mediators can either be self-produced and secreted by the microbes, such as

phenazines (Rabaey, Boon, Höfte, & Verstraete, 2005) and flavins (Marsili et al., 2008), or externally added to the system. The selection of an appropriate mediator is primarily governed by its redox potential, which must align with the molecular interaction site within the electron transport chain. Most of these known interaction sites are located on the cytoplasmic membrane, necessitating the transport of the mediator across the outer membrane. However, the mechanisms by which mediators, particularly exogenous and synthetic ones, are transported across the microbial membrane are still not well understood, posing a significant challenge to improving indirect electron transfer efficiency (Gemünde, Lai, Pause, Krömer, & Holtmann, 2022).

Another form of indirect electron transfer to the anode involves $H_2$ produced during fermentation (Fig. 2-4D). This mechanism is primarily applicable in microbial fuel cells and requires a catalytic anode, e.g. coated with platinum, to facilitate current production. Unlike the other electron transfer mechanisms described above, the microorganism is not using the anode for energy conservation. As a result, these microbial fuel cells tend to be less efficient in generating high power densities and coulombic efficiencies, as the energy is primarily diverted toward metabolite production rather than extracellular electron transfer (Niessen, Schröder, Harnisch, & Scholz, 2005).

The selection of an extracellular electron transfer mechanism depends on the specific application. One major limitation of direct electron transfer is that microorganisms must stay in close proximity to the electrode surface. Biofilms formed on the electrode do not fully utilize the bulk liquid in the reactor and are limited by the diffusion rates of reactants and products, which can lead to product accumulation and substrate depletion within the biofilm (Scott & Yu, 2015). In contrast, indirect electron transfer (mediator-based) processes allow for the full utilization of the reactor volume. However, some mediators can be toxic to cells at higher concentrations (Yonei, Noda, Tachibana, & Akasaka, 1986), requiring careful control and efficient stirring. The toxicity of some mediators is also an important point to consider regarding downstream processing. For natural

(self-produced) mediators, factors like energy and carbon costs, as well as stability, need to be considered (Gemünde, et al., 2022). In contrast, artificial mediators impose no additional metabolic burden on the cells, and their concentration can be more precisely controlled.

### 2.2.3 Employing *Pseudomonas putida* in a bio-electrochemical system

The obligate aerobic *P. putida* can generate ATP and redox power under oxygen-limited or even anaerobic conditions, when growing in the presence of an anode (Lai, et al., 2016; Schmitz, et al., 2015; Weimer, et al., 2024). Using *P. putida* for electrochemical conversions offers advantages, as the microbe lacks fermentative pathways, which are commonly associated with the production of undesirable by-products in facultative anaerobes (Nelson, et al., 2002). Although *P. putida* is not naturally electrogenic, redox mediators can act as electron acceptors. To adapt *P. putida* to the bio-electrochemical system, both natural (under oxygen-limited conditions) and inorganic metal complexes (under anaerobic conditions) have been employed as redox mediators (Lai, et al., 2016; Schmitz, et al., 2015).

Interestingly, certain Pseudomonas species, like *P. aeruginosa*, naturally interact with solid electrodes by secreting phenazines - organic compounds that facilitate electron transfer (Rabaey, et al., 2005). The phenazine production pathway of *P. aeruginosa* has been successfully transferred into *P. putida* KT2440 for the biosynthesis of phenazine derivatives, phenazine-1-carboxylic acid (PCA; *phzA-G*) and pyocyanin (PYO; *phzA-G*, *phzM*, *phzS*) (Schmitz et al., 2015). The engineered strains were able to produce phenazine derivates from glucose, using them as mediator to transfer electrons to the anode (Schmitz et al., 2015). However, the stability of PYO was found to be relatively low, with a half-life of just one day (Chukwubuikem, Berger, Mady, & Rosenbaum, 2021; Clifford et al., 2021). Additionally, its redox activity in the bio-electrochemical system is only semi-reversible (Bosire, Blank, & Rosenbaum, 2016), making PYO unsuitable as a

mediator for long-term processes. In contrast, PCA is a more promising mediator, with a half-life exceeding 10 days and reversible redox activity in the bio-electrochemical system (Bosire, et al., 2016; Chukwubuikem, et al., 2021). By utilizing self-secreted phenazines as redox mediators in an oxygen-limited bio-electrochemical system, *P. putida* primarily converts glucose into biomass, with gluconate as minor by-product (Schmitz, et al., 2015). This corresponds closely to the distribution of carbon flow in cells growing under aerobic conditions (Kohlstedt & Wittmann, 2019). This approach has shown to be advantageous for producing compounds such as rhamnolipids, valuable bio-detergents, that are more conveniently produced under microaerobic conditions due to problems with foam formation during aeration in aerobic systems (Askitosari et al., 2020). However, the use of self-secreted natural mediators has several drawbacks, including the metabolic costs associated with their biosynthesis, significant carbon loss, and less controllable concentrations as compared to the use of artificial added mediators (Gemünde, et al., 2022).

As a second strategy an artificial mediator can be supplied for enabling anaerobic (<15 ppb) electrochemical activity. Redox mediators that exhibit a potential greater than 0.207 V (versus a standard hydrogen electrode, SHE) resulted in the detection of analytic current in the bio-electrochemical system using *P. putida* (F1 and KT2440). Among these mediators are positively charged compounds, such as $[Co(bpy)_3]^{3+/2+}$, as well as negatively charged mediators such as $[Fe(CN)_6]^{3-/4-}$(Fig. 2-5B) (Lai, et al., 2016). This provides flexibility in selecting mediators that best fit process requirements, such as facilitating downstream processing (mediator separation). Notably, providing an anodic potential and artificial redox mediators significantly redirects *P. putida*'s metabolism in the absence of oxygen, resulting in a distinct anode-driven, electrogenic phenotype, capable of non-growth production of chemicals with high yield and selectivity. Driven by continuous electron flow from cells to mediators, *P. putida* KT2440 primarily converts glucose via periplasmic glucose oxidation into 2KG ($Y_{2KG/GLC}$ >90%), with gluconate as

an intermediate. Acetate is produced as the main cytosolic byproduct (Pause, et al., 2023; Weimer, et al., 2024). Under aerobic conditions, 90% of the carbon flux bypasses this periplasmic pathway, favoring cytoplasmic glycolysis. However, under anaerobic bio-electrochemical system conditions, periplasmic glucose oxidation to 2KG is crucial for current generation, as direct cytosolic glucose uptake or uptake via gluconate does not support current formation (Pause, et al., 2023). 2KG is a commercially valuable compound with diverse applications, including its use in the industrial synthesis of isoascorbic acid, an antioxidant approved for food preservation in the European market (Pappenberger & Hohmann, 2014). The high anaerobic 2KG yield using glucose is only achievable in the bio-electrochemical system, where the presence of the anode enables decoupling of carbon and electron balance. Examining the degree of reduction (DoR) of the substrate and final product: glucose (DoR = 4), 2KG (DoR = 3.33), and acetate (DoR = 4), shows that the products are overall more oxidized than glucose, without the formation of a more reduced byproduct, as typically seen in fermentation processes.

In addition, the bio-electrochemical performance of KT2440 was enhanced by overexpression of Gcd (Gluconate dehydrogenase) (Yu, et al., 2018). Moreover, cytochrome c reductase ($bc_1$, complex III) was identified as a key player in extracellular electron transfer through inhibitor studies. Specifically, antimycin A, a complex III-specific inhibitor, completely abolished electron transfer. In contrast, inhibition of cytochrome c oxidases and NADH dehydrogenase using sodium azide and rotenone had no significant effect on current output. Although the involvement of the periplasmic subunit of cytochrome c oxidase in extracellular electron transfer cannot be entirely ruled out, these findings suggest that complex III is the key component in electron transfer in the bio-electrochemical using *P. putida*, while the terminal oxidases, which are crucial for aerobic respiration, likely play only a minor or negligible role (Fig. 2-5A, Fig. 2-5C) (Lai, Bernhardt, & Krömer, 2020).

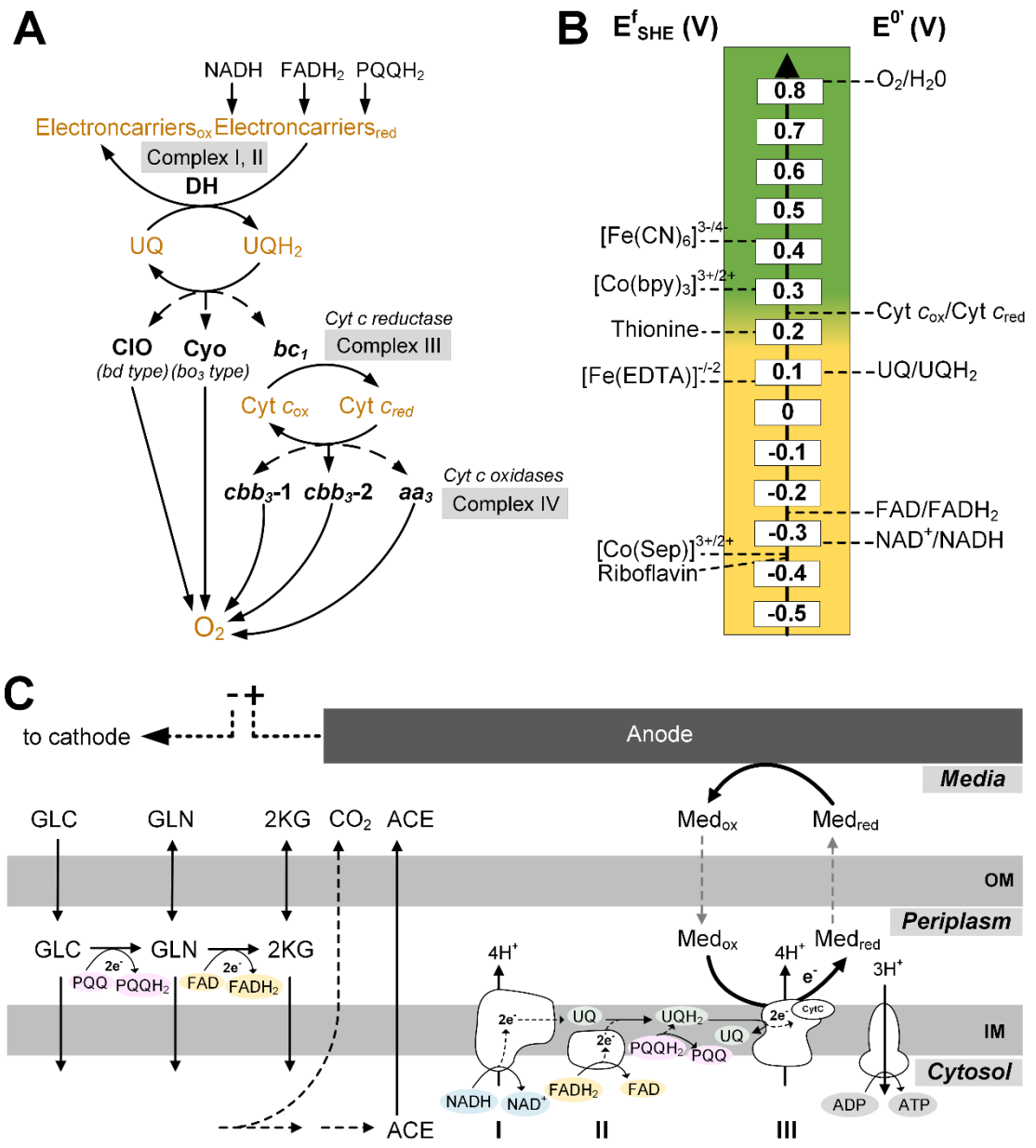


Figure continued next page

**Fig. 2-5**: **Electron transport chain and mediator-driven extracellular transfer using *P. putida* KT2440.** Schematic diagram of *P. putida* electron transport chain illustrating the possible routes of electron transfer (A). Formal redox potentials of artificial redox chemicals tested with *P. putida* in the bio-electrochemical system - only mediators with a potential greater than 0.207 V resulted in the detection of a catalytic current (in green) (Lai, et al., 2016), and standard redox potential of key redox reactions in the electron transport chain (White, Drummond, James, & Fuqua, 2011) (B). Schematic of electron transport chain of *P. putida* under bio-electrochemical conditions. Periplasmic glucose oxidation serves as the primary electron source. Electron donors transfer electrons to quinone carriers through dehydrogenases. The key site for mediator reduction has been

identified as cytochrome c reductase (III) (Lai et al., 2020). Electrons pumped by complexes I and III contribute to the formation of ATP through the action of ATP synthase. The mediator gets re-oxidized at the anode. Complex I: NADH dehydrogenase, Complex II: succinate dehydrogenase, Complex III: cytochrome $bc_1$, GLC: glucose, GLN: gluconate, 2KG: 2-ketogluconate, ACE: acetate

In addition to glucose, *P. putida* can convert other sugars in a bio-electrochemical system to their respective (keto-)sugar acids, allowing to produce a variety of valuable products. This included even non-growth-supporting sugars, such as L-arabinose, and D-galactose (Nguyen, et al., 2021). Moreover, the product spectrum can be further expanded by introducing carbon sources beyond sugars. For instance, when citrate was used as the sole substrate, recombinant *P. putida* KT2440 oxidized it into para-hydroxybenzoate, achieving a 70% higher yield compared to an aerobic setup (Hintermayer, Yu, Krömer, & Weuster-Botz, 2016).

In summary, the application of *P. putida* in a bio-electrochemical system containing artificial mediators shows strong potential for producing compounds that benefit from anodic electro-fermentation. However, challenges remain, particularly the lack of anaerobic growth and low carbon turnover rates (0.2 mmol $(g_{CDW}\ h)^{-1}$ compared to 14.2 mmol $(g_{CDW}\ h)^{-1}$ under aerobic conditions (Pause, et al., 2023), which must be addressed to optimize the system for broader applications.

# 3 Material and Methods

## 3.1 Bacterial strains and plasmids

*P. putida* KT2440 (DSM 6125) was obtained from the German Collection of Microorganisms and Cell Cultures (Leibniz-Institute DSMZ - Deutsche Sammlung von Mikroorganismen und Zellkulturen GmbH, Braunschweig, Germany), and served as the wild-type strain. The *E. coli* strains DH5αλpir (Biomedal Life Science, Seville, Spain), CC118λpir (de Lorenzo & Timmis, 1994), and HB101 were used for cloning purposes (plasmid amplification and tri-parental mating). All strains used in this work are listed in Table 3-1, all plasmids used in this work are listed in Table 3-2. Plasmid pSEVA234 was kindly donated by Prof. Víctor de Lorenzo (Centro Nacional de Biotecnología (CSIC), Madrid, Spain). For long-term storage, bacterial strains were preserved at -80 °C in stocks containing 20% (v/v) glycerol.

**Table 3-1:** Bacterial strains used in this work.

| ***E. coli*** | **Description** | **Reference** |
|---|---|---|
| DH5αλpir | Host for plasmid amplification: *supE44*, *ΔlacU169* (*φ80 lacZΔM15*), *hsdR17* ($rk^-mk^+$), *recA1*, *endA1*, *thi1*, *gyrA*, *relA*, *λpir* lysogen | Biomedal Life Sci., Seville, Spain |
| CC118λpir | Mating donor strain: *Δ(ara-leu)*, *araD*, *ΔlacX174*, *galE*, *galK*, *phoA*, *thi1*, *rpsE*, *rpoB*, *argE (Am)*, *recA1*, lysogenic *λpir* | (de Lorenzo & Timmis, 1994) |
| HB101 | Mating helper strain: *SmR*, *hsdR-M*$^+$, *pro*, l*eu*, *thi*, *recA* | (Sambrook, Fritsch, & Maniatis, 1989) |
| ***P. putida*** | **Description** | **Reference** |
| KT2440 | Wild type | (Nelson, et al., 2002) |
| *ΔscpC* | KT2440 derivative: *ΔscpC (ΔPP_0154)* | This work |
| *ΔPP_5266* | KT2440 derivative: *ΔPP_5266* | This work |
| *ΔacsAI ΔacsAII* | KT2440 derivative: *ΔacsAI* (*ΔPP_4487*) *ΔacsAII* (*ΔPP_4702*) | This work |
| *ΔaldBI ΔaldBII* | KT2440 derivative: *ΔaldBI* (*ΔPP_0545*) *ΔaldBII* (or *pedI*, *ΔPP_2680*) | This work |
| KT2440_control | KT2440 pSEVA6213S | This work |
| *ΔexbBD ΔtonB* | KT2440 derivative: *ΔPP_5306-5308* pSEVA6213S | This work |
| *ΔPP_1446* | KT2440 derivative: *ΔPP_1446* | This work |
| *ΔPP_3325* | KT2440 derivative: *ΔPP_3325* | This work |
| *ΔPP_1446 ΔPP_3325* | KT2440 derivative: *ΔPP_1446 ΔPP_3325* | This work |
| KT/234 | *P. putida* KT2440 pSEVA234 | This work |
| KT/234-oprF | *P. putida* KT2440 pSEVA6213S pSEVA234-oprF | This work |
| ΔTonB/234 | *P. putida ΔexbBD ΔtonB* pSEVA6213S pSEVA234 | |
| ΔTonB/234-oprF | *P. putida ΔexbBD ΔtonB* pSEVA6213S pSEVA234-oprF | This work |

**Table 3-2:** Plasmids used in this work.

| Plasmids | Description | Reference |
|---|---|---|
| pGNW2 | Suicide plasmid for integration/deletion: *Km$^R$, oriR6K, lacZα* with two flanking I-SceI sites, P 14g→msfGFP | (Wirth, Kozaeva, & Nikel, 2020) |
| pGNW2_Δ0154 | pGNW2 bearing regions up/downstream *PP_0154* | This work |
| pGNW2_Δ5266 | pGNW2 bearing regions up/downstream *PP_5266* | This work |
| pGNW2_Δ4487 | pGNW2 bearing regions up/downstream *PP_4487* | This work |
| pGNW2_Δ4702 | pGNW2 bearing regions up/downstream *PP_4702* | This work |
| pGNW2_Δ0545 | pGNW2 bearing regions up/downstream *PP_0545* | This work |
| pGNW2_Δ2680 | pGNW2 bearing regions up/downstream *PP_2680* | This work |
| pGNW2_Δ5306-8 | pGNW2 bearing regions up/downstream *PP_5306*-8 | This work |
| pGNW2_Δ1446 | pGNW2 bearing regions up/downstream *PP_1446* | This work |
| pGNW2_Δ3325 | pGNW2 bearing regions up/downstream *PP_3325* | This work |
| pSEVA6213S | Helper plasmid: *Gm$^R$, oriV* (RK2), *xylS*, PEM7→I-SceI | (Wirth, et al., 2020) |
| pSEVA234 | *Km$^R$*; oriV (RK2), lacIq-Ptrc | (Silva-Rocha et al., 2012) |
| pSEVA234-oprF | pSEVA234 bearing oprF (*PP_2089*) | This work |

## 3.2 Strain construction

### 3.2.1 Polymerase chain reaction

Polymerase chain reaction (PCR) was performed for DNA amplification and strain validation. For colony PCR, used to verify the accuracy of clones from transformation events, Phire Green Hot Start II PCR Master Mix (Thermo Fisher Scientific, Rochester, NY, USA) was employed. For amplifying fragments for plasmid construction, High-Fidelity PCR Master Mix with GC buffer or Phusion Plus DNA Polymerase (Thermo Fisher Scientific, Waltham, MA, USA) was used. The composition of the PCR reaction mixture is provided in Table 3-3, and the thermal cycler program parameters are detailed in Table 3-4. All Primers used in this work can be found in Supplementary Table 6-1.

**Table 3-3:** PCR reaction mixture components.

| Component | Volume [µL] | Final concentration |
|---|---|---|
| 2X PCR master mix | 10 | 1X |
| Forward primer (10 µM) | 0.5 | 250 nM |
| Reverse primer (10 µM) | 0.5 | 250 nM |
| Template DNA | * | 1–10 ng plasmid<br>5–100 ng genomic DNA |
| DMSO | 0.6 | 3% (v/v) |
| Water, nuclease free | add to 20 µL | |

**Table 3-4:** Parameters for thermal cycler program.

| Step | Temperature [°C] | Time [min] | Cycles |
|---|---|---|---|
| Initial Denaturation | 98 | 5 | 1 |
| Denaturation | 98 | 0.5 | |
| Annealing | * | 0.5 | 30 |
| Elongation | 72 | ** | |
| Final Elongation | 72 | 5 | 1 |
| | 8 | ∞ | 1 |

*Calculated for each primer pair using Tm Calculator (Thermo Fisher Scientific), 60 °C for Phusion Plus

**Phire: 15 sec $kb^{-1}$, Phusion: 30 sec $kb^{-1}$

### 3.2.2 Gel electrophoresis

To verify the correct size of PCR products and plasmid digestions, samples were analyzed by electrophoretic separation on 1–2% (w/v) agarose gels in 1X TAE buffer, run at 120 V for 40–60 minutes, depending on the expected fragment size. DNA samples were mixed with GelRed (MilliporeSigma, Burlington, MA, USA) for DNA staining, and loading dye (Gel Loading Dye, Purple 6X, New England Biolabs, Frankfurt am Main, Germany) before loading onto the gel. As standard either a 1kb DNA ladder (DNA Marker BLUE 1000 bp, GeneON, Ludwigshafen, Germany) or a 50 bp Marker (DNA Ladder 50 bp ready-to-use, GeneON, Ludwigshafen, Germany) were applied. The resulting bands were visualized by UV transillumination using the E-BOX CX5 TS gel documentation system (Vilber, Marne-la-Vallée, France).

### 3.2.3 Isolation and purification of plasmid DNA

For plasmid isolation and purification, the QIAprep Spin Miniprep Kit (Qiagen, Hilden, Germany) was used following the manufacturer's instructions, utilizing overnight cultures grown in Luria-Bertani (LB) liquid medium. If necessary, the eluted DNA was further concentrated using a SpeedVac Concentrator DNA 120 (Thermo Fisher Scientific, Waltham, MA, USA). DNA concentrations were measured using a NanoDrop 1000 spectrophotometer (Thermo Fisher Scientific, Waltham, MA, USA).

### 3.2.4 Purification of DNA fragments

PCR-amplified and digested DNA were purified using the WIZARD SV Gel and PCR Clean-Up System (Promega, Madison, WI, USA) according to the manufacturer's instructions. DNA concentrations were measured using a NanoDrop 1000 spectrophotometer (Thermo Fisher Scientific, Waltham, MA, USA).

### 3.2.5 Assembly of plasmids

All designs for cloning procedures were created with SnapGene software Version 7.2.1 (www.snapgene.com). Integrative plasmids were constructed using Gibson assembly (Gibson et al., 2009). The plasmid pGNW2 was digested with FastDigest enzymes (Thermo Fisher Scientific, Waltham, MA, USA) following the manufacturer's protocol. The DNA fragments to be inserted into the plasmid backbone were PCR-amplified using primers containing 20 bp homologous overlap regions. After verification and purification of both, the digested backbone and DNA fragments, 200 ng of the backbone and an equimolar amount of the DNA fragments were combined with 15 µL of Gibson master mix (Table 3-5). Nuclease-free water was added to bring the final volume to 20 µL.

**Table 3-5:** Gibson assembly mix.

| Component | | Volume final [µL] |
|---|---|---|
| **Gibson 5X assembly buffer** | | |
| Tris-HCl (1 M), pH 7.5 | 3 mL | 320 |
| $MgCl_2$ (100 mM) | 300 µL | |
| dGTP (100 mM) | 60 µL | |
| dATP (100 mM) | 60 µL | |
| dCTP (100 mM) | 60 µL | |
| dTTP (100 mM) | 60 µL | |
| DTT (1 mM) | 300 µL | |
| PEG-800 | 1.5 g | |
| NAD | 20 mg | |
| Water, nuclease free | 2.16 mL | |
| T5 Exonuclease | | 0.64 |
| Phusion Polymerase | | 20 |
| Taq ligase | | 160 |
| Water, nuclease free | | 699.4 |

The reaction mixture was incubated at 50 °C for 1 h. For transformation, 4 µL of the assembled product was added to 50 µL of competent cells.

The episomal plasmid pSEVA234-oprF was constructed by ligation using the Rapid DNA Ligation Kit (Thermo Fisher Scientific, Waltham, MA, United States) according to manufactures instructions, using BamHI-XbaI restriction sites. The correctness of all constructed plasmid was verified by PCR and sequencing (GENEWIZ, Inc. Burlington, MA, United States).

### 3.2.6 Transformation by heat shock

To prepare heat shock-competent *E. coli* DH5λpir cells, a 5 mL overnight culture was grown in LB medium supplemented with 20 mM $MgSO_4$ at 37 °C and 230 rpm on an orbital shaker (Multitron, Infors AG, Bottmingen, Switzerland). For the main culture, 125 mL of LB + 20 mM $MgSO_4$ in a 1 L flask was inoculated with 1 mL of the overnight culture and incubated at room temperature (23°C) at 250 rpm until the $OD_{600}$ reached 0.4–0.6. The cells were then cooled on ice for 10 min with frequent swirling. The cells were harvested by centrifugation (6000 × *g,* 10 min, 4 °C) in pre-cooled 50 mL Falcon tubes. The pellet was resuspended in 40 mL of cold TB buffer (Table 3-6) and centrifuged again under the same conditions. The cell pellet was then resuspended in 10 mL of cold TB buffer, followed by the addition of 0.75 mL DMSO. The cells were incubated on ice for 10 min. Finally, 100 µL aliquots were distributed into pre-cooled 1.5 mL tubes and stored at -80 °C until use.

**Table 3-6:** Composition of TB-Buffer (100 mL).

| Component | Volume [mL] |
|---|---|
| Pipes-NaOH (0.5 M), pH 6.7 | 2 |
| $CaCl_2$ (0.5 M) | 3 |
| KCl (2 M) | 12.5 |
| $MnCl_2$ (1 M) | 5.5 |
| Ultrapure water | 77 |

For heat shock transformation, competent cells were thawed on ice and mixed with 5-50 ng of DNA. The mixture was incubated on ice for 30 min, followed by heat shocking at 45 °C for 45 sec, and then placed back on ice for 2 min. Afterward, 900 µL of LB medium was added, and the cells were incubated for 1 h at 37 °C with shaking at 220 rpm. The transformed cells were plated on $LB^{kan}$ plates and incubated overnight at 37 °C.

### 3.2.7 Transformation by electroporation

Electrocompetent *E. coli* cells were prepared by inoculating 1 L of LB in a 2 L baffled flask inoculated with an overnight culture grown at 37 °C in 10 mL of LB. The culture was incubated at 37 °C and 250 rpm until an $OD_{600}$ of 0.35–0.4 was reached. The culture was then cooled on ice for 10 min with frequent swirling. Cells were transferred into pre-cooled 50 mL Falcon tubes, centrifuged (5000 × *g*, 10 min, 4 °C), and the resulting pellet was resuspended in 400 mL of ice-cold 10% (v/v) glycerol. Cells were centrifuged again under the same conditions, resuspended in 30 mL of cold glycerol, and centrifuged (8000 × *g*, 5 min, 4 °C). This washing step was repeated twice. Finally, the pellet was resuspended in 0.3 mL of cold glycerol, and 80 µL aliquots were distributed into pre-cooled 1.5 mL tubes before being snap-frozen in liquid nitrogen. The electrocompetent cells were stored at -80 °C until use.

For preparing electrocompetent *P. putida* cells, a 50 mL LB culture was grown overnight at 30 °C with shaking at 200 rpm. The cells were harvested by centrifugation (6000 × *g*, 10 min, RT) and resuspended in 50 mL of 300 mM sucrose. The cells were then centrifuged under the same conditions, resuspended in 1 mL of 300 mM sucrose, and centrifuged again (8000 × *g*, 2 min, RT). The pellet was resuspended in 250 µL of 300 mM sucrose, and 100 µL aliquots were transferred into pre-cooled 1.5 mL tubes and stored at -80 °C until needed.

For electroporation, one aliquot of competent cells was thawed on ice and mixed with either 50-200 ng of plasmid DNA or 4 µL of Gibson assembly reaction mixture. The cell-DNA mixture was transferred to a 2 mm gap electroporation cuvette (Gene Pulser cuvette, Bio-Rad, Hercules, CA, USA) and incubated on ice for 10 minutes. Electroporation was performed using a Gene Pulser Xcell (Bio-Rad, Hercules, CA, USA) with the following settings: 2.5 kV, 25 µF, and 200 Ω. Immediately after electroporation, 400 µL of LB was added, and the cells were incubated for 1 h at 30 °C for *P. putida* or 37 °C for *E. coli*. Finally, the cells were plated on LB agar containing the appropriate antibiotics and incubated overnight.

### 3.2.8 Tri-parental mating

To deliver integrative plasmids to *P. putida*, the donor *E. coli* CC118λpir strain (containing the plasmid), the helper *E. coli* HB101 strain, and the recipient *P. putida* strain were grown overnight in 20 mL LB medium supplemented with 50 µg $mL^{-1}$ kanamycin for the donor strain, 30 µg $mL^{-1}$ chloramphenicol for the helper strain, at 230 rpm, and 37 °C for *E. coli* and 30 °C for *P. putida*. Cells were harvested by centrifugation (13,000 rpm, 3 min, RT), and the pellets were resuspended in 1 mL of 10 mM $MgSO_4$.

For conjugation, 100 µL of the donor and helper strain suspensions were mixed with 200 µL of the recipient *P. putida* suspension in 4.6 mL of 10 mM $MgSO_4$. The mixture was centrifuged (6000 × *g*, 3 min, RT), and the resulting pellet was resuspended in 10 µL of 10 mM $MgSO_4$. This suspension was spotted onto the center of an LB agar plate and incubated overnight at 30 °C. The following day, the cells were recovered from the plate using an inoculation loop, resuspended in 5 mL of 10 mM $MgSO_4$, and centrifuged again (13,000 rpm, 3 min, RT). The pellet was resuspended in 100 µL of 10 mM $MgSO_4$ and plated onto M9 citrate plate (Table 3-7) containing 50 µg $mL^{-1}$ kanamycin. The plate was incubated overnight at 30 °C.

**Table 3-7:** Composition of M9 citrate plates.

| Component | Stock concentration [g/L] | Volume [mL] |
|---|---|---|
| **Salts (10X)** | | |
| $Na_2HPO_4$ | 68 | 100 |
| $KH_2PO_4$ | 30 | |
| NaCl | 5 | |
| $NH_4Cl$ | 10 | |
| $MgSO_4 \cdot 7H_2O$ | 246.4 | 2 |
| Agar | 16 | 888 |
| Sodium citrate $2H_2O$ | 228 | 10 |

### 3.2.1 Genomic modifications

Gene deletions were done based on homologous recombination-based technique for genome engineering in *P. putida*, which involves two rounds of recombination (Martínez-García & de Lorenzo, 2011; Wirth, et al., 2020). First, the suicide plasmid pGNW2 (derivate of pEMG) containing recognition sequences for the yeast intron-encoded I-*Sce*I homing endonuclease, was constructed in vitro by Gibson assembly using the linearized integrative plasmid and 500 bp PCR amplified fragments, reflecting the upstream and downstream flanking regions of genes to be deleted. The assembled plasmid was verified by PCR and delivered to *P. putida* via tri-parental mating. Integration in the genome was verified using the construction primers (forward primer upstream region and reverse primer downstream region). Obtained *P. putida*::pGNW2-UP/DW clones were transformed with the plasmid pSEVA6213S (bearing I-*Sce*I) for counter-selection. Extended passaging was required to lose the counter-selection plasmid pSEVA6231S in the *P. putida ΔexbBD ΔtonB* derivative, resulting in an apparent phenotype change on LB plates, evidenced by larger colonies. To rule out other unintended genomic changes, *P. putida ΔexbBD ΔtonB* pSEVA6231S was used. The wild type was accordingly transformed with pSEVA6231S for comparison. All deletions were verified by PCR and sequencing (GENEWIZ Azenta Life Sciences, Leipzig, Germany).

## 3.3 Cultivation

### 3.3.1 Growth media

Cells were grown in a defined M9 glucose medium (DM9) (Lai, Nguyen, & Krömer, 2019) (Table 3-8). For aerobic cultivations the medium contained 5 g $L^{-1}$ glucose. For anaerobic cultivations the medium contained 1.5 g $L^{-1}$ glucose. The pH was adjusted to 7 with 5 M NaOH.

**Table 3-8:** Composition of DM9 Media.

| Component | Stock concentration [g/L] | Concentration [g/L] |
|---|---|---|
| **Salts (5X)** | | |
| $Na_2HPO_4$ | 30 | 6 |
| $KH_2PO_4$ | 15 | 3 |
| $NH_4Cl$ (10X) | 1 | 0.1 |
| $MgSO_4 \cdot 7H_2O$ (1000X) | 100 | 0.1 |
| $CaCl_2 \cdot 2H_2O$ (1000X) | 15 | 0.015 |
| $C_6H_{12}O_6 \cdot H_2O$ | 200 | * |
| **Trace elements (1000X)** | **[mg/L]** | **[mg/L]** |
| $FeCl_3 \cdot 6H_2O$ | 1500 | 1.5 |
| $H_3BO_3$ | 150 | 0.15 |
| $CuSO_4 \cdot 5H_2O$ | 30 | 0.03 |
| KI | 180 | 0.18 |
| $MnCl_2 \cdot 4H_2O$ | 120 | 0.12 |
| $Na_2MoO_4 \cdot 2H_2O$ | 60 | 0.06 |
| $ZnSO_4 \cdot 7H_2O$ | 120 | 0.12 |
| $CoCl_2 \cdot 6H_2O$ | 150 | 0.15 |
| EDTA (acid) | 10,000 | 10 |
| $NiCl_2 \cdot 6H_2O$ | 23 | 0.023 |
| Ultrapure water | | Add to 1L |

### 3.3.2 Pre-culture preparation

A single colony from a fresh LB agar plate was used to inoculate a baffled shake flask, filled to ≤ 15% of its total volume with DM9 medium. The flasks were incubated overnight (16 hours) at 30 °C and 230 rpm on a rotary shaker (Infors, Bottmingen, Switzerland). Cells were harvested in exponential phase by centrifugation (6000 x *g*, 5 min, RT) and used to inoculate the main culture.

To enhance aerobic growth of *P. putida ΔexbBD ΔtonB*, the medium was supplemented with 20 µM $FeCl_3$. Strains harboring pSEVA234-oprF were induced with 1 mM IPTG at an $OD_{600}$ of 0.2. If necessary, precultures were supplemented with antibiotics at the

following concentrations: gentamycin 30 µg $mL^{-1}$ and kanamycin 50 µg $mL^{-1}$. The anaerobic main cultures did not contain antibiotics or inducers, as the cells do not grow under these conditions.

### 3.3.3 Cultivation in a miniaturized microtiter plate system

The growth rates of wild type *P. putida* and its Δ*exbBD* Δ*tonB* derivate at different iron concentration (10, 20, 40 µM $FeCl_3$) were screened using a miniaturized bioreactor system (BioLector). Cultures were grown in triplicate in a 48-well flower plates at 1,300 rpm, 30 °C, and 85% humidity (Beckman Coulter GmbH, Baesweiler, Germany), with each well filled with 1 mL DM9 medium and inoculated to an initial $OD_{620}$ of 0.2. Cell growth was measured online at $OD_{620}$. The maximum specific growth rate was determined by regression of ln $OD_{620}$ over time during exponential growth.

### 3.3.4 Cultivation in a bio-electrochemical system

The bio-electrochemical cultivation was carried out using DM9 medium containing 1.5 g $L^{-1}$ glucose and 1 mM ferricyanide ($[Fe(CN)_6]$) or 1 mM cobalt bipyridine ($[Co(bipy)_3]$) as the electron mediator. The reactors were inoculated to an initial optical density ($OD_{600}$) of approximately 1. Reactor setup and operation followed the protocol detailed elsewhere (Lai, et al., 2019). In brief, a custom-designed, double-jacketed cylindrical glass reactor with a working volume of 320 mL was used. The reactor's lids and plugs were made from polyether ether ketone (PEEK). The anodic (working) chamber was separated from the cathodic (counter) chamber by an ion-exchange membrane (CMI-7000, Membranes International Inc., Ringwood, NJ, USA). Titanium wire (0.5 mm diameter; TI5555, Advent, Oxford, England) was used as the electrical conductor. The cathode consisted of stainless-steel mesh (CMI-7000, Membranes International Inc.), while the anode was a 5 × 5 cm piece of carbon cloth (1071 HCB,

AvCarb Material Solution, Lowell, MA, USA) pre-treated with cetyltrimethylammonium bromide (CTAB). The reactor was sparged with $N_2$ at a flow rate of 2 L $h^{-1}$. A condenser was connected to the system to minimize water loss (0.09 mL $h^{-1}$ with condenser) due to reactor gassing and to maintain pressure balance. It was operated with cooled water at 12 °C. The reactor system was connected to an 8-channel potentiostat (VSP-3e, BioLogic, Seyssinet-Pariset, France). The bio-electrochemical system cultivation was operated using chronoamperometry, with the anode (working electrode) held at a set potential of 0.5 V using $[Fe(CN)_6]$ or 0.3 V using $[Co(bipy)_3]$ versus the reference electrode (Ag/AgCl, saturated KCl, RE-1CP, ALS, Tokyo, Japan). For isotopic tracer studies, glucose was substituted with 99% $[^{13}C_6]$ glucose (CLM-1396-10, Cambridge Isotope Laboratories, Tewksbury, MA, USA).

### 3.3.5 Cultivation in anaerobic serum flasks

The mediator reduction rate of ferricyanide was screened in 30 mL serum bottles. The bottles were filled with 25 mL DM9 media containing 1.5 g $L^{-1}$ glucose, which were then tightly sealed with aluminum caps, sparged with $N_2$ (2 min) to make them anaerobic, and inoculated to a starting $OD_{600}$ of 1. The bottles were incubated on a rotary shaker at 30 °C and 180 rpm (Infors, Bottmingen, Switzerland). Three biological replicates were carried out for each condition, and cell-free bottles were used as control.

### 3.3.6 Cultivation in oxygen-depleted well plates

The mediator reduction rate of ferricyanide at different concentrations (0.5, 1, 2, 4 mM) and varying $FeCl_3$ concentrations (5.5, 15.5, 25.5 µM) was conducted in 24 well plates. The different conditions were prepared in 50 mL Falcon tubes in DM9 media (1.5 g $L^{-1}$ glucose) with a starting $OD_{600}$ of 1, and then separated in four different plates, with a filling volume per well of 2 mL and each condition in duplicate. An oxygen-depleted

atmosphere was generated using Anaerocult™ C mini (Merck, Millipore, Darmstadt, Germany). The plates were incubated on a rotary shaker at 30 °C and 160 rpm (Infors, Bottmingen, Switzerland). Each plate was harvested at different time points to obtain a time course of mediator reduction.

## 3.4 Analytics

### 3.4.1 Quantification of cells, substrates, and products

Cell concentration was spectrophotometrically measured as optical density ($OD_{600}$). The concentration of ferricyanide ($[Fe(CN)_6]^{3-}$) was determined spectrophotometrically at 420 nm (Lai, et al., 2016). Glucose concentration was quantified using HPLC (1260 Infinity Series, Agilent, Darmstadt, Germany) with a MetaCarb 87C column (Agilent) maintained at 80 °C as the stationary phase, and deionized water as the mobile phase at a flow rate of 1 mL $min^{-1}$. Detection of glucose was performed via refractive index, and external standards were employed for quantification. Organic acids, including gluconate, 2-ketogluconate, pyruvate, acetate, succinate, and lactate, were analyzed by HPLC (1260 Infinity Series, Agilent) using an Aminex HPX-87H column (Bio-Rad, Hercules, CA, USA) at 40 °C as the stationary phase, with isocratic elution using 50 mM $H_2SO_4$ at a flow rate of 0.5 mL $min^{-1}$ as the mobile phase. These analytes were detected by UV absorption at 210 nm and quantified using external standards.

### 3.4.2 Extraction and quantification of fatty acids

Cellular fatty acid analysis was conducted by DSMZ Services (Leibniz Institute DSMZ - Deutsche Sammlung von Mikroorganismen und Zellkulturen GmbH, Braunschweig, Germany). The total fatty acid content in the biomass was quantified as previously described (Dietrich, Jovanovic-Gasovic, Cao, Kohlstedt, & Wittmann, 2023). Briefly, a 5 mg sample of freeze-dried cell material was transferred into a glass vial and mixed with

300 µL of a solvent containing methanol, toluene, and 95% sulfuric acid (50:50:2 v/v/v) for extraction and transesterification. Subsequently, 15 µg of n-3 heneicosapentaenoic acid methyl ester (HPA, 22:5; Cayman Chemical, Ann Arbor, MI, USA) was added as an internal standard. The mixture was incubated at 80 °C for 24 h. After cooling to room temperature, 250 µL of stopping solution (0.5 M $NH_4HCO_3$ and 2 M KCl in $H_2O$) was added, and the mixture was centrifuged (12,000 x *g*, 5 min, RT). The upper organic phase was collected for GC-MS analysis (Dietrich et al., 2023).

### 3.4.3 Extraction and quantification of intracellular CoA thioesters

The analysis of intracellular CoA thioesters was performed as previously described (Gläser et al., 2020). Briefly, 8 mg of cells were harvested and transferred into cooled extraction and quenching buffer (95% acetonitrile, 25 mM formic acid, -20 °C), then incubated on ice for 10 min. The mixture was centrifuged (15,000 x *g*, 10 min, 4 °C), and the supernatant was combined with 10 mL of super-cooled deionized water. The pellet was resuspended in 8 mL of super-cooled deionized water and centrifuged likewise. The collected supernatants were combined and snap-frozen in liquid nitrogen, freeze-dried, and re-dissolved in 500 µL of cooled resuspension buffer (25 mM ammonium formate, pH 3.0, 2% MeOH, 4 °C). Prior to analysis, the sample was filtered (Ultrafree-MC 0.22°µm, Merck, Millipore, Germany). The analysis was conducted using a triple quadrupole mass spectrometer (QTRAP 6500+, AB Sciex, Darmstadt, Germany) coupled with an Agilent Infinity 1290 HPLC system, equipped with a core-shell reversed-phase column (Kinetex XB-C18, 100 × 2.1 mm, 2.6 µm, 100 Å, Phenomenex) maintained at 40 °C. For the analysis, 10 µL of the sample was injected and separated using a gradient of formic acid (50 mM, pH 8.1, with 25% ammonium hydroxide in $H_2O$, A) and methanol (B) at a flow rate of 300 µL $min^{-1}$. The gradient profile was as follows: 0–7 min, 0–10% B; 7–10 min, 10–100% B; 10–11 min, 100% B; 11–12 min, 100–0% B; 12–15 min, 0% B.

### 3.4.4 GC-MS $^{13}C$ labeling analysis of amino acids

Protein-bound amino acids were analyzed using 2 mg of cells by hydrolyzing the sample in 100 µL of 6 M HCl at 100 °C for 24 h. After hydrolysis, the cell debris was removed by filtration using a 0.2 µm Ultrafree-MC filter (Merck-Millipore, Darmstadt, Germany). The resulting hydrolysate was dried under a nitrogen stream, then resuspended in 50 µL of N,N-dimethylformamide containing 1% (v/v) pyridine. It was then derivatized with 50°µL of N-methyl-t-butyldimethylsilyl-trifluoroacetamide (MBDSTFA, Macherey-Nagel, Düren, Germany) by heating at 80 °C for 30 min (Wittmann, Hans, & Heinzle, 2002).

For the analysis of $^{13}C$-labeled free intracellular amino acids, 4 mL of bio-electrochemical system sample was harvested by fast vacuum filtration (cellulose nitrate membrane filter, 0.2 µm, 47 mm, Sartorius), followed by hot water extraction. The filter was rinsed with 15 mL of NaCl solution, adjusted to match the medium's ionic strength, and placed in a plastic container. After incubation at 100 °C for 10 min, the extract was cooled on ice and centrifuged (13,000 x *g*, 5 min, 4 °C) (Bolten, Kiefer, Letisse, Portais, & Wittmann, 2007). From the obtained supernatant 1 mL was vacuum-dried and derivatized similarly to the protein-bound amino acid samples.

The mass isotopomer distributions (MIDs) of derivatized amino acids were analyzed via GC-MS (Agilent 7890A, Quadrupole Mass Selective Detector 5975C, Agilent Technologies), equipped with an HP-5MS column (30 m, 250 µm × 0.25 µm, Agilent Technologies) and helium 5.0 as the carrier gas (flow rate: 1.7 mL $min^{-1}$). The GC-MS temperature program was set as follows: 120 °C for 2 min, followed by an 8 °C $min^{-1}$ increase (2–12 min), a 10 °C $min^{-1}$ increase (12–24.5 min), and a final hold at 325 °C (24.5–27 min). Additional settings included the inlet at 250 °C, the transfer liner at 280°°C, the ion source at 230 °C, and the quadrupole at 150 °C. Selective ion monitoring (SIM) was used to quantify the MIDs of amino acid fragments with suitable quality, including alanine (m/z 260), valine (m/z 288), leucine (m/z 274), threonine (m/z 404), aspartate (m/z 418), serine (m/z 390), and proline (m/z 258) (Wittmann, 2007).

### 3.4.5 GC-MS and LC-MS $^{13}C$ labeling analysis of organic acids

The mass isotopomer distributions (MIDs) of fragment ions from secreted organic acids - acetate (m/z 43), pyruvate (m/z 174), and succinate (m/z 289) - were analyzed by GC-MS using an HP-5MS column (Agilent) as the stationary phase and helium 5.0 as the mobile phase. To eliminate isobaric interference between the analytes of interest and the sample matrix, all samples were initially measured in scan mode before applying SIM (Selective Ion Monitoring) mode. For acetate analysis, 100 µL of the supernatant was mixed with 100 µL of $H_2SO_4$ (10% v/v) and 20 µL of *n*-pentanol, then incubated at 80 °C for 15 min (Adler, Bolten, Dohnt, Hansen, & Wittmann, 2013). After cooling on ice, the ester formed was extracted with 200 µL of *n*-hexane. The following GC-MS temperature program was applied: 75 °C for 2 min, followed by a ramp of 25 °C $min^{-1}$. For pyruvate analysis, 200 µL of supernatant was evaporated under a nitrogen stream. The residue was dissolved in 50 µL of methoxyamine hydrochloride in pyridine (20 mg $mL^{-1}$) and incubated at 80 °C for 30 min. Then, 50 µL of MSTFA (Macherey-Nagel, Düren, Germany) was added, and the mixture was incubated again at 80 °C for 30 min. The GC-MS temperature program used was: 30 °C (0-1 min), followed by a 10 °C $min^{-1}$ increase (1-10 min) and a 40 °C $min^{-1}$ increase (10-15.125 min). For succinate analysis, 50 µL of supernatant was dried under a nitrogen stream. The derivatization and instrument settings were the same as those used for amino acid measurements (Becker, et al., 2013).

The labeling patterns of 2-ketogluconate and gluconate were analyzed as fragment ions via LC-MS/MS using a triple quadrupole mass spectrometer (QTRAP 6500+, AB Sciex, Darmstadt, Germany) coupled to an HPLC system (Agilent Infinity 1290) with an Acquity UPLC BEH Amide column (100 x 2.1 mm, 1.7 µm, 130 Å, Waters) at 40 °C. For analysis, 10 µL of the sample was injected and separated using a gradient of $NH_4OH$ (0.1%,

pH 8.9, A) and acetonitrile (B) at a flow rate of 200 µL $min^{-1}$ as follows: 0–7 min, 100% B; 7–10 min, 100-70% B; 10–14 min, 70-50% B; 15 min, 50-100% B.

All $^{13}C$ enrichments were corrected for the natural abundance of isotopes (van Winden, Wittmann, Heinzle, & Heijnen, 2002) and reported as summed fractional labeling (SFL) (Wittmann & Heinzle, 2005).

### 3.4.6 Calculation of electron and carbon balances

The electron balance (EB) was determined using Equation 3-1 (Lai, et al., 2016):

$$EB\ [\%]=((\sum_{i=n}^{n}\left(C_{i_{t_{end}}}*m_i*\gamma\right)+e_{anode\ t_{end}})/(\sum_{i=n}^{n}\left(C_{i_{t_0}}*m_i*\gamma\right)+e_{anode\ t_0}))*100$$

(Eq. 3-1)

In this equation, $C_i$ represents the quantities of each compound at the initial time point ($t_0$) and the final time point ($t_{end}$), m denotes the number of carbon atoms in each molecule, and γ indicates the degree of reduction for the respective compounds. Additionally, $e_{anode}$ refers to the quantity of electrons collected at the anode at both the initial time point ($t_0$) and the final time point ($t_{end}$).

The carbon recovery (CR) was determined using Equation 3-2 (Lai, et al., 2016):

$$CR\ [\%]=(\sum_{i=n}^{n}\left(C_{i_{t_{end}}}*m_i\right)/\sum_{i=n}^{n}\left(C_{i_{t_0}}*m_i\right))*100$$

(Eq. 3-2)

In this equation, $C_i$ represents the quantity of each compound at the initial time point ($t_0$) and the final time point ($t_{end}$), and m denotes the corresponding number of carbon atoms in each molecule.

### 3.4.7 Analysis of elemental biomass composition

The CHN content of freeze-dried biomass (2 mg, n = 3) was analyzed using elemental analysis with an Elementar Vario MICRO instrument (Elementar Analysensysteme GmbH, Langenselbold, Germany). The CHN Elemental analysis was conducted by Susanne Harling (Inorganic Solid State Chemistry, Saarland University, Saarbrücken, Germany).

### 3.4.8 Quantification of adenylate energy metabolites

A cell sample (5 mg cell dry weight) was harvested from the cultivation using vacuum filtration (Durapore Membrane, PVDF, 0.45 µm, 47 mm, Millipore Merck, Darmstadt, Germany) (Wordofa et al., 2017). The filter was immersed in 4 mL of boiling ethanol/water (75:25 v/v, 70 °C). The mixture was vortexed for 30 sec, followed by centrifugation (17,000 x *g*, 5 min, 4 °C). The resulting cell debris was discarded, and the supernatant was transferred to pre-cooled 50 mL Falcon tubes, diluted with ice-cold water to achieve a final ethanol concentration of 20% (v/v), frozen at -80 °C, and lyophilized. The resulting lyophilizate was resuspended in 0.5 mL of ATP assay buffer (ab113849, Abcam, Cambridge, UK). Protein was removed using a 10 kDa filter (Vivaspin 500, GE Healthcare, Freiburg, Germany). The ATP content in the extract was quantified following the manufacturer's protocol (ab113849 Kit, Abcam) with a GloMax microplate reader (Promega, Madison, WI, US). Prior to analysis, ADP and AMP were enzymatically converted to ATP. For ADP conversion, 100 µL of the extract was incubated with 25 µL of reaction buffer (75 mM potassium phosphate, pH 7.3; 15 mM $MgCl_2$; 0.5 mM phosphoenolpyruvate; and 36 mg $mL^{-1}$ pyruvate kinase (P9136, Sigma-Aldrich)). For AMP conversion, 100 µL of the extract was incubated with 25 µL of reaction buffer, supplemented with 4 mg $mL^{-1}$ myokinase (M5520, Sigma-Aldrich). Each reaction mixture was incubated for 15 min at 37 °C, after which the enzymes were inactivated by

heating at 100 °C for 2 min. Based on the data, the adenylate energy charge (AEC) was calculated using Equation 3-3 (Atkinson, 1968):

$$AEC\ [-] = \frac{[ATP]+0.5*[ADP]}{[ATP]+[ADP]+[AMP]}$$

(Eq. 3-3)

The quantification of adenylate energy metabolites was performed in collaboration with Laura Pause (Systems Biotechnology Group, Helmholtz Centre for Environmental Research (UFZ), Leipzig, Germany).

### 3.4.10 NPN uptake assay

Cells were cultivated in DM9 minimal medium (5 g $L^{-1}$ glucose) until reaching mid-exponential phase. A 1 mL aliquot of cells was harvested by centrifugation (5,500 x *g*, 3 min, RT), then washed with PBS buffer (pH 7.3) and centrifuged again under the same conditions. The cells were then resuspended to a final optical density of 0.4 ($OD_{600}$). A 200 µL portion of this cell suspension was mixed with 4 µL of NPN working solution (0.5 mM, with PBS diluted 5 mM stock solution in acetone) to achieve a final concentration of 10 µM. For fluorescence measurement black 96-well plates were used. The change in intensity was measured directly using an excitation wavelength of 350 nm and emission spectra from 390 to 490 nm on a BioTek Synergy H1 Multimode Reader (BioTek, Santa Clara, CA, United States). Samples were measured in triplicate.

### 3.4.11 Global gene expression analysis

A custom microarray (eArray, SurePrint G3, 8 × 60K, Agilent Technologies) was designed based on the updated genome sequence of *Pseudomonas putida* KT2440 (Belda et al., 2016). The array included three distinct 60-mer probes per gene along with internal controls. For sampling, 2 mL of culture was quickly centrifuged (13,000 rpm, 30 sec,

4 °C), the supernatant discarded, and the cell pellet snap-frozen in liquid nitrogen. Total RNA was extracted and purified using the RNeasy Mini Kit (Qiagen, Hilden, Germany) and TURBO DNA-free Kit (Thermo Fisher Scientific, Waltham, MA, USA), followed by quantification (NanoDrop 1000, Peqlab Biotechnology, Erlangen, Germany). RNA quality was assessed with a Bioanalyzer System (RNA 6000 Nano Kit, 2100 Bioanalyzer, Agilent Technologies), and only samples with an RNA integrity number (RIN) >8 were used for further processing.

For labeling, 50 ng of RNA was chemically labeled according to the manufacturer's instructions (Low Input Quick Amp WT Labeling One-Color Kit, RNA Spike-In One-Color Kit, Agilent Technologies). The labeled RNA was then purified (RNeasy Mini Spin Columns, Agilent Technologies), and cRNA was quantified (NanoDrop 1000, Peqlab, Erlangen, Germany). At least 600 ng of cRNA with a specific activity of 15 pmol Cy3 $\mu g^{-1}$ cRNA was hybridized onto the microarray. Hybridization was performed following the manufacturer's protocol (Gene Expression Hybridization Kit, SureHyb chamber, Agilent Technologies). After hybridization, the microarray was washed (Gene Expression Wash Buffer Kit, Agilent Technologies), loaded into the SureScan microarray scanner cassette (G2600D, Agilent Technologies), and scanned using the SureScan Microarray Scanner G4900DA (Agilent Technologies) with the AgilentG3_GX_1color scanning protocol at 3 µm double resolution.

Data extraction and processing were performed using Agilent Technologies' microarray and feature extraction software (Version 12.1.1.1). Transcriptomic analysis and visualization were carried out with GeneSpring software (Version 14.9, Agilent Technologies) and Perseus Version 1.6.15 (Tyanova et al., 2016). Statistical analysis was done using an unpaired t-test, with p-values adjusted for multiple testing via the Benjamini-Hochberg method (Benjamini & Hochberg, 1995). A q-value threshold of 0.05 was applied. Genes were further filtered based on a $\log_2$fold change of ≤ -2 or ≥ 2 and a

p-value ≤ 0.05. The full dataset is available on GEO under accession number GSE266590.

### 3.4.12 Proteome analysis

For total proteome analysis, a shotgun approach was employed. For sampling, 2 mL of culture were centrifuged (13,000 x *g*, 1 min, 4 °C), and the resulting cell pellets were immediately snap-frozen in liquid nitrogen. Cell disruption was performed using freeze-thaw cycles by dissolving the pellets in 50 µL of 50 mM ammonium bicarbonate buffer, followed by freezing in liquid nitrogen and incubating at 40 °C with shaking at 750 rpm for 60 sec. This cycle was repeated three times. After the final cycle, the samples were placed in an ultrasonic bath for 30 sec. Protein concentration was quantified using the 2D-Quant kit (Cytiva, Marlborough, MA, USA), and 10 µg of protein was used for further processing. An internal standard, 0.04 µg of glyceraldehyde 3-phosphate dehydrogenase (from *Staphylococcus aureus* Mrsa252, 336 aa residues), was added.

Subsequently, 2 µL of 1 M dithiothreitol was added, and the samples were incubated at 30 °C for 1 h at 400 rpm. This was followed by the addition of 15 µL of 400 mM iodoacetamide, with incubation at room temperature and 400 rpm for 1 hour in the dark. Protein digestion was initiated by adding 0.63 µg of sequencing-grade trypsin (Promega, Madison, WI, United States) and incubating overnight at 37 °C with shaking at 400 rpm. The digestion reaction was terminated by adding 1 µL of 100% formic acid. The samples were then desalted using ZipTip-µC18 columns (Merck Millipore, Darmstadt, Germany), lyophilized, and reconstituted in 0.1% formic acid.

For analysis, the samples were subjected to nano-liquid chromatography (Dionex Ultimate 3000RSLC, Thermo Scientific, USA), coupled to an Orbitrap Fusion Tribrid mass spectrometer (MS/MS; Thermo Scientific, USA) according to previously published

LC-MS/MS parameters (Seidel, Kühnert, & Adrian, 2018). Data were processed using Perseus Version 1.6.15, where the initial step involved log2 transformation and contaminant filtering. Proteins with fewer than three valid values per condition were excluded. Following normalization by mean subtraction, statistical comparisons between samples were made using a two-sided unpaired t-test, with permutation-based FDR (S0 = 0.1). Only proteins with p-values and q-values below 0.05 and $log_2$fold changes of < -1 or > 1 were regarded as significant. Significantly altered proteins were categorized based on their gene ontology “biological process” annotations, obtained from the Perseus annotation database. Hierarchical clustering was applied to the fold-change data within each group. The full dataset is available on MassIVE (MSV000094887).

Sample preparation was performed by Laura Pause (Systems Biotechnology group, Helmholtz Centre for Environmental Research (UFZ), Leipzig, Germany), while LC-MS/MS measurement were conducted by Benjamin Scheer (Department of Molecular Environmental Biotechnology, Helmholtz Centre for Environmental Research (UFZ), Leipzig, Germany). Data processing was carried out in collaboration with Dr. Fabian Ries (Institute of Systems Biotechnology, Saarland University, Saarbrücken, Germany).

### 3.4.13 Ribosome analysis

For ribosome profiling, cells equivalent to 10 mg of cell dry weight were harvested in a 50 mL Falcon tube containing 25 g of ice and 50 µL of chloramphenicol (CAP) (100 mg $mL^{-1}$). The sample was then centrifuged (5,000 x *g*, 5 min, 4 °C). The resulting cell pellet was resuspended on ice in 1 mL of buffer (50 mM Tris, pH 8, 100 mM NaCl, 10 mM $MgCl_2$, 100 µg $mL^{-1}$ CAP, 1 mM DTT) and transferred to a 2 mL tube. After a second centrifugation under the same conditions, the supernatant was discarded, and the pellet was resuspended in 250 µL of the same buffer. The cell suspension was

directly pipetted into liquid nitrogen, forming frozen droplets that were collected into 2 mL tubes and stored at -80 °C.

For analysis, three samples were pooled and resuspended in 250 µL of lysis buffer (50 mM Tris, pH 8, 100 mM NaCl, 10 mM $MgCl_2$, 100 µg $mL^{-1}$ CAP, 1 mM DTT, 0.75 mg $mL^{-1}$ lysozyme (L-6876, Sigma-Aldrich, Taufkirchen, Germany), 1% (w/v) TRITON X-100, 10 mM Ribonucleoside Vanadyl Complex (S1402S, NEB, Frankfurt am Main, Germany), 1% (v/v) Protease Inhibitor Cocktail (P8849-1ML, Sigma-Aldrich, Taufkirchen, Germany). Cell lysis was performed using two cycles in a homogenisator (Precellys 24, Bertin Technology, France) with 6,500 rpm and 30 sec each, and 1 min intervals on ice between cycles. The lysate was then centrifuged (13,000 rpm, 10 min, 4 °C) to remove cell debris. A 500 µL aliquot of the clarified extract was layered onto a sucrose gradient (10-50%) (Table 3-9) and subjected to ultracentrifugation (Optima LE-80K, Beckman Coulter, USA) (34,500 x *g*, 2 h, 4 °C). The absorbance of the samples was continuously monitored at 260 nm with a pump rate of 1 mL $min^{-1}$ to assess ribosome profiles. Ribosome analysis was carried out in collaboration with Dr. Fabian Ries (Institute of Systems Biotechnology, Saarland University, Saarbrücken, Germany).

**Table 3-9:** Sucrose gradient (10-50%) preparation.

| Component | **10%** [mL] | **23.3%** [mL] | **36.7%** [mL] | **50%** [mL] |
|---|---|---|---|---|
| **Sucrose (60% in *TNM)** | 4.17 | 9.70 | 15.30 | 20.80 |
| ***TNM** | 20.78 | 15.25 | 9.65 | 4.15 |
| **DTT (1 M)** | 0.025 | 0.025 | 0.025 | 0.025 |
| **CAP (100 µg $mL^{-1}$)** | 0.025 | 0.025 | 0.025 | 0.025 |

*TNM (50 mM Tris pH 8, 100 mM NaCl, 10 mM $MgCl_2$)

### 3.4.14 Statistical analysis

Results are expressed as mean values ± standard deviations. Statistical analysis was performed using either Student's t-test or one-way analysis of variance (ANOVA). Differences were considered statistically significant when the p-value was less than 0.05

(*), and highly significant when below 0.01 (**). The analyses were conducted using OriginLab (OriginPro 2023b), and Perseus (Version 1.6.15).

# 4 Results and Discussion

## 4.1 Systems biology of electrogenic *P. putida* KT2440

The obligate aerobe *P. putida* KT2440 can engage in non-growth anaerobic production within a bio-electrochemical system when supplemented with redox mediators. However, the underlying mechanisms of this phenotype remain poorly understood. To gain insight into the anoxic electrogenic behavior of *P. putida* KT2440, a systems-level study was conducted during the bio-electrochemical oxidation of glucose. This investigation included transcriptomic, proteomic, and metabolomic analyses to reveal previously unexplored metabolic reactions and pathway activities under these conditions.

### 4.1.1 Anaerobic bio-electrochemically driven metabolism

*P. putida* KT2440 produces various mono- and dicarboxylic acids when cultured on glucose in a bio-electrochemical system equipped with an anode to capture electrons produced during glucose oxidation in the absence of oxygen (Lai, et al., 2016; Weimer, et al., 2024) (Fig. 4-1). Since *P. putida* cannot directly interact with the anode, the minimal medium was supplemented with 1 mM of the external electron mediator ferricyanide to facilitate electron transfer. Glucose conversion in the bio-electrochemical system took approximately 380 hours (Fig. 4-1B), leading to the production of gluconate, 2-ketogluconate (2KG) via the periplasmic glucose oxidation pathway (del Castillo et al., 2007). Additionally, pyruvate, lactate, acetate, and succinate were produced in varying amounts, derived from Embden-Meyerhof-Parnas pathway and the TCA cycle, indicating a more complex metabolic activity beyond pure periplasmic glucose oxidation (Fig. 4-1C, Fig. 4-1D). Shortly after inoculation into the bio-electrochemical system, the cells rapidly adapted to the electrochemical environment, initiating electron current generation. The process proceeded through four distinct phases, each characterized by different metabolic activities (Fig. 4-1B, Fig. 4-1C, Fig. 4-1D, Fig. 4-1F). During phase I (0-24 hours), all observed products were released into the medium, and cell

concentration decreased. During phase II (24-75 hours), succinate production ceased, lactate was re-consumed, and the formation of gluconate, 2KG, acetate, and pyruvate continued. Current generation increased while cell concentration further decreased. In phase III (75-140 hours), cells displayed the highest electrochemical activity. Cell concentration stabilized, and significant amounts of gluconate, 2KG, and acetate were produced. Peak current density reached 0.047 mA/cm² (± 0.007). During phase IV (140-380 hours), the current generation decreased. Gluconate, succinate, and pyruvate were re-consumed, while 2KG and acetate production continued. The accumulation and subsequent re-consumption of organic acids in *P. putida* have been reported under various conditions and appear to be a natural response to specific culture environments. For instance, citrate accumulation was observed during polyhydroxyalkanoate (PHA) production from glycerol (Poblete-Castro, Binger, Oehlert, & Rohde, 2014), while succinate and malate accumulation occurred during continuous PHA production (Beckers, Poblete-Castro, Tomasch, & Wittmann, 2016). Moreover, pyruvate and acetate accumulation has been associated with the stringent response to (p)ppGpp accumulation in *P. putida* (Vogeleer & Létisse, 2022), for *P. putida* mutants which lack the global regulator Crc (Molina, La Rosa, Nogales, & Rojo, 2019) and are driven into metabolic overflow by the saturation of catabolic enzymes and the deregulation of substrate uptake (Bujdoš, et al., 2023). To gain a clearer understanding of the observed dynamics in organic acid production and re-consumption, it would be beneficial to analyze the organic acid profiles during the initial adaptation of *P. putida* in the bio-electrochemical system with shorter sampling intervals and greater detail. This approach could provide valuable insights into the underlying mechanisms, further illuminating the microbe's adaptive strategies under electrogenic conditions.

Throughout the process, both oxidized and reduced forms of the mediator were present (**Fig. 4-1B**). Initially, the mediator was fully oxidized ($OD_{420}$ = 1.13 ± 0.04, equivalent to 1.14 mM oxidized mediator). At peak current, approximately 50% of the mediator

remained oxidized (0.55 ± 0.07 mM), suggesting limitations of diffusion in the bulk liquid and oxidation at the anode surface as electron generation increased.

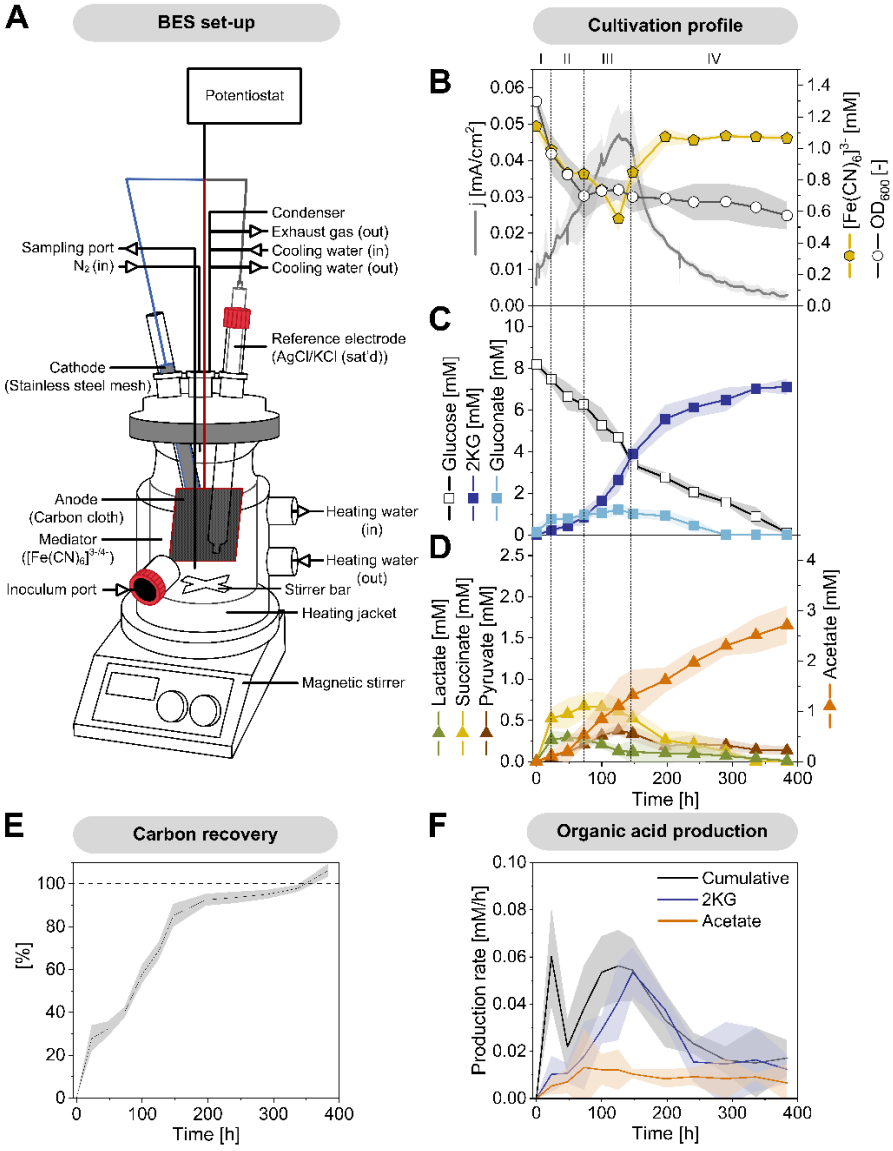


**Fig. 4-1**: **Bio-electrochemical fermentation of *P. putida* KT2440 on glucose.** The data comprise the time profiles of current density (mA/cm$^2$), cell concentration ($OD_{600}$), and $[Fe(CN)_6]^{3-}$ (mM) (B), glucose (mM) , gluconate (mM), and 2-ketogluconate (mM) (C), and other organic acids (mM) (D). The data was corrected for evaporation effects (Supplementary, Table 6-2, Fig. 6-1) and used to estimate the carbon balance (E), as well as the yields and specific production rates of 2-ketogluconate, acetate, and cumulative acid production over time, respectively (F), n=4.

Notably, the time course of current generation closely aligned with the specific rate of 2KG formation (Fig. 4-1B, Fig. 4-1F), suggesting that 2KG production served as the main pathway for anodic electron transfer.

A stoichiometric analysis of the process revealed several peculiarities: Based on the degree of reduction of glucose and the products, the overall electron balance (104.9 ± 2.7%) was not fully closed, indicating that more electrons were captured by the anode than could be accounted for by glucose conversion alone. The primary product, 2KG, was produced at a concentration of 7.9 mM, yielding 88.4% (0.88 mol $mol^{-1}$ glucose). Acetate, the second most abundant product, reached a concentration of 3.0 mM with a yield of 0.34 mol $mol^{-1}$ glucose. However, the stoichiometry suggested that available glucose was insufficient to account for the synthesis of both 2KG and acetate. While 2KG production consumed 88.4% of the glucose, an additional 16.9% would be required for acetate formation (accounting for one $CO_2$ molecule per acetate), implying that not all acetate was derived from glucose. This was further supported by carbon recovery calculations, where the recovered carbon in the products exceeded that from the substrate glucose (106.3 ± 2.6%) (Fig. 4-1E). Similar to the electron balance, the carbon balance did not close, likely due to contributions from biomass breakdown. This hypothesis is supported by the observed decrease in cell concentration (Fig. 4-1B) and recent findings indicating that bio-electrochemical cultivated *P. putida* degrades biomass as a carbon source (Pause, et al., 2023).

### 4.1.2 Energy state under electrogenic conditions

The production of gluconate and 2KG generated electrons that were transferred to the anode in the reactor through the external mediator ferricyanide (Fig. 4-1). This electron transfer was essential for ATP generation in electrogenic *P. putida* (Lai, et al., 2016). Notably, the non-growing cells remained metabolically active throughout the entire process (16 days), maintaining their adenylate energy charge (AEC) at a level of

0.52 ± 0.01 (Fig. 4-2), which is significantly higher than the AEC observed for oxygen-starved *P. putida*, at 0.32 ± 0.01 (Demling et al., 2021), and 0.28 ± 0.04 (Nikel & de Lorenzo, 2013). This suggests that electrogenic metabolism facilitated a more favorable energy balance compared to oxygen-limited conditions. However, the ATP content decreased over time. After 100 hours of bio-electrochemical fermentation the ATP content was significantly lower with 1.2 ± 0.01 µmol $g_{CDW}^{-1}$ than that of the cells analyzed at the beginning of the process with 6.9 ± 0.1 µmol $g_{CDW}^{-1}$ (Fig 4-2), implying that the cells were subjected to stress.

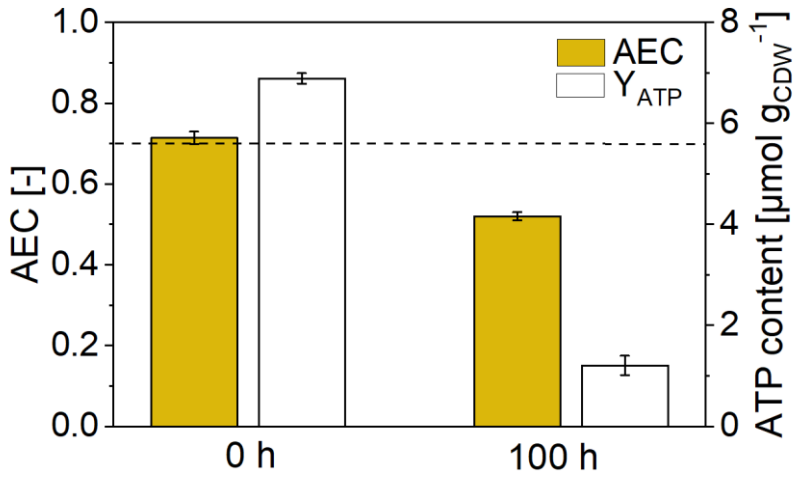


**Fig. 4-2: Changes in energy metabolism during bio-electrochemical fermentation of *P. putida* KT2440 on glucose.** The data show the ATP content (µmol $g_{CDW}^{-1}$) and the adenylate energy charge (ACE) after 0 h and 100 h. n=3

A previous study showed that *P. putida*, when exposed to stress-inducing toxic aromatics, experiences a notable decrease in ATP content while still maintaining its adenylate energy charge over extended periods (Kohlstedt, et al., 2018). This ability to sustain metabolic activity and energy charge despite stress highlights the finely tuned resource allocation in *P. putida* KT2440, enabling prolonged metabolic function and productivity.

### 4.1.3 Isotopic $^{13}C$ tracer studies for metabolite tracing

Under anaerobic bio-electrochemical conditions, *P. putida* produced six distinct organic acids (Fig 4-1C, Fig 4-1D). To trace their metabolic origins,$^{13}C$ isotope profiling was employed (Berger et al., 2014). Bio-electrochemical cultivations were performed using 99% [$^{13}C_6$] glucose, inoculated with cells from a non-labeled pre-culture. Newly synthesized organic acids were expected to show $^{13}C$ labeling, whereas organic acids derived from biomass would remain unlabeled, indicating incorporation of carbon from pre-existing cell material. After 100 hours, samples were collected for GC-MS and LC-MS $^{13}C$ labeling analysis of 2KG, gluconate, acetate, pyruvate, and succinate. Although lactate was not present at the sampling point, its precursor, pyruvate, provided the necessary labeling information. Summed fraction labeling (SFL) data revealed the relative abundance of $^{13}C$ atoms in the organic acids, indicating the degree to which they were derived from glucose ($^{13}C$) or biomass ($^{12}C$) (Fig. 4-3A). Gluconate and 2KG were fully $^{13}C$ enriched, confirming their de novo synthesis from glucose. In contrast, acetate, pyruvate, and succinate showed incorporation of both $^{13}C$ from glucose and $^{12}C$ from biomass-derived carbon, aligning with the decrease in cell concentration observed early in the process (Fig. 4-1B, Fig. 4-1D). Pyruvate showed SFL of 75.4%, indicating that most of its carbon originated from glucose metabolized through the ED and lower EMP pathways, while the remaining 24.6% was derived from biomass breakdown. In contrast, acetate (SFL = 39.4%) and succinate (SFL = 30.7%) exhibited significantly lower $^{13}C$ enrichment, suggesting that these metabolites were predominantly sourced from the degradation of biomass components (Fig. 4-3A). This discovery influenced the carbon and energy balances, which had previously been overestimated based solely on stoichiometric analysis. Assuming the SFL of acetate remained constant until the end of the process, with only 39.4% of acetate derived from glucose, the recalculated electron balance was 98.2 ± 2.4%. Likewise, the carbon balance was adjusted to 96.9% ± 2.6%. While this estimate is based on the $^{13}C$ labelling pattern of acetate after 100 hours (and

not at the end of the process, where no sample was taken) and should be therefore interpreted cautiously, both balances closed more accurately. Incorporating $^{13}$C-tracer information therefore proves useful, as it allows to validate the origin of products.

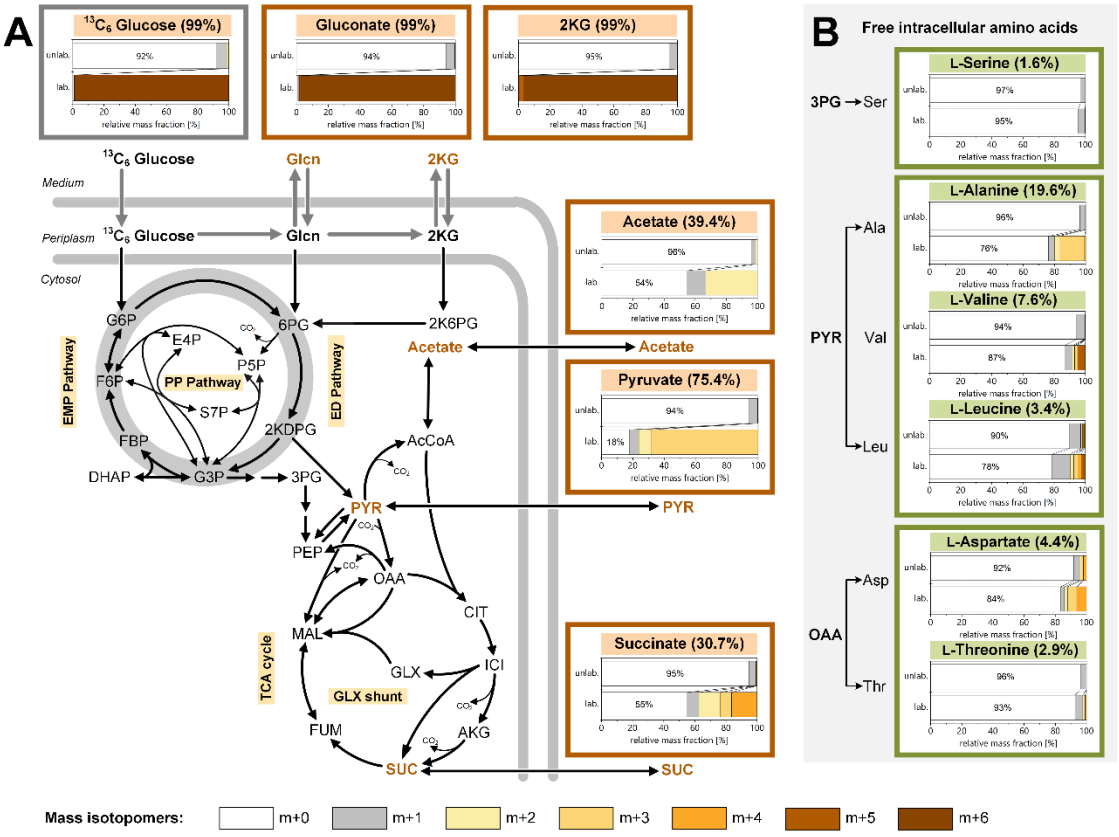


**Fig. 4-3: Isotopic profiling of anoxic-electronic *P. putida* KT2440 grown on [$^{13}C_6$] glucose.** The data display the $^{13}$C enrichment of extracellular accumulated organic acids (A) and intracellular amino acids (B), sampled after 100 h from the bio-electrochemical process using [$^{13}C_6$] glucose as the substrate. For comparison, the bio-electrochemical process was conducted using naturally labeled glucose, i.e. non-$^{13}$C-labeled glucose, as the substrate. The bar graphs represent the measured mass isotopomer distributions of the analytes (m+0 to m+x) using [$^{13}C_6$] glucose (lower bars, lab.) and non-$^{13}$C-labeled glucose (upper bars, unlab.) The numbers, given above the bar charts, display the summed fraction labeling from the tracer study on [$^{13}C_6$] glucose, calculated after correction of the measured labeling data for natural isotope abundance. As shown, gluconate and 2-ketogluconate exclusively originate from glucose, while the other organic acids partially stem from the [$^{13}C_6$]-labeled glucose and (non-labeled) biomass constituents. Amino acids are largely derived from biomass.

Further analysis of the $^{13}C$ labeling pattern in free intracellular amino acids after 100 hours of bio-electrochemical fermentation revealed that amino acids belonging to the pyruvate and oxaloacetate families were significantly enriched in $^{13}C$ (Fig. 4-3B), indicating ongoing de novo synthesis from glucose. Among these, alanine exhibited the highest SFL at 19.6%, whereas serine showed a low $^{13}C$ enrichment with an SFL of 1.6% (Fig. 4-3B). Additionally, $^{13}C$ labeling was detected in amino acids incorporated into proteins obtained through cell protein hydrolysis, with SFL ranging from 0.5% to 2.0%. These values were approximately ten times lower than those found in the free intracellular pools but remained significantly above the natural labeling threshold of 0.02 ± 0.02%. Given that free-form amino acids likely represented only about 1% of the total cellular pool, the observed $^{13}C$ incorporation into protein biomass clearly indicated new protein synthesis (Supplementary, Fig. 6-2). However, the relatively low degree of labeling suggests that protein (re)synthesis was limited, potentially confined to a specific subset of proteins. Notably, the carbon-to-nitrogen (C:N) ratio of cells increased from 3.44 ± 0.01 at the process start to 3.87 ± 0.03 after 100 hours, suggesting loss of nitrogen in cellular chemical composition (Fig. 4-4A).

### 4.1.4 Changes in CoA thioester pools, and fatty acid content

Acetate was a significant by-product (Fig. 4-1D), with a considerable portion not originating from pyruvate. Many microbes typically convert pyruvate to acetate through acetyl-CoA under anaerobic conditions (Wolfe, 2005). In electrochemically cultivated *P. putida* approximately half of the acetate was derived from biomass, bypassing pyruvate entirely, as indicated by its significantly lower SFL of acetate compared to pyruvate (Fig. 4-3A). To gain deeper insights into this process, the abundance of intracellular CoA thioesters was analyzed using LC-MS/MS (Gläser, et al., 2020) (Fig. 4-4B, Fig. 4-4C).

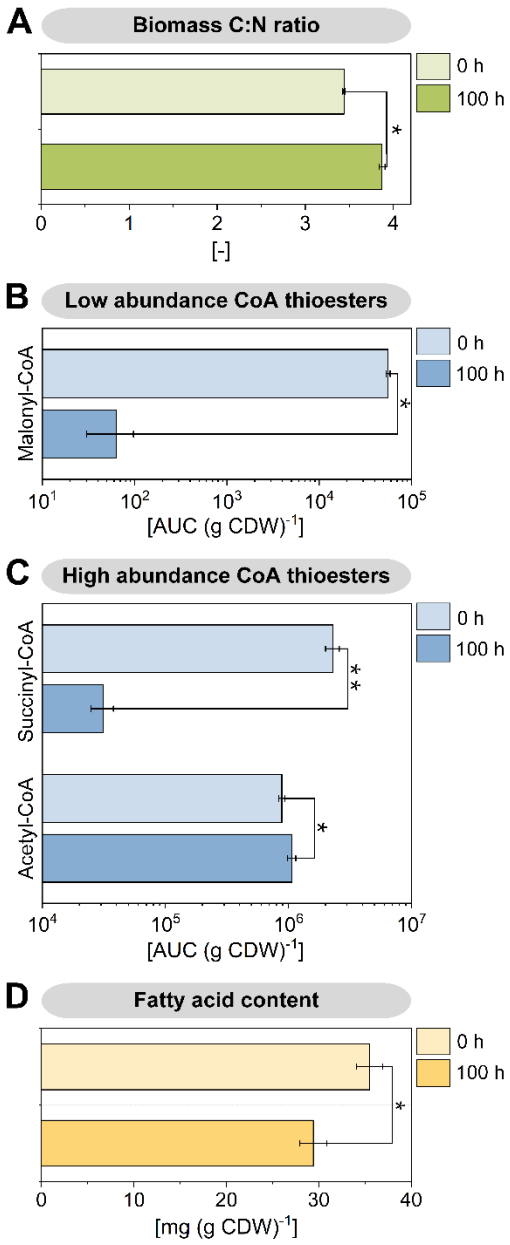


**Figure 4-4: Metabolomic changes during bio-electrochemical fermentation of *P. putida* KT2440 on glucose.** The data show the C:N ratio of the biomass (A), the abundance of intracellular CoA thioesters (B, C), and the fatty acid content of the biomass after 0 h and 100 h. The significance of differences between the time points is indicated as follows: * ($p < 0.05$) and ** ($p < 0.01$). $n = 3$.

Succinyl-CoA levels were notably reduced in cells cultured under bio-electrochemical conditions compared to those grown aerobically, likely as a result of the disrupted TCA cycle in the absence of oxygen. Furthermore, malonyl-CoA levels in cells from the

bio-electrochemical reactor were 1000-fold lower, suggesting reduced fatty acid synthesis, which typically initiates with malonyl-CoA (Jovanovic Gasovic et al., 2023). Interestingly, *P. putida* cultured under bio-electrochemical conditions exhibited a 20% increase in acetyl-CoA levels (Fig. 4-4C). Labelling experiments suggested the involvement of acetyl-CoA in exchange reactions between the EMP pathway and the TCA cycle (Fig. 4-3A) (Wittmann, 2002; Wittmann, Kiefer, & Zelder, 2004). These reactions have been previously documented in *P. putida* KT2440 and *P. aeruginosa* PAO-1 during aerobic growth on glucose (Kohlstedt & Wittmann, 2019; Nikel, et al., 2015). The elevated acetyl-CoA level likely resulted from fatty acid degradation via β-oxidation, as indicated by a substantial decrease in the overall fatty acid content of the cells during the bio-electrochemical process (Fig. 4-4D). Lipid degradation for energy and redox balance during stationary phase has been observed in various microbes (Beganovic et al., 2023; Jovanovic Gasovic, et al., 2023; Stegmüller et al., 2024). Given an average fatty acid carbon chain length of 16 (Supplementary, Table 6-3), the breakdown of a single fatty acid molecule yields 7 FADH, 7 NADH, and 8 acetyl-CoA. This suggests that intracellular lipids served as a carbon source, and the elevated acetyl-CoA levels may have contributed to acetate synthesis (Fig. 4-1D). Moreover, fatty acid degradation probably acted as a supplementary source of energy and reducing power for electrogenic *P. putida*.

### 4.1.5 Adaption to electrogenic conditions at the transcriptional level

To gain a deeper understanding of the observed electrogenic phenotype of *P. putida*, samples were collected at 0, 24, and 100 hours to investigate adaptation at the transcriptional level using microarray analysis and at the translational level through shotgun proteomics with LC-MS/MS.

High-quality mRNA was collected, demonstrating significant reproducibility among biological replicates (Fig. 4-5). *P. putida* exhibited significant changes in gene expression

throughout the process (Supplementary, Fig. 6-3A). After 24 hours, compared to process start (0 hours), 2,011 genes (36.1% of 5,564 coding sequences) were significantly upregulated ($p_{adj} < 0.05$, log2-fold change > 2), while 176 genes (3.2%) were significantly downregulated ($p_{adj} < 0.05$, log2-fold change < -2) (Fig. 4-6A, Supplementary, Fig. 6-3A). This suggests a broad adaptive response to the anaerobic conditions.

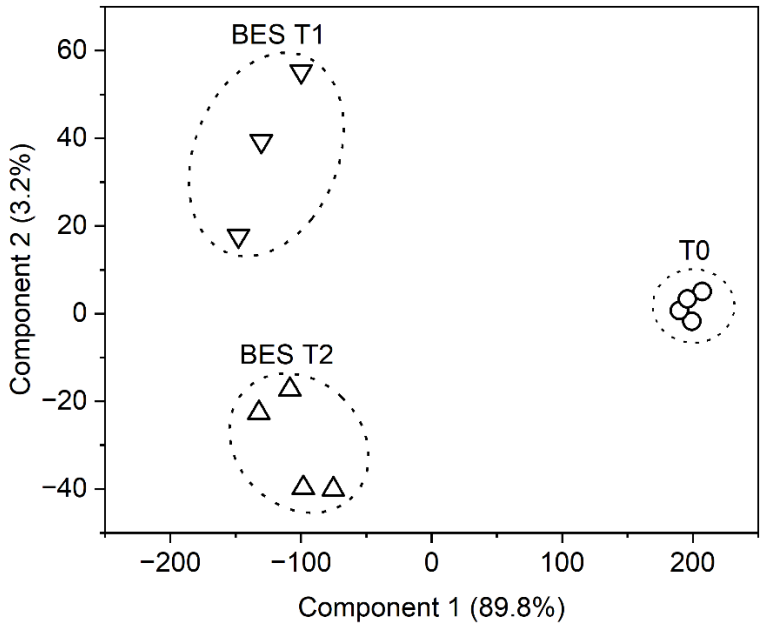


**Figure 4-5: Principal component analysis of transcriptome samples.** T0 (preculture 0 h, circle), T1 (Bio-electrochemical system 24 h; down-pointing triangle), T2 (Bio-electrochemical system 100 h; up-pointing triangle).

The upregulated genes were primarily associated with membrane-related processes, including transport, secretion, and cell wall organization. In contrast, the downregulated genes were mostly linked to cell mobility. Gene Ontology (GO) enrichment analysis revealed several biological processes that were significantly overrepresented at the 24-hour sample point. These included siderophore transport (96%), DNA integration (65%), ion transport (61%), secretion (55%), transmembrane transport (53%),

transposition (52%), amino acid transport (52%), establishment of localization (51%), and cell wall organization (49%) (Fig. 4-6B). In contrast, categories such as cell mobility (24%) and amine transport (13%) showed lower enrichment. Notably, the ATP-intensive flagellar motor was significantly downregulated (Supplementary, Table 6-4), likely in response to the lower ATP content observed (Fig. 4-2). Significant changes were also observed in central carbon metabolism (Fig. 4-6C, Supplementary, Table 6-5). Genes encoding the gluconate-2-dehydrogenase complex (*PP_3382, PP_3383, PP_3384*) were upregulated, aligning with 2KG being the primary product, while the nonspecific subunit *PP_3623* was not upregulated. Furthermore, genes associated with the pyruvate node (*pycAB*, *aceF*, *acoABC*) and the glyoxylate shunt were significantly upregulated. Increased levels of acetyl-CoA have been reported to enhance the kinase activity of isocitrate dehydrogenase kinase/phosphatase (AceK), resulting in phosphorylation and partial inactivation of isocitrate dehydrogenase (Icd) (Crousilles, Dolan, Brear, Chirgadze, & Welch, 2018). In accordance with this, *icd* was downregulated, likely redirecting metabolic flux toward the glyoxylate shunt. Additionally, acetate symporters (*actP-I*, *actP-II*, *actP-III*) were upregulated. There was also a shift in expression from the cytosolic NADH-forming malate dehydrogenase (*mdh*) to the membrane-bound quinol-forming malate dehydrogenases (*mqo-1*, *mqo-2*), which may be linked to adaptations in electron transport. In electrogenic *P. putida*, cytochrome c reductase has been identified as the key enzyme for electron transfer to the mediator $[Fe(CN)_6]^{3-}$ (Lai, et al., 2020), with quinol acting as a direct substrate for the cytochrome c reductase complex. In contrast, genes involved in glucose oxidation and phosphorylation (*gtsABCD*), triose recycling (*tpiA*, *fda*, *fbp*, *pgi*), and the pentose phosphate (PP) pathway (*zwf*, *pgl*) remained largely unchanged or showed slight downregulation. Overall, the expression pattern remained stable during the later phases, with over 80% of the upregulated genes consistently expressed at both the 24 and 100-hour time points.

Temporal differences were more pronounced among the downregulated genes (Supplementary, Fig. 6-3A).

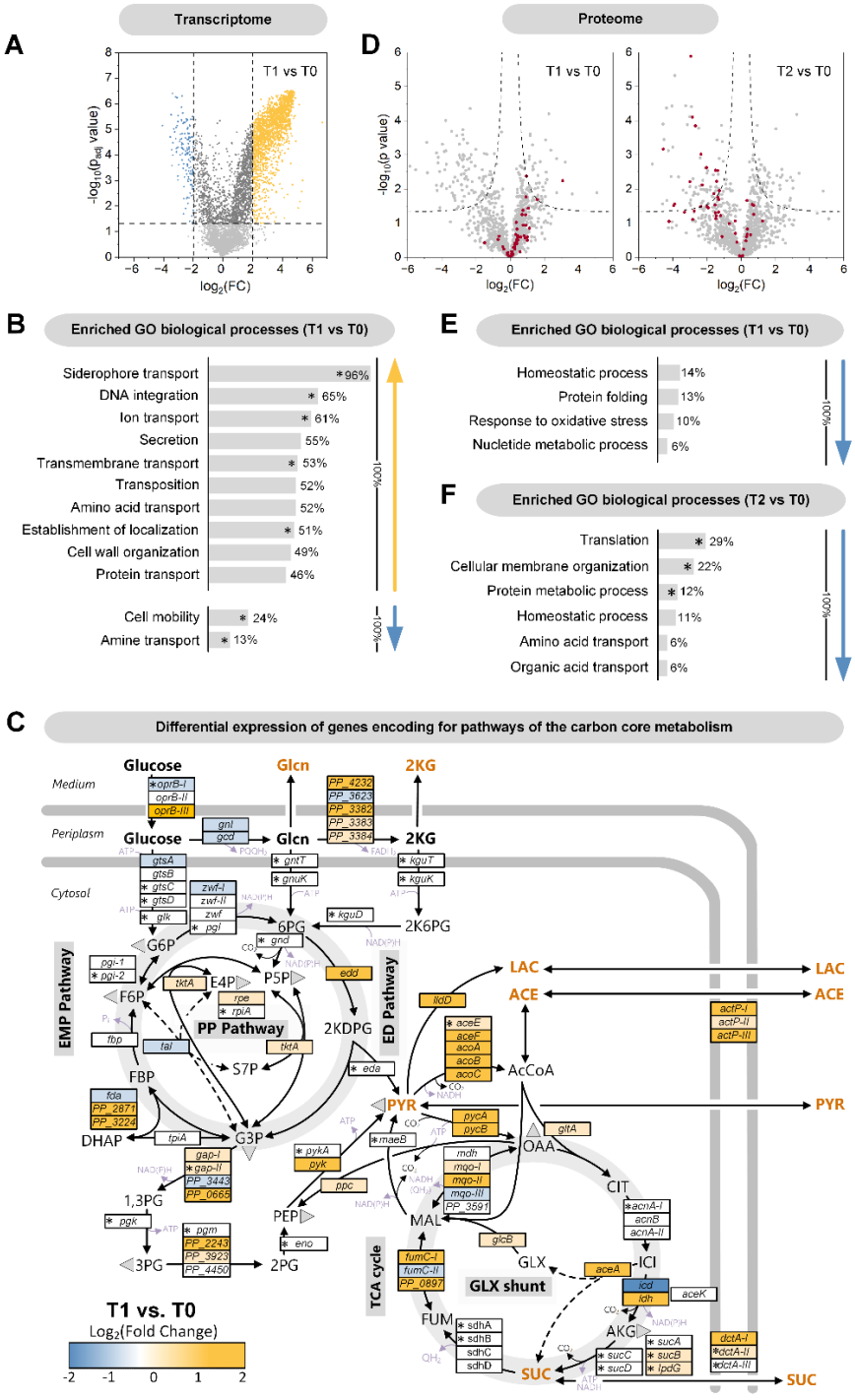


Figure continued next page

**Figure 4-6: Transcriptomic and proteomic changes during bio-electrochemical fermentation of *P. putida* KT2440 on glucose.** Volcano plot of global transcriptomic

differences between 0 h (T0) and 24 h (T1) (A). Assignment of transcriptional changes between 0 h and 24 h to GO biological processes (Gene Ontology), n = 4. (B). The given percentage depicts the coverage of a category by significantly changed transcripts. Significantly enriched GO biological processes are marked * (Fisher's exact test). Expression dynamics of genes related to the central carbon core metabolism between 0 h and 24 h (C). For completeness, non-significantly changed genes are included (marked *, Benjamini–Hochberg FDR > 0.05), n = 4. Volcano plots of global proteomic changes between 0 h (T0), 24 h (T1), and 100 h (T2) (D), n = 3. Ribosomal proteins are labelled red. Assignment of proteomic changes between 0 h and 24 h (E), as well as 0 h and 100 h (F) to GO biological processes. The given percentage depicts the coverage of a category by significantly changed proteins. Significantly enriched GO biological processes are marked * (Fisher's exact test).

The reduction of the fatty acid content in the biomass, sampled after 100 hours of bio-electrochemical cultivation (Fig. 4-4D), suggests that fatty acid degradation served as an additional source of energy and reducing power for electrogenic *P. putida* KT2440. The importance of fatty acid catabolic reactions is underscored by their transcriptional activation. For instance, genes involved in β-oxidation (*fadA*, *paaF*, *paaH*, *pcaF-I*) were upregulated. Simultaneously, genes encoding enzymes for de novo fatty acid synthesis were downregulated at both the transcript level (*mmgF*, *prpC*, *accA*, *accB*, *atoB*, *fabA*) and the protein level (FabD, AcpP) (Supplementary, Table 6-6). The absence of odd-chain fatty acids explained the downregulation of genes associated with the methyl-citrate cycle (Supplementary, Table 6-6) (Dolan et al., 2020; Dolan et al., 2022). Furthermore, fatty acid metabolism was likely adapted for structural reasons: Notably, *fabA* and *fabD* are involved in the synthesis of unsaturated fatty acids, and the saturation degree of the cellular fatty acid pool, sampled after 100 hours of bio-electrochemical cultivation was increased compared to cellular fatty acid pool of the samples from 0 hours (Supplementary, Table 6-3). This could serve as a mechanism to adjust membrane fluidity (Heipieper & de Bont, 1994; Loffhagen, Härtig, & Babel, 1995). Additionally, the share of *trans*-unsaturated fatty acids significantly increased after 100 hours

(Supplementary, Table 6-3). Given the shutdown of fatty acid biosynthesis (Supplementary, Table 6-6), these *trans*-unsaturated fatty acids were likely not synthesized de novo. Based on the observed fatty acid spectrum, these likely originated from the *cis*-*trans* isomerization of existing unsaturated fatty acids. This conclusion is supported by the strong upregulation of the non-reversible *cis*-*trans* isomerase (*cti*) (Supplementary, Table 6-6). Consequently, the overall *cis*-*trans* fatty acid ratio shifted dramatically from 25.1 at the process start to 0.6 after 100 hours, indicating that most of the *cis*-oriented fatty acids were converted (Supplementary, Table 6-3). This type of adaptation has been shown to occur in *P. putida* strains (P8, NCTC 10936, and KT2440) when subjected to abrupt disturbances without the ability to synthesize new fatty acids (Härtig, Loffhagen, & Harms, 2005). The isomerization process, which occurred without altering the double bond position and without requiring a cofactor or energy, provided an efficient mechanism for adjusting the membrane composition (Heipieper, Meinhardt, & Segura, 2003; Pedrotta & Witholt, 1999; von Wallbrunn, Richnow, Neumann, Meinhardt, & Heipieper, 2003). The resulting membrane composition has higher rigidity and tighter packing with reduced fluidity (Okuyama, Sasaki, Higashi, & Murata, 1990), which can enhance cellular resilience. It is important to note that the modified membrane composition likely contributed to the sustained long-term efficiency of the involved electron transport chain complexes, as well as the transporters responsible for substrates, products, and mediator.

### 4.1.5 Adaption to electrogenic conditions at the translational level

Changes at the protein level were restricted to relatively few enzymes and regulators compared to the transcriptome (Fig. 4-6D, Supplementary, Fig. 6-3B). After 24 hours, 95 proteins showed a decrease in abundance, while 40 proteins exhibited a significant increase. This suggests that the bacterium selectively modified its protein composition in response to anoxic-electrogenic conditions.

Proteins that exhibited significant changes over time (24 h, 100 h, 380 h) were predominantly associated to carbon and nitrogen metabolism, transport processes, and translation (Fig. 4-7). For instance, enzymes involved in the electron transport chain (PP_2867, NuoC, SdhA, NuoE, CyoB, Ndh) increased in abundance, likely reflecting their role in electron transfer to the external mediator. Additionally, the glyoxylate shunt enzyme AceA, gluconate 2-dehydrogenase (PP_3383), and the acetate symporter ActP-I showed increased abundance, aligning with the transcriptome data. In contrast, several energy-dependent ABC transporters were less abundant. A significant number of the affected proteins had unknown functions (Fig. 4-7). Notably, the proteome analyzed at 100 and 380 hours closely resembled that of the 24-hour time point, with one notable exception: proteins associated with translation were significantly impacted during the later stages (Fig. 4-7). Up to the 24-hour time point, ribosomal proteins remained stable in abundance, suggesting active translation during this phase (Fig. 4-6D, Fig. 4-6E). However, after 100 hours, many proteins associated with translation showed decreased abundance, making translation a significantly enriched GO biological process with reduced protein levels (Fig. 4-6D, Fig. 4-6F). The translation initiation factor IF-1 (InfA, PP_4007) showed a decrease, while the energy-dependent translational throttle protein EttA (PP_0674), which acts as an ADP/ATP ratio sensor and translation inhibitor, showed an increase. The latter restricts translation in response to reduced energy levels (Fig. 4-2) (Boël et al., 2014). Additionally, the abundance of 27 structural ribosomal proteins declined, with reductions of up to 24-fold, as seen for RpsU (PP_0389), a component of the small 30S ribosomal subunit (Fig. 4-7). Under optimal growth conditions, up to 80% of the ATP required for anabolic processes is utilized for protein and rRNA synthesis (Stouthamer & Bettenhaussen, 1973; Tempest & Neijssel, 1984). Consequently, the reduction in overall translation output was vital for sustaining the performance of *P. putida* in the bio-electrochemical system over an extended period, given the observed lower ATP content (Fig. 4-2).

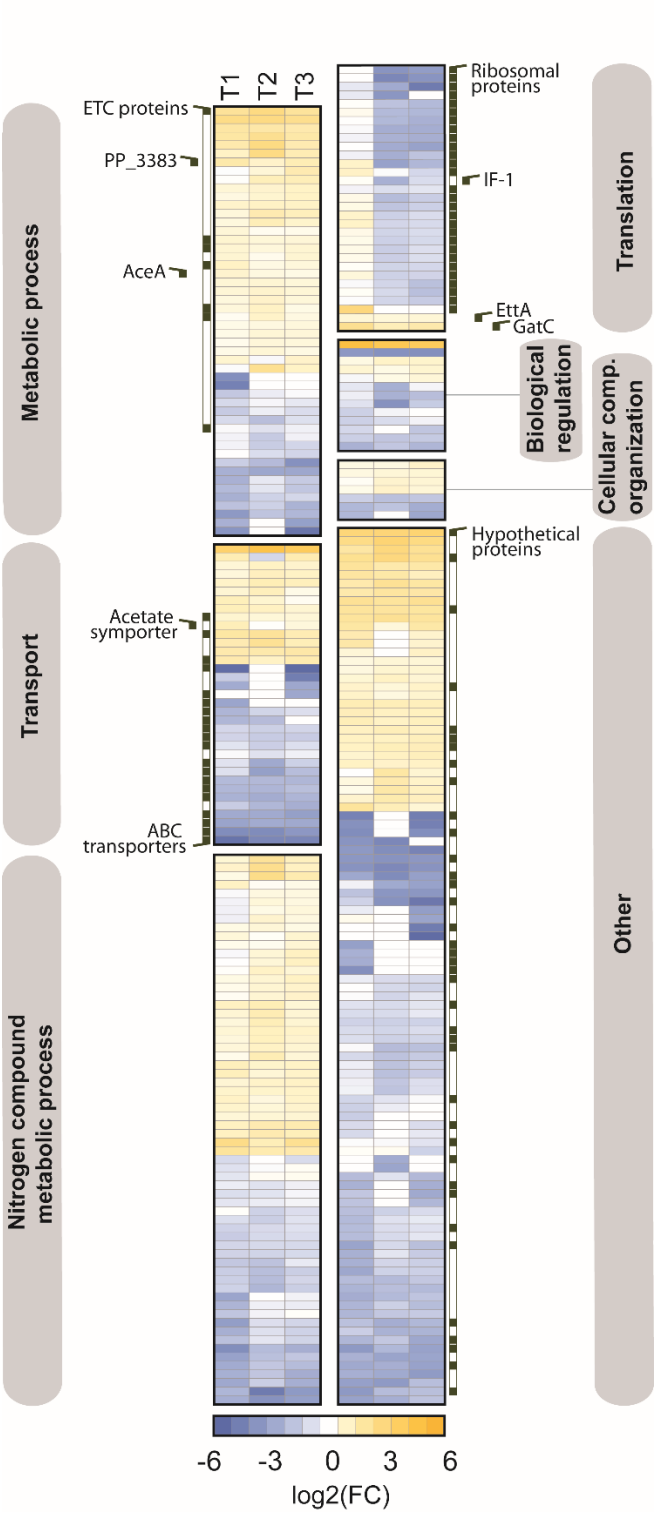


**Figure 4-7: Hierarchical clustering of proteomic changes during bio-electrochemical fermentation of *P. putida* KT2440 on glucose.** The heatmap depicts significant changes in the proteome between 0 h and 24 h (T1), 100 h (T2), as well as 380 h (T3), n=3. Significantly changed proteins (-1 > log2-fold > 1, p value < 0.05) are grouped with one way ANOVA against the start sample, whereby the grouping is based on the corresponding Gene Ontology “biological process” annotations.

To assess how these changes affected the functionality of the translation machinery, sucrose gradient sedimentation analysis was performed (Fig. 4-8). Early in the process, the cells contained a significant fraction of polysomes, indicating active translation. Both polysomes and monosomes, essential for translation, were observed. By 100 hours, both forms had nearly vanished, indicating a substantial reduction in translation activity.

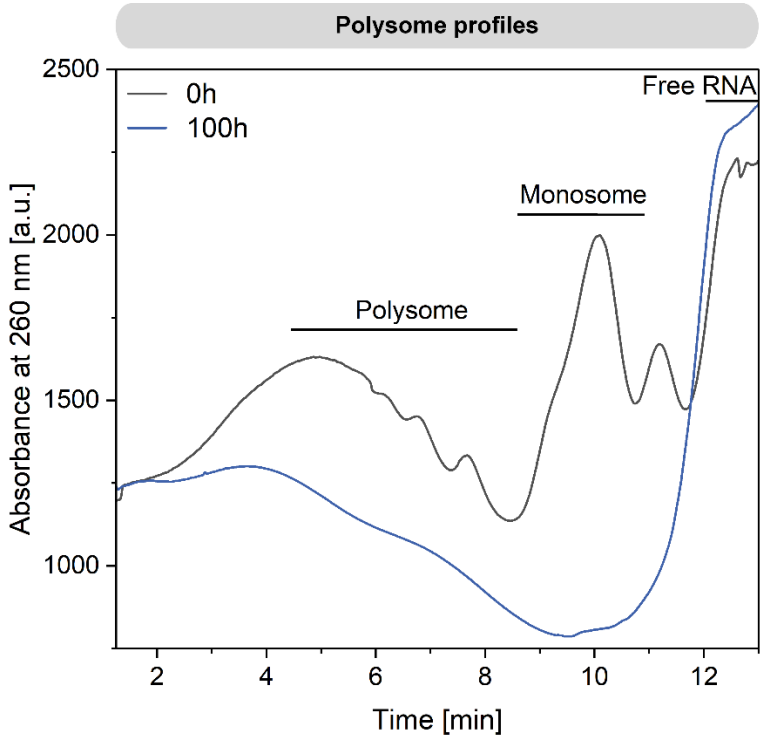


**Figure 4-8: Ribosome profiling during bio-electrochemical fermentation of *P. putida* KT2440 on glucose.** The data display the abundance of different ribosome variants after 0 and 100 h.

Under unfavorable conditions, bacteria typically stabilize ribosomes in two forms: as 70S particles, with Factor pY bound to the small subunit, or as 100S particles, a complex of two 70S units linked by the Hibernation Promoting Factor (HPF) and the Ribosome Modulation Factor (RMF) (Trösch & Willmund, 2019; Wilson & Nierhaus, 2007). However, hibernating ribosome complexes were not formed in electrogenic

*P. putida* KT2440. *P. putida* lacks a gene encoding Factor pY in its genome, and HPF was significantly downregulated at both the transcript and protein levels. This accounts for the absence of 70S and 100S particles observed in the sucrose gradients (Fig. 4-8). In contrast, *P. aeruginosa*, which can grow anaerobically in the presence of nitrate and nitrite, induces ribosome hibernation under anaerobic conditions (Trunk et al., 2010). This suggests that anoxic-electrogenic *P. putida* may prioritize the degradation and recycling of proteins and ribonucleic acids for catabolic processes rather than maintaining a hibernating ribosome pool, aligning with the growth arrest observed in later phases (Bergkessel, Basta, & Newman, 2016). Such degradation processes would lead to nitrogen loss, consistent with the increased C:N ratio observed during the process (Fig. 4-4A). *P. putida* appeared to have entered a new state of homeostasis to sustain metabolic activity throughout the extended fermentation period (380 hours). In this state, existing proteins were preserved and remained active with lower energy requirements. To maintain cellular protein homeostasis, the abundance of key ATP-dependent chaperones GroEL/S (log2-fold change 0.08 and 0.45), DnaK (log2-fold change 0.31), and the ATP-independent chaperone Trigger Factor (log2-fold change 0.49) remained stable.

These observations led to a re-evaluation of the transcriptome data from the later stages (100 hours) (Supplementary, Fig. 6-4). The apparent decline in active ribosomes suggested that mRNA levels at this stage might represent transcriptional responses that could no longer be fully translated into proteins. Furthermore, technical factors may have influenced the transcriptome data beyond the 100-hour sample. The protocol required total RNA as input, and since rRNA makes up the majority of RNA in bacterial cells (80-90%) (Culviner, Guegler, & Laub, 2020; Rosenow, Saxena, Durst, & Gingeras, 2001), a reduction in the rRNA pool could have caused a relative increase in mRNA abundance in samples from the later stages of the process used for microarray analysis. This may have led to an overestimation of gene expression. Therefore, the primary conclusions

regarding transcriptional adaptation should be drawn from the 24-hour sample, as was done previously.

### 4.2 Metabolic engineering for enhanced 2-ketogluconate production

Acetate accumulation was significant under anoxic-electrogenic conditions (Fig. 4-1D). Its biosynthesis pathway in *P. putida* KT2440 remains poorly understood, as acetate is typically not produced aerobically in this strain (Vogeleer & Létisse, 2022). This contrasts with other microbes where acetate is a well-studied overflow metabolite (Millard, Enjalbert, Uttenweiler-Joseph, Portais, & Létisse, 2021; Wittmann et al., 2007). In addition, *P. putida* lacks the gene for acetate kinase (*ackA*), unlike facultative anaerobic relatives such as *P. aeruginosa* (Dolan, et al., 2020; Kampers, et al., 2021; Nikel & de Lorenzo, 2013; Sohn, Kim, Park, & Lee, 2010). Previous studies have yielded mixed results concerning the effects of heterologous expression of *ackA* on enhancing the anaerobic survival of *P. putida* (Kampers, et al., 2021; Nikel & de Lorenzo, 2013; Sohn, et al., 2010). Given the substantial formation of acetate under bio-electrochemical conditions, different mutants were constructed to elucidate the underlying biosynthesis pathways.

*P. putida* KT2440 has four potential pathways for acetate biosynthesis from acetyl-CoA: (i) the acetyl-CoA synthase (ACS) pathway, which functions in reverse to generate ATP, (ii) the ATP-independent acetyl-CoA hydrolase (ACH) pathway, (iii) the NAD(P)H-generating aldehyde dehydrogenase (ALD) pathway, and (iv) the acetate CoA-transferase (AST) pathway, which couples ATP formation to the regeneration of succinyl-CoA to succinate via succinyl-CoA synthetase (Fig. 4-9). To investigate the impact of these different pathways, four mutants were constructed, each lacking one of the potential pathways. For pathways involving two enzymes, both corresponding genes were sequentially deleted. The mutant *P. putida* KT2440 *ΔacsAI ΔacsAII* lacked both

ACS-encoding genes, which are located in different genomic regions. The strain *ΔPP_5266* was deficient in the ACH enzyme, encoded by *PP_5266*. The two ALD variants were sequentially eliminated to create the double mutant *ΔaldBI ΔaldBII*. Finally, *P. putida* KT2440 *ΔscpC* was constructed to lack the AST pathway. All strains were compared to the wild type (Fig. 4-9). This approach enabled a systematic dissection of each pathway's contribution to acetate production under anoxic-electrogenic conditions, offering insights into the primary metabolic activities of *P. putida* KT2440 in the anaerobic bio-electrochemical environment. The elimination of each acetate biosynthetic pathway significantly impacted acetate production and overall metabolism. Notably, the deletion of the two acetyl-CoA synthase encoding genes (*ΔacsAI ΔacsAII*) led to a 30% reduction in acetate titer compared to the wild type, while gluconate formation increased substantially at the expense of 2KG production (Fig. 4-9C, Fig. 4-9D). Although the peak current achieved by the mutant was comparable to that of the wild type, it was reached 130 h later. Notably, this mutant displayed a brief phase of intense acetate production right at the onset of the process, which was not observed in the wild type. The strain lacking acetyl-CoA hydrolase (*ΔPP_5266*) produced less acetate than the wild type (Fig. 4-9E); however, it accumulated more gluconate and generated a current that was 20% higher. In this mutant, gluconate was further oxidized to 2KG only after glucose depletion. The acetate:succinate CoA-transferase-deficient strain (*ΔscpC*) produced 60% less acetate and converted glucose into 2KG approximately three days faster than the wild type (Fig. 4-9F). Notably, *P. putida* KT2440 *ΔaldBI ΔaldBII* exhibited the most significant differences compared to the wild type (Fig. 4-9G). Acetate production decreased by 80%, indicating that the aldehyde dehydrogenase pathway was the primary route for acetate formation. Remarkably, this mutant demonstrated a glucose conversion rate that was twice as fast, with complete substrate consumption achieved in just 200 h. During this time, the cells converted glucose to 2KG with a yield of 0.96 mol $mol^{-1}$ with minimal gluconate accumulation (Fig. 4-9G).

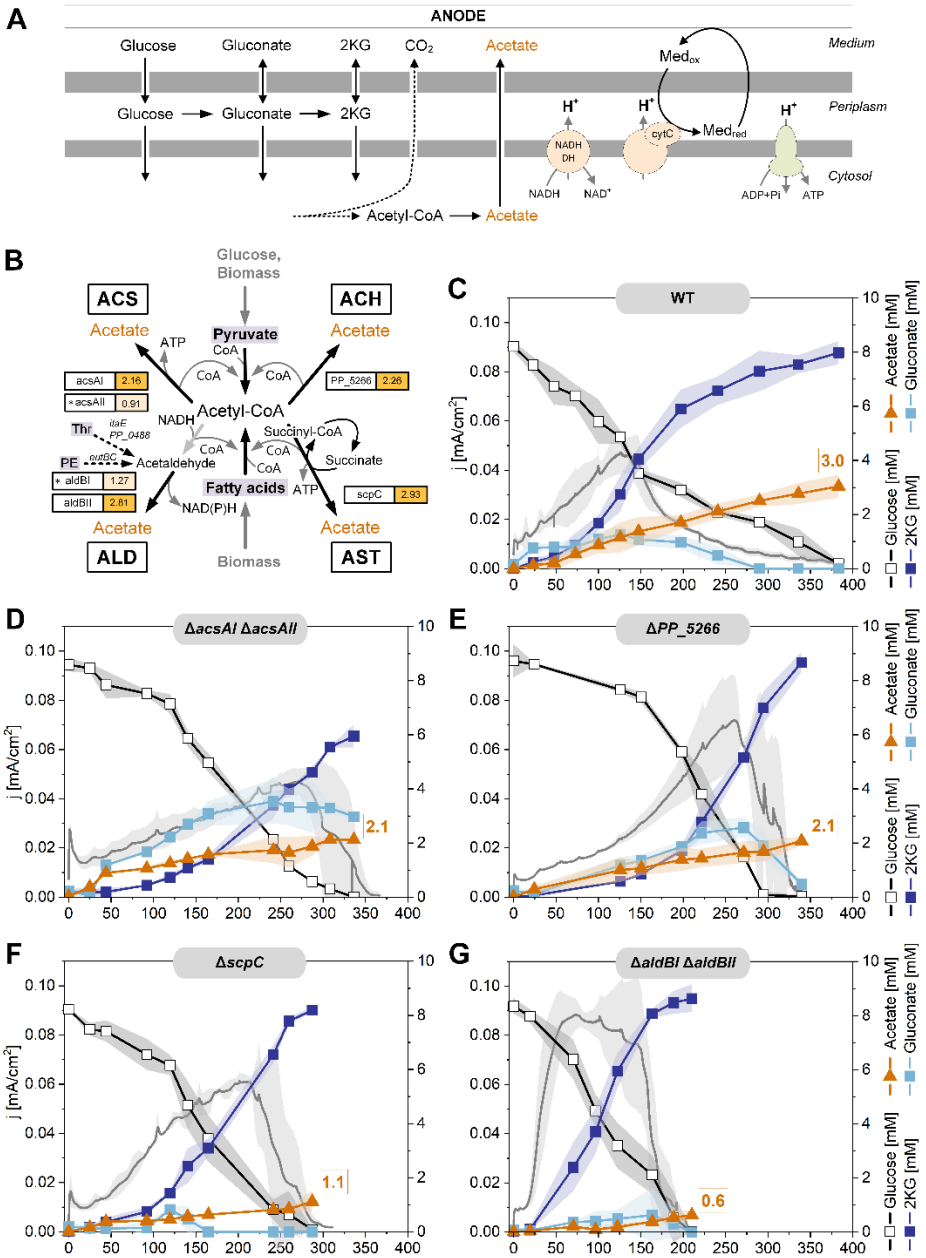


**Figure 4-9: Impact of acetate production during bio-electrochemical fermentation of *P. putida* KT2440 on glucose.** Schematic representation of the major energy-yielding pathways and processes under these conditions, including periplasmic glucose oxidation, cytosolic acetate formation, proton translocation by cytochrome c reductase and NADH dehydrogenase, respectively, and ATP generation by ATPase (A). Potential routes for acetate biosynthesis in *P. putida* KT2440, all originating from acetyl-CoA and connected to catabolic breakdown of glucose and biomass constituents (B). Fermentation profiles of KT2440 and deletion mutants, each lacking one of the four acetate biosynthetic routes (C-G). The data represent the current density (mA/cm$^2$) and the concentrations of glucose, gluconate, 2-ketogluconate, and acetate, n=4. Additional data on cell concentrations and by-products are given in the Supplementary, Fig. 6-6.

From a biotechnological perspective, the ALD mutant outperformed the wild type in terms of yield, selectivity, and productivity for 2KG production. Additionally, transcriptional analysis revealed that all four acetate biosynthesis pathways were upregulated (Fig. 4-9B). Eliminating any of these pathways led to reduced acetate levels (Fig. 4-9, Supplementary, Fig. 6-5). Notably, the acetate:succinate CoA-transferase (AST) and reverse acetyl-CoA synthase (ACS) pathways are directly associated with ATP formation, while the aldehyde dehydrogenase (ALD) pathway generates NAD(P)H. When these pathways were deleted, *P. putida* strengthened its primary ATP synthesis route: periplasmic glucose oxidation (Fig. 4-9). It appears that both the catabolic breakdown of biomass components and acetate production contributed to the energy and redox power supply (Fig. 4-3, Fig. 4-4). This adaptive response is similar to that observed in other microbes, which enhance their ATP supply mechanisms under energy-limiting conditions (Wittmann, et al., 2007). Additionally, there were also notable differences in cell concentration decrease among the strains (Supplementary, Fig. 6-6). For the best performing *ΔaldBI ΔaldBII* mutant (Fig. 4-9G), despite its distinct phenotype, the exact pathway components responsible acetate formation remains unclear. Our data suggest that the pathway likely begins with acetyl-CoA and progresses through acetaldehyde to acetate, with the final step involving the two aldehyde dehydrogenases (AldBI/II). However, no gene encoding an acylating acetaldehyde dehydrogenase, which would convert acetyl-CoA to acetaldehyde, was identified in the *P. putida* KT2440 genome. Alternative sources of acetaldehyde could include threonine (degraded via *ltaE* and *PP_0488*) and the phospholipid phosphatidylethanolamine (degraded via *eutB* and *eutC*) (Fig. 4-9B). Threonine degradation was transcriptionally upregulated, with a log2-fold change of 1.0 for *ltaE* and a log2-fold change of 2.6 for *PP_0488*, likely triggered as part of protein and amino acid catabolism to facilitate resource allocation. In contrast, phosphatidylethanolamine degradation was downregulated (log2-fold change for *eutB*: -3.02; *eutC*: -3.08). However, these alternative sources were likely insufficient to

explain the large amount of unlabeled acetate (1.8 mM) observed (Fig. 4-3A). Additional research is required to fully clarify the complete acetate biosynthesis pathway in this strain.

In three of the four mutants, *ΔaldBI ΔaldBII*, *ΔscpC*, and *ΔPP_5266*, reduced acetate production led to increased glucose oxidation to 2KG, highlighting the elimination of acetate formation as a metabolic engineering strategy to boost product formation in electrogenic *P. putida*. This represents the first successful metabolic engineering strategy targeting pathways beyond the 2KG biosynthetic route in anaerobic electrogenic *P. putida* KT2440. 2KG is a commercially valuable chemical with a wide range of applications, much like other organic acids (Becker, Kuhl, Kohlstedt, Starck, & Wittmann, 2018; Lange et al., 2017; Rohles et al., 2018). It is utilized in metal complexes for antitumor treatments (Burgos, Belchior, & Sinisterra, 2002) and serves as a bioactive ingredient in cosmetics to enhance hyaluronic acid production, thereby improving skin rejuvenation and elasticity (Marini & Saxena, 2017). According to the International Nomenclature of Cosmetic Ingredients (INCI), 2KG is found in over 20 commercial products. Furthermore, it is used industrially to synthesize isoascorbic acid, an antioxidant approved for food preservation in the European market (Pappenberger & Hohmann, 2014). The obligate aerobic metabolism of *P. putida* presents challenges for its industrial applications. Aerobic processes often lead to increased capital costs, restrict reactor size, and result in significant carbon loss through $CO_2$ production, which in turn lowers yields compared to anaerobic conditions (Hannon, et al., 2007; Lai, et al., 2016). In this context, the newly engineered *P. putida* mutants optimized for anoxic-electrogenic production of 2KG offer an attractive alternative. These mutants can be utilized in various operational modes, including batch processes with high initial glucose levels, fed-batch processes with continuous glucose feeding, or a two-stage process: an initial aerobic phase for biomass formation followed by an anaerobic phase for non-growth 2KG production. This approach could result in significant overall yields (Fig. 4-9) and

long-term operation (Fig. 4-1B). Additionally, *P. putida* can efficiently oxidize other sugars, such as fructose, under bio-electrochemical conditions, achieving high yields (Lai, et al., 2019; Nguyen, et al., 2021). For example, arabinose and galactose can be converted into L-arabonic and L-galactonic acid, respectively, both of which are commercially valuable chemicals (Jones et al., 2004; Mehtiö et al., 2016). It would be interesting to investigate whether the synthesis of these valuable products is similarly enhanced in the *P. putida ΔaldBI ΔaldBII* mutant. However, the present performance of these mutants appears to fall short of industrial efficiency, necessitating further optimization. The combined deletion of *aldBI, aldBII*, and *scpC* holds promise for further reducing or even completely eliminating acetate formation while improving the yields of target products. Moreover, the highest performing 2KG-producing mutant, *P. putida ΔaldBI ΔaldBII*, reached a plateau in current output, indicating potential bottlenecks in the electrogenic process that go beyond metabolic engineering. Factors such as bioreactor design or mediator turnover likely need to be optimized to further enhance performance (Supplementary, Fig. 6-7).

### 4.3 Mediator transport for extracellular electron transfer

For effective cellular electron shuttling between cells and mediators in the bio-electrochemical system, the interaction site must be accessible to the mediator, and their respective redox potentials must be compatible. Notably, many known mediator interaction sites are localized on the cytoplasmic membrane (Gemünde, et al., 2022). In the case of *P. putida*, mediators with a potential above 0.207 V have been shown to produce a detectable catalytic current in the bio-electrochemical system (Lai, et al., 2016), with cytochrome c reductase as a key interaction site for electron transfer (Lai, et al., 2020). This underscores the necessity for oxidized mediators to be transported across the outer membrane into the periplasm, where they are reduced at their molecular interaction site, before being transported out of the periplasm for re-oxidation at the anode. This bidirectional transport is crucial for efficient extracellular electron transfer in *P. putida* in the absence of oxygen. Its efficiency is directly linked to the electron transfer rate. However, the transport mechanisms for exogenous synthetic hydrophilic mediators, which cannot freely diffuse across the outer membrane, remain largely unknown so far (Gemünde, et al., 2022). Gaining a comprehensive understanding of these processes between the cell, mediator, and electrode is essential for optimizing the performance of *P. putida* in bio-electrochemical systems. In this context, potential targets for enhancing periplasmic mediator transport should be identified.

#### 4.3.1 A system view on periplasmic mediator transport in *P. putida*

Restricted bacterial membrane permeability, particularly for hydrophilic redox mediators, is a limiting factor that constrains mediated electron transfer between microbes and electrodes. For natural mediators, e.g. riboflavin, proteins like Bfe in *Shewanella oneidensis* (Kotloski & Gralnick, 2013), and YeeO in *E. coli* (McAnulty & Wood, 2014), are known to play roles in secretion. Several receptors and transporters have been proposed to facilitate riboflavin uptake (García-Angulo, 2017). However, the use of

natural mediators introduces challenges such as metabolic burden and stability issues (Chukwubuikem, et al., 2021). Unlike natural mediators, artificial mediators are not inherently part of the microbial system, necessitating their uptake through active transport mechanisms. To identify potential periplasmic mediator transport systems, the expression data of genes, predicted to be localized on the outer membrane, were evaluated, as compiled in the Pseudomonas Genome Database (Winsor et al., 2016). In total 149 genes encoding proteins localized on the outer membrane were identified. Around half of them were significantly upregulated (log2-fold change ≥ 2, $p \leq 0.05$) (Supplementary, Table 6-7). Among the 74 upregulated genes, 15 encode porin or porin-like proteins, 6 are associated with RND efflux pumps, and 9 encode proteins with unknown function. Notably, 27 of the significantly upregulated genes were TonB-dependent receptors (TBDR) (Fig. 4-10). TBDRs are widespread among gram-negative bacteria. They are active transporters, which mediate substrate specific transport across the outer membrane (Hiroshi Nikaido, 2003). TBDRs are fueled by energy, derived from the proton motive force generated at the inner membrane by the so called TonB complex (TonB, ExbB, ExbD) (Noinaj, Guillier, Barnard, & Buchanan, 2010). While the TonB complex is primarily known for its role in iron uptake (Klebba et al., 2021), it has also been implicated in drug and solvent tolerance (Godoy, Ramos-González, & Ramos, 2001) and the transport of other substrates, such as saccharides (Bolam & van den Berg, 2018) and lignin-derived aromatic compounds (Fujita et al., 2019). This broad substrate range underscores the versatility of TBDRs in facilitating diverse uptake. The genome of *P. putida* KT2440 contains a total of 30 TBDRs (Pierre Cornelis & Bodilis, 2009). Although the individual components of the TonB complex (*tonB*, *exbB*, *exbD*) did not show significant upregulation (Fig. 4-10), the notable upregulation of almost all TBDRs suggested that the TonB complex as a promising target for investigating periplasmic mediator uptake. Furthermore, two TBDRs, PP_1446 and PP_3325, were

also found to be significantly more abundant in the corresponding proteome dataset (log2-FC 1.63 for PP_1446, and 1.53 for PP_3325) (Fig. 4-10B).

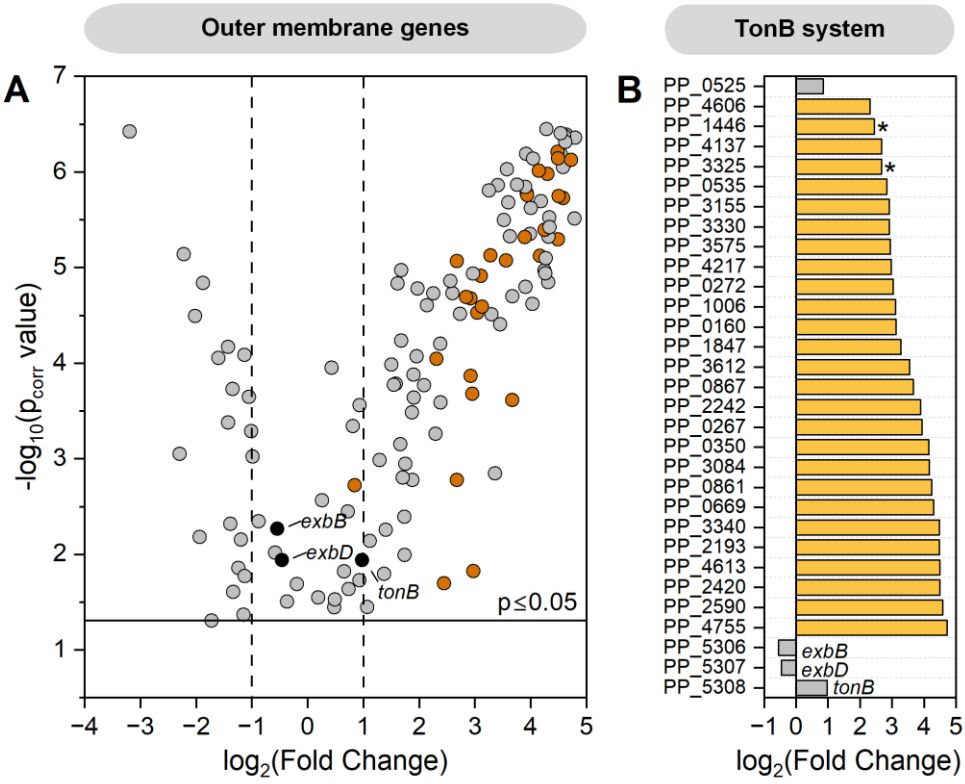


**Figure 4-10**: **Gene expression change of genes localized on the outer membrane ($p_{corr}$ ≤ 0.05).** Volcano plot depicts expression data of outer membrane genes. TBDRs are marked in orange, *tonB*, *exbB*, *exbD* are marked in black (A). Log2-fold change of TBDRs and *tonB*, *exbB*, *exbD* ($p_{corr}$ ≤ 0.05). Significantly changed genes in orange (log2-fold change ≥ 2, $p_{corr}$ ≤ 0.05). '*' Significantly higher abundant TBDRs in the proteomic data set. PP_1446 (log2-fold change 1.63), PP_3325 (log2-fold change 1.53) (B). Cells from 24 hours of bio-electrochemical cultivation were compared to cells at process start (0 h) (n=4).

While the involvement of porins in mediator transport across the outer membrane was shown before for *E. coli* using riboflavin as the mediator (Yong et al., 2013), and suggested for *Cupravidus necator* using ferricyanide as mediator (Gemünde, Ruppert,

& Holtmann, 2024), the involvement of the TonB system in periplasmic mediator transport has not yet been established.

A key factor in transmembrane transport is the cell's perception of the substrate. In the medical field, the concept of taking advantage of active transport is widely explored to overcome membrane barriers for drug delivery, for instance through strategies like siderophore-drug conjugates (Luscher et al., 2018). Notably, the presence of ferricyanide not only triggered the expression of TBDRs but also upregulated genes associated with metal homeostasis, such as *PP_2408* (*czcC-II*, log2-FC 4.8), *PP_5385* (*czcC*, log2-FC 4.6), *PP_0045* (*czcC-I*, log2-FC 3.9), *PP_2204* (*copB-I*, log2-FC 4.0), and part of the pyoverdine efflux system *PP_4211* (*ompQ*, log2-FC 4.2) (Supplementary, Table 6-7). The latter is a fluorescent siderophore produced by various species of *Pseudomonas*. Siderophores are molecules that bind and transport iron, especially in environments where iron is scarce (Bonneau, Roche, & Schalk, 2020). This response suggests that the cell may treat inorganic metal mediators like ferricyanide as metal nutrient/stressor, a field which has been rarely studied so far.

Disrupting the TonB complex is expected to impair TBDR-dependent uptake across the outer membrane (Fig. 4-11A), thereby allowing to investigate the impact of TBDRs on periplasmic mediator uptake. Experimentally, the mediator turnover was studied in two ways (Fig. 4-11B): The first approach used simple cultivation in anaerobic well plates and serum flasks, which allowed for fast screening. In these experiments, the oxidized mediator (ferricyanide) added at the start of the cultivation becomes fully reduced over time due to the absence of an anode. This reduction results in a distinct color change from yellow (ferricyanide, $[Fe(CN)_6]^{3-}$) to colorless (ferrocyanide, $[Fe(CN)_6]^{4-}$) (Fig. 4-11B). The concentration of the oxidized form of the mediator can readily be measured spectrophotometrically. In the bio-electrochemical system, the mediator is continuously re-oxidized at the anode, prolonging the cultivation duration. This process enables the cells to fully oxidize the added substrate, glucose, allowing for a more

detailed and comprehensive analysis of the product profile over time. In addition to monitoring the concentration of oxidized mediator, the current signal (mediator re-oxidation) can be directly studied as a measure of electron transfer from the cells.

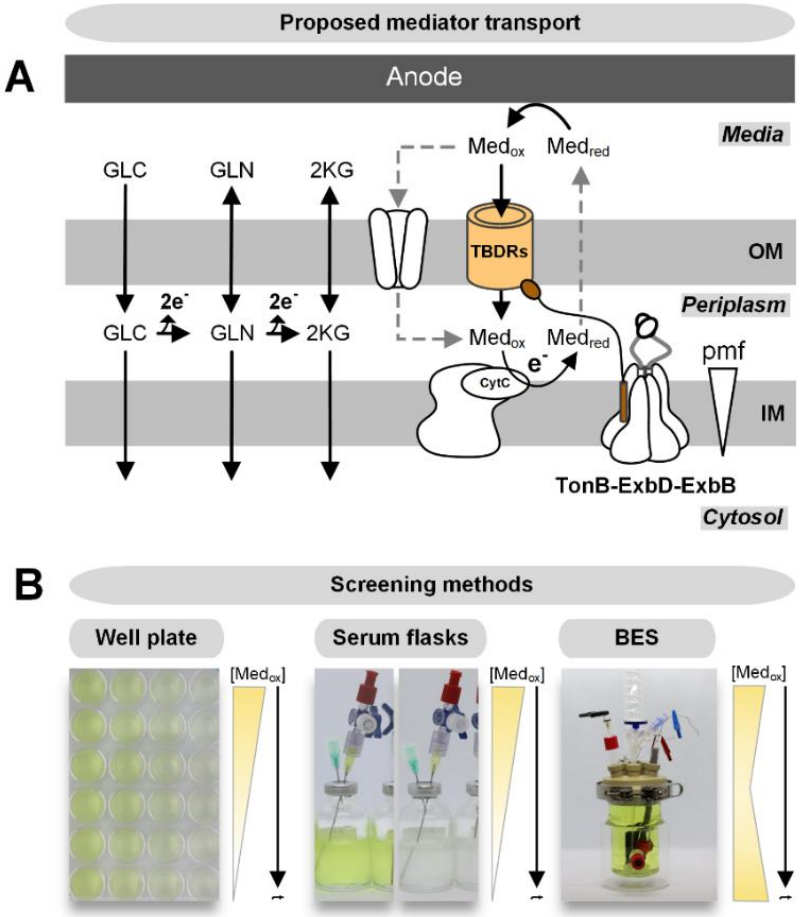


**Figure 4-11: Proposed mediator transport across the outer membrane and employed screening methods to study mediator reduction.** The TonB complex (TonB-ExbD-ExbB) localized on the inner membrane utilizes the proton motive force (pmf) to transduce energy to TBDRs (orange) localized on the outer membrane via TonB (brown), which allows substrate specific uptake. TBDRs are proposed to be involved in periplasmic uptake of the hydrophilic, oxidized mediator ($Med_{ox}$, $[Fe(CN)_6]^{3-}$). In the periplasm the mediator gets reduced at the cytochrome c reductase as the key interaction site (Lai, et al., 2020) ($Med_{red}$, $[Fe(CN)_6]^{4-}$) (A). The mediator reduction rate was investigated with well plates, serum flasks, and in a bio-electrochemical system (BES). In contrast to the bio-electrochemical system, the mediator gets fully reduced in the well plates and serum flasks (B).

### 4.3.2 Aerobic phenotype of *P. putida ΔexbBD ΔtonB*

To investigate the role of the TonB complex in mediator transport, a mutant strain with an in-frame deletion of the *exbB*, *exbD*, and *tonB* genes (PP_5306-5308) was constructed (Fig. 4-12A). The suicide plasmid, used for homologous recombination, was assembled *in vitro* using Gibson assembly, incorporating 500 bp regions corresponding to the 5′ and 3′ flanking regions of the *exbBD*, and *tonB* gene cluster. These genes are likely part of an operon, given their close genomic arrangement (Fig. 4-12C), suggesting coordinated transcription and regulation, as proposed for other *P. putida* strains (Bitter, Tommassen, & Weisbeek, 1993).

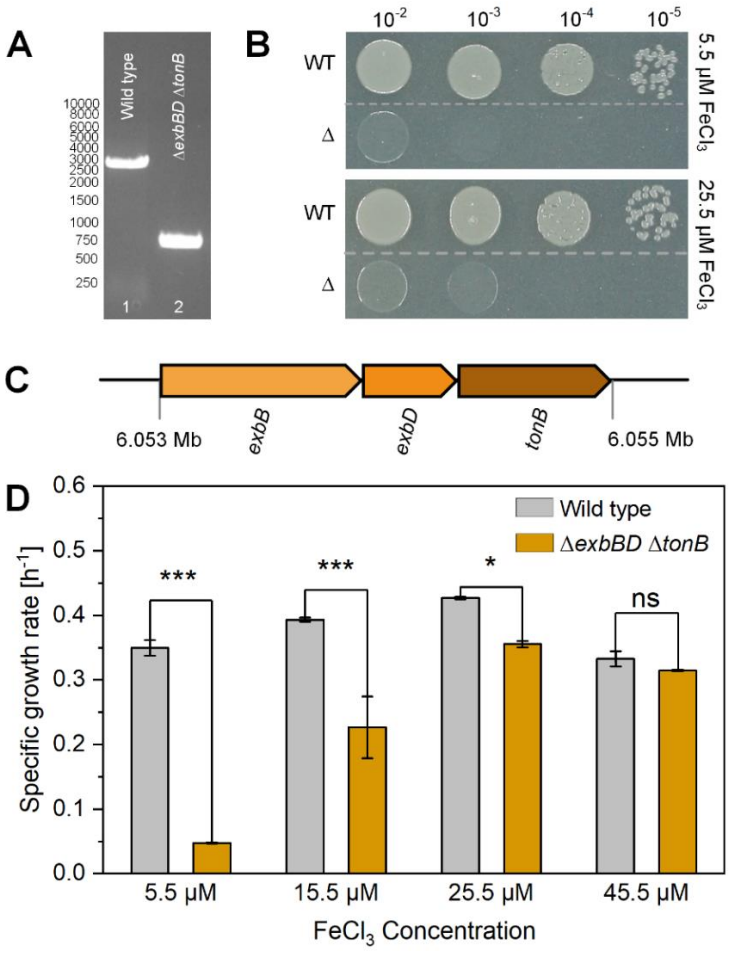


Figure continued next page

**Figure 4-12: Growth of *P. putida* KT2240 and its *ΔexbBD ΔtonB* derivative at different iron concentrations.** PCR analysis of wild type and mutant band with

difference of 2123 bp (*ΔexbBD tonB*) (A). Dilution series on LB agar plates with supplementation of iron using *P. putida* KT2440 (WT) and its *ΔexbBD ΔtonB* (Δ) derivative (B). Genomic organization of *exbB*, *exbD* and *tonB* (C). Specific growth rates ($h^{-1}$) with additional $FeCl_3$ (10, 20, 40 µM) in DM9 medium (initial $FeCl_3$ concentration of 5.5 µM) of *P. putida* KT2440 (grey bars) and its *ΔexbBD ΔtonB* derivative (orange). Each value is the mean of n = 3. ns: not significant ($p > 0.05$), *: $p < 0.05$, **: $p < 0.01$ Student's t-test (OriginLab) (D).

In line with previous findings, the *ΔexbBD ΔtonB* mutant displayed impaired aerobic growth (Godoy, Ramos-González, & Ramos, 2004; Godoy, et al., 2001; Poole, Zhao, Neshat, Heinrichs, & Dean, 1996). The TonB complex is particularly important for iron uptake, and supplementing the media with additional iron partially restored aerobic growth in the mutant (Fig. 4-12B, Fig. 4-12D). In minimal DM9 medium with a basic $FeCl_3$ concentration of 5.5 µM, the mutant exhibited a reduced growth rate, approximately sevenfold lower than that of the wild type (Fig. 4-12D). Supplementing the media with 20 µM $FeCl_3$ markedly increased growth of the mutant, raising the growth rate to about 80% of the wild type's rate. However, further increasing the $FeCl_3$ concentration to 40 µM appeared inhibitory, reducing growth rates in both mutant and wild type (Fig. 4-12D). These findings underscore the crucial role of the TonB complex in the cell's essential nutrient uptake and emphasize the importance for iron supplementation (20 µM $FeCl_3$) in the media for experiments involving the *ΔexbBD ΔtonB* mutant.

### 4.3.3 Extracellular electron transfer properties of *P. putida ΔexbBD ΔtonB*

To evaluate the difference in the reduction rate of the mediator, the wild type and the *ΔexbBD ΔtonB* mutant were tested in anaerobic serum flasks, supplemented with 1 mM ferricyanide (Fig. 4-13A, Fig. 4-13B). Notably, *P. putida* Δ*exbBD* Δ*tonB* exhibited a significantly lower mediator reduction rate (0.026 ±0.001 mM/h), compared to the wild type (0.056 ±0.009 mM/h). This suggests that the TonB complex plays a significant role

in mediator transport in *P. putida*, with its deletion markedly impairing extracellular electron transfer. Unlike aerobic growth, supplementation with additional $FeCl_3$ (10 µM, 20 µM) did not affect the reduction rate for either strain (Fig. 4-13C). This is likely due to the absence of growth under anaerobic conditions, which may reduce *P. putida*'s overall iron requirement.

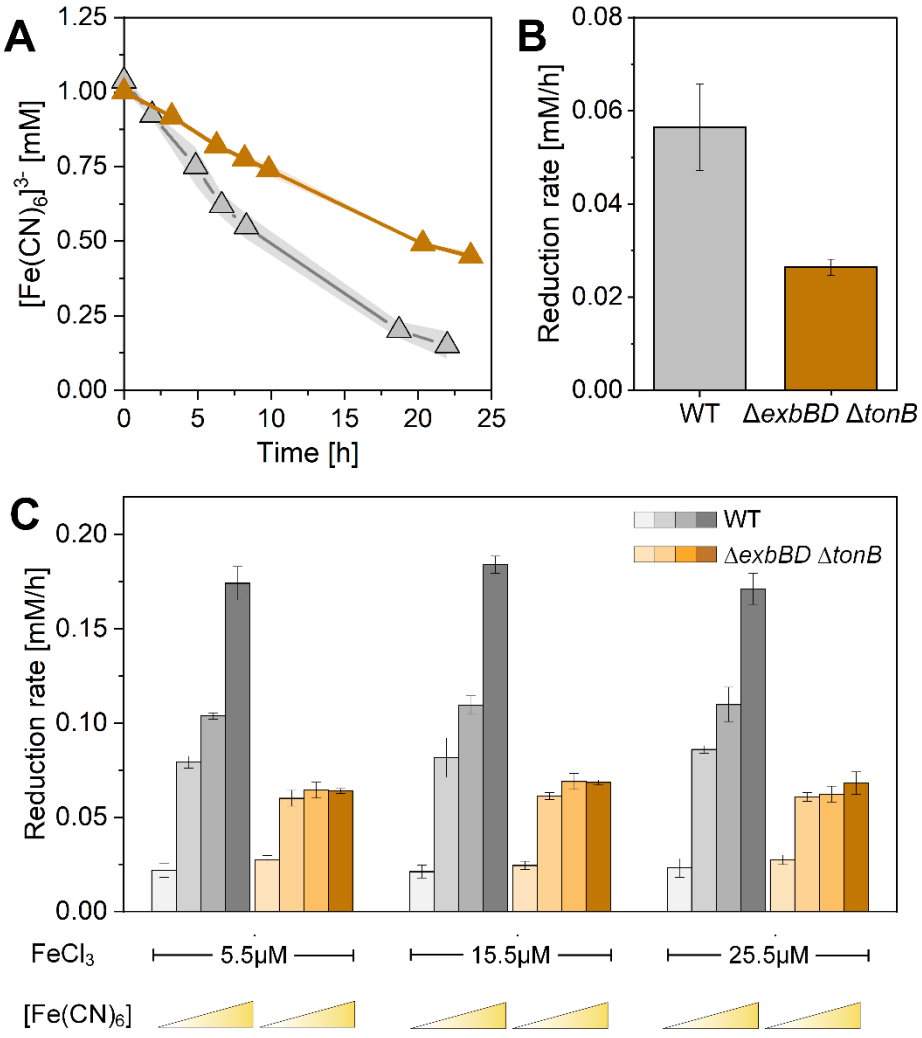


**Figure 4-13: Mediator $[Fe(CN)_6]^{3-}$ reduction of *P. putida* KT2440 (WT, grey) and its *ΔexbBD ΔtonB* derivate (orange).** Reduction of the mediator (1 mM) in anaerobic serum flasks (A), and the respective mediator reduction rates (B). Mediator reduction rates in well plates at different mediator (0.5, 1, 2, 4 mM) and iron concentrations (5.5 µM, 15.5 µM, 25.5 µM) (C). (n=3)

Additionally, at the tested concentrations, there seemed to be no competition between iron and the mediator for TBDR mediated periplasmic uptake, as the reduction rate of the mediator remained unchanged across different iron concentrations (Fig. 4-13C). Interestingly, the still detectable mediator reduction in *P. putida ΔexbBD ΔtonB* suggested the involvement of an alternative mediator transport mechanism beyond the TonB complex (Fig. 4-13A).

Next, to investigate the potential role of passive diffusion through porins, the impact of different mediator concentrations (0.5, 1, 2, 4 mM) was investigated (Fig. 4-13C). Notably, the reduction rate of the wild type continued to rise with increasing mediator concentrations (up to the tested 4 mM), which suggested that passive diffusion through porins was a possible mechanism for mediator uptake, in addition to the TonB system. In contrast, the reduction rate of the *ΔexbBD ΔtonB* mutant increased less markedly: while the reduction rate doubled when the mediator concentration was increased from 0.5 to 1 mM, the mediator reduction rate then plateaued and further increase in mediator concentration did not lead to a proportional rise in the reduction rate (Fig. 4-13C). This outcome was unexpected, given that porins generally facilitate diffusion according to the concentration gradient. As mediator concentrations increased, a corresponding rise in periplasmic concentration would be expected in both strains, ultimately resulting in an enhanced rate of extracellular electron transfer and, consequently, an increased mediator reduction rate. However, this finding reveals a previously unrecognized role of the TonB system in mediator transport, suggesting that TonB plays a critical role in enhancing the mediator reduction rate, even in transport processes typically associated with passive diffusion.

Additionally, single and double mutants for the TBDRs - PP_1446 and PP_3325, both of which were upregulated in the transcriptome and proteome datasets (Fig. 4-10B), were constructed to evaluate their effect on mediator reduction. This investigation served as a first step to identify specific TBDR(s), among the 30 encoded in the *P. putida* genome,

that are responsible for mediator uptake, which could facilitate targeted engineering approaches in the future. However, neither the single nor the double mutants led to a decrease in the reduction rate (Fig. 4-14). This finding suggests that multiple TBDRs among the 30 identified may be involved in mediator uptake, indicating potential redundancy or functional overlap among them. It has been shown that members of the *Pseudomonas* genus possess several TBDRs with a high degree of redundancy for the uptake of substrates such as ferric citrate, heme, and pyoverdines (P. Cornelis & Matthijs, 2002; Hartney et al., 2011), all of which are important for iron acquisition. This redundancy enhances bacterial survival and adaptability in diverse and changing environments by enabling efficient nutrient acquisition, but it complicates the identification of specific TBDR(s) involved in mediator transport, necessitating a more elaborate combinatorial gene deletion approach for TBDR identification.

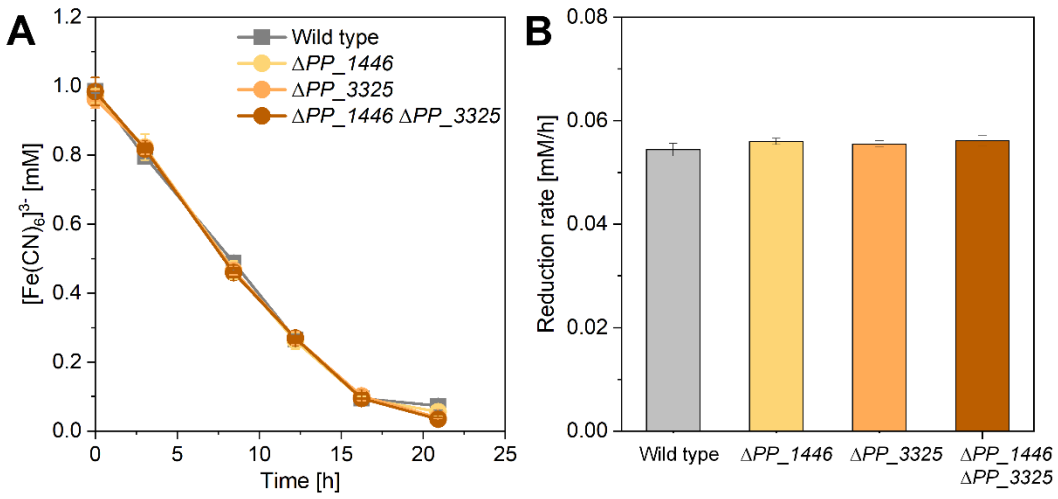


**Figure 4-14: Mediator reduction rate of *P. putida* KT2440 and TBDR mutants.** Mediator reduction rate in anaerobic serum flasks (A) and the respective reduction rates (B) of the wild type (grey), and mutants of TBDR(s), found significantly higher abundant in the transcriptome and proteome data set - ΔPP_1446 (yellow), ΔPP_3325 (orange), and ΔPP_1446 ΔPP_3325 (brown).

Subsequently, the bio-electrochemical performance of *P. putida ΔexbBD ΔtonB* was evaluated in comparison to the wild type to determine whether the reduced mediator reduction rates observed in serum flasks and plate screenings would translate into differences in current output and product spectrum. Additionally, the role of the TonB complex in the periplasmic uptake of inorganic, hydrophilic metal mediators other than ferricyanide should be assessed. All bio-electrochemical cultivations were supplemented with 1 mM of the positively charged mediator cobalt bipyridine ($[Co(bipy)_3]^{3+/2+}$) or negatively charged mediator ferricyanide ($[Fe(CN)_6]^{3-/4-}$) (Fig. 4-15).

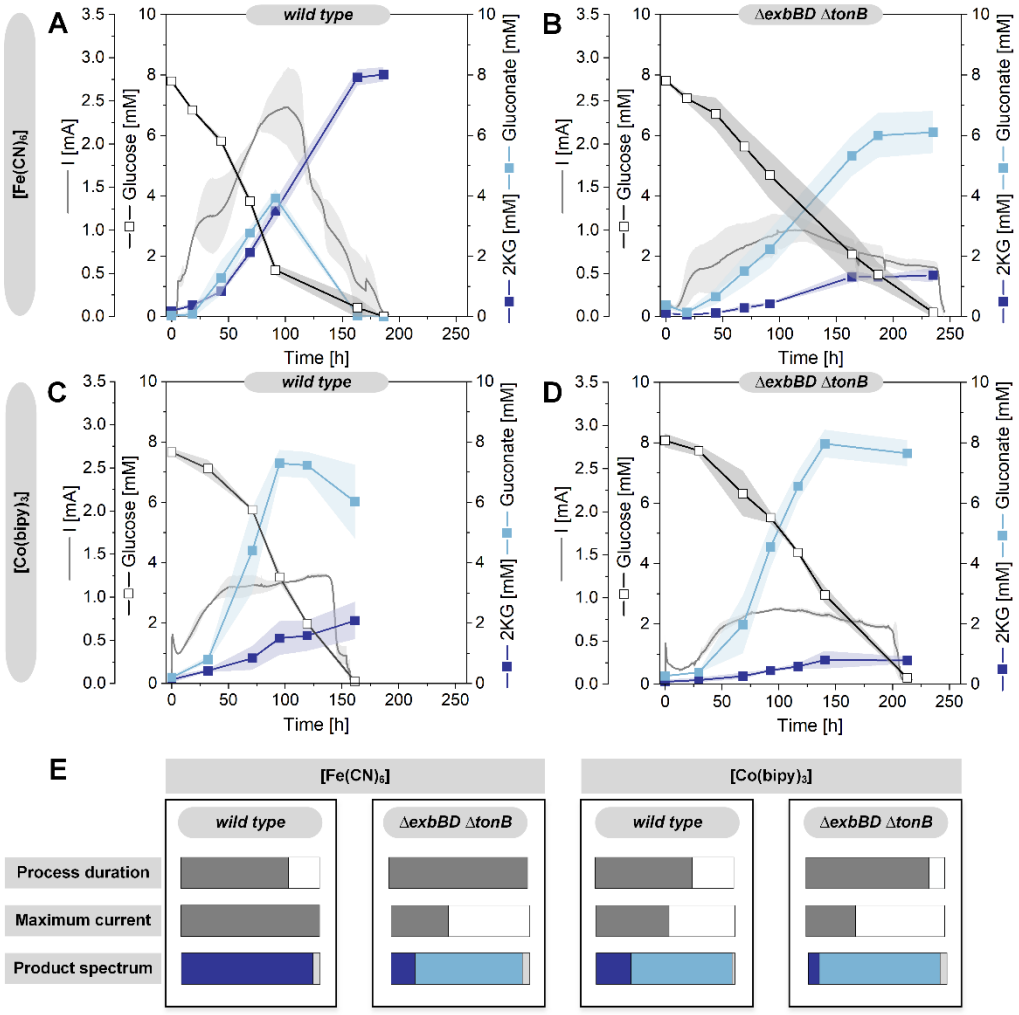


Figure continued next page

**Figure 4-15: Bio-electrochemical cultivation of *P. putida* KT2440 and its *ΔexbBD ΔtonB* derivate on glucose.** The data represent the current (mA) and the

concentrations of glucose (mM), gluconate (mM), and 2-ketogluconate (mM) of *P. putida* KT2440 and its *ΔexbBD ΔtonB* derivate using either $[Fe(CN)_6]$ (A, B) or $[Co(bipy)_3]$ (C, D) as mediator. The panel below, compares the overall process performance, highlighting the key metrics - process duration, maximum current output, and the product spectrum (gluconate and 2-ketogluconate) for *P. putida* and its *ΔexbBD ΔtonB* derivative using $[Fe(CN)_6]$ or $[Co(bipy)_3]$ (E). (n=3)

**Table 4-1.** Product yields of *P. putida* KT2440 and its *ΔexbBD ΔtonB* derivate using different mediators.

| **Yields [$mol_{product}/mol_{glucose}$]** | **KT2440 $[Fe(CN)_6]$** | ***ΔexbBD ΔtonB* $[Fe(CN)_6]$** | **KT2440 $[Co(bipy)_3]$** | ***ΔexbBD ΔtonB* $[Co(bipy)_3]$** |
|---|---|---|---|---|
| $Y_{2KG}$ | 0.93 ± 0.03 | 0.17 ± 0.01 | 0.25 ± 0.10 | 0.08 ± 0.01 |
| $Y_{gluconate}$ | 0.00 | 0.77 ± 0.08 | 0.73 ± 0.17 | 0.87 ± 0.08 |

For both strains, the primary products derived from glucose were gluconate and 2KG (Fig. 4-15). When using $[Fe(CN)_6]$ as the mediator, the wild-type produced 2KG as the main product, with no detectable gluconate remaining at the end of fermentation (Fig. 4-15A, Table 4-1). The complete conversion of glucose took around 186 hours, resulting in a maximum current output of 2.42 ± 0.43 mA. In contrast, when $[Co(bipy)_3]$ was used as the mediator, full glucose conversion took around 168 hours and the wild type produced higher levels of gluconate ($Y_{GLC}$ 0.73 ± 0.17 mol $mol^{-1}$) and lower amounts of 2KG ($Y_{2KG}$ 0.25 ± 0.10 mol $mol^{-1}$) (Fig. 4-15C, Table 4-1). This shift in product spectrum was reflected by a twofold lower current peak (1.25 ± 0.02 mA) (Fig. 4-15C). The oxidation of glucose to gluconate or 2KG generates two and four electrons, respectively. The two mediators differ in their redox potential, $[Fe(CN)_6]$ has a higher redox potential than $[Co(bipy)_3]$ (+0.31 and +0.42V versus SHE) (Lai, et al., 2016). The redox potential of a mediator determines its ability to accept and donate electrons. $[Fe(CN)_6]$ has a greater capacity to pull electrons from glucose due to its higher redox potential. This results in increased electron flow, higher current output, and more oxidized product (Gluconate: Degree of Reduction: 3.67, 2KG: Degree of Reduction: 3.33). These findings

demonstrate that $[Fe(CN)_6]$ is the superior choice for bio-electrochemical production of 2KG using *P. putida*.

Notably, the *ΔexbBD ΔtonB* mutant required approximately 50 hours longer for full glucose conversion (240 h), when $[Fe(CN)_6]$ was used as the mediator, with a significantly reduced current peak of 1.0 ± 0.14 mA (Fig. 4-15B). Additionally, there was a notable shift in the product spectrum, with 80% lower yield of 2KG ($Y_{2KG}$ 0.17 ± 0.01 mol $mol^{-1}$) and production of gluconate as the main product ($Y_{GLC}$ 0.77 ± 0.08 mol $mol^{-1}$) (Table 4-1). This reflects a diminished extracellular electron transfer likely due to lower mediator access in the absence of the TonB system. Likewise, when using $[Co(bipy)_3]$, the *ΔexbBD ΔtonB* mutant exhibited reduced glucose consumption, with a prolonged fermentation duration of around 50 hours (213 h) (Fig. 4-15A, Fig. 4-15D). This was accompanied by a 30% reduction of the current peak (0.87 ± 0.02 mA) and a shift of the product spectrum towards a higher yield of gluconate (Table 4-1). The impact of the TonB complex on the bio-electrochemical performance of *P. putida* was more pronounced when using $[Fe(CN)_6]$ as the mediator. However, remarkably, the TonB system influenced electron transfer and glucose conversion using either $[Fe(CN)_6]$ or $[Co(bipy)_3]$, resulting in overall longer process durations, reduced current outputs and a shift towards the more reduced product gluconate (Fig. 4-15E). This highlights the critical role of the TonB system in extracellular electron transfer efficiency for different mediators and underscores its importance for the bio-electrochemical performance of *P. putida*.

### 4.3.3 Metabolic engineering for accelerated extracellular electron transport

As shown, different concentrations of $[Fe(CN)_6]$ boosted mediator reduction (Fig. 4-13B), suggesting that, in addition to the TonB complex, diffusion through porins might contribute to mediator transport across the outer membrane. To further investigate this aspect, the porin OprF (PP_2089) was overexpressed. Although, its expression was not significantly altered in the transcriptome dataset (log2-fold change of -1.15,

Supplementary, Table 6-7), previous studies reported that OprF can enhance current output in *E. coli* within a microbial fuel cell (Yong, et al., 2013). Therefore, the role of OprF in *P. putida* deserved further inspection. The *oprF* gene, along with a ribosomal binding site (RBS) (Supplementary Table 6-1), was PCR-amplified and cloned into the Isopropyl β-d-1-thiogalactopyranoside (IPTG)-inducible vector pSEVA234 using restriction enzyme digestion followed by ligation, generating pSEVA234-oprF. Both the empty plasmid and pSEVA234-oprF were introduced into *P. putida* KT2440 and its *ΔexbBD ΔtonB* derivative, resulting in the strains KT/234, KT/234-oprF, ΔTonB/234, and ΔTonB/234-oprF.

Firstly, to assess changes in cell permeability resulting from OprF overexpression, an N-phenylnaphthylamine (NPN) uptake assay was performed (Fig. 4-16A, Fig. 4-16B). NPN is a hydrophobic fluorescent probe that shows minimal fluorescence in aqueous environments but becomes highly fluorescent in nonpolar or hydrophobic surroundings (Träuble & Overath, 1973). The outer membrane's highly structured outer leaflet, composed of hydrophilic lipopolysaccharides (LPS), serves as a barrier, restricting the access of hydrophobic molecules like NPN (H. Nikaido, 1989). However, when the outer membrane is compromised such as through increased permeability caused by porin overexpression or membrane damage, NPN can penetrate and interact with the hydrophobic regions inside the membrane, leading to increased fluorescence. This makes the assay particularly valuable for assessing membrane permeability and integrity (Hancock & Wong, 1984; Helander & Mattila-Sandholm, 2000; Loh, Grant, & Hancock, 1984). For the assay, cells were induced overnight (16 h) with 1 mM IPTG at a starting $OD_{600}$ of 0.2. The overnight culture was diluted to an $OD_{600}$ of 0.4, ensuring that the same cell concentration was used in the final NPN reaction mixture.

OprF overexpression led to a 3.6-fold increase in fluorescence intensity for the KT/234-oprF strain (Fig. 4-16A), reflecting a higher membrane permeability with OprF overexpression. As cell permeability increased, the KT/234-oprF strain showed a

threefold increase in the reduction rate in anaerobic serum flasks using 1 mM ferricyanide (Fig. 4-16C), demonstrating that OprF is involved in mediator transport and represents a promising target for accelerating extracellular electron transfer.

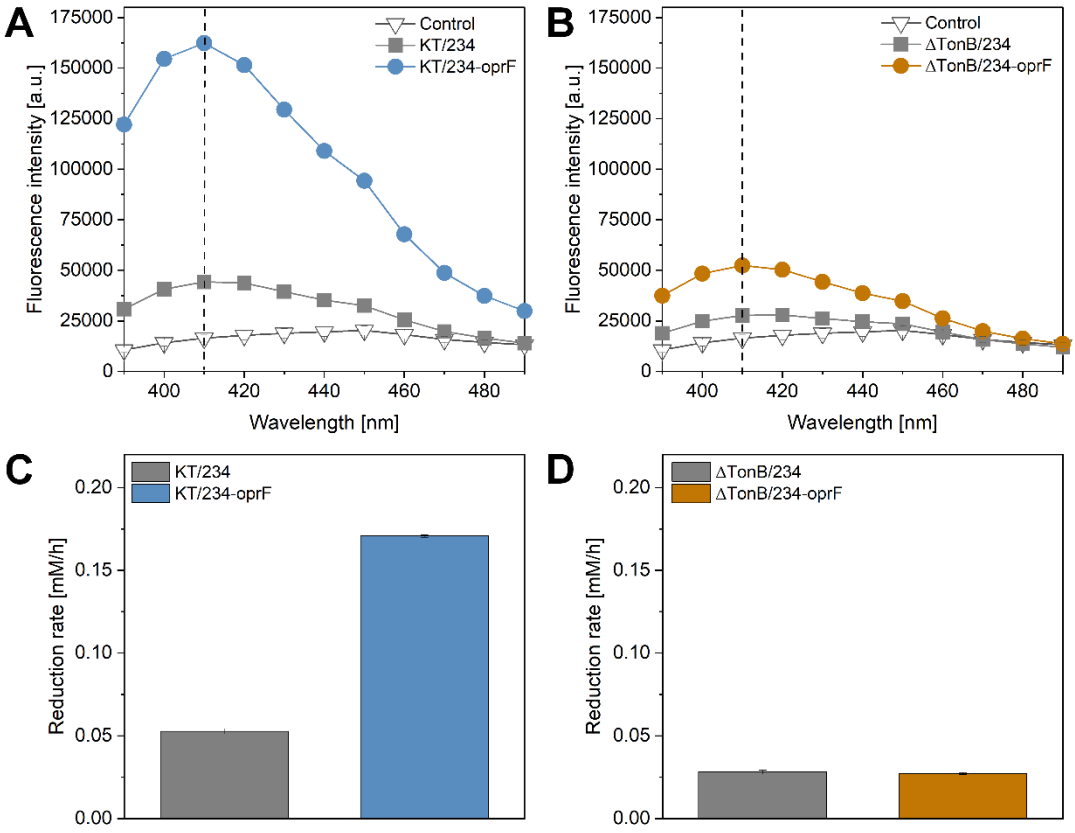


**Figure 4-16: Effect of overexpression of the general porin oprF on cell permeability and reduction rate of $[Fe(CN)_6]$.** NPN uptake assay of KT/234 (grey square), KT/234-oprF (blue circle) and control without cells (white triangle) (A) and ΔTonB/234 (grey square), ΔTonB/234-oprF (orange circle), and control without cells (white triangle) (B). Anaerobic serum flask $[Fe(CN)_6]^{3-}$ reduction rate (mM/h) for KT/234 (grey), KT/234-oprF (blue) (C), ΔTonB/234 (grey), and ΔTonB/234-oprF (orange) (D).

In contrast, the ΔTonB/234-oprF strain showed not the same increase in reduction rate (Fig. 4-16D), despite its higher cell permeability (Fig. 4-16B). Differing OprF levels between KT/234-oprF and the ΔTonB/234-oprF cannot be ruled out, but the 1.8-fold

increase in cell permeability observed in the mutant, although less pronounced than in the KT/234-oprF, still indicates elevated OprF levels and should have correspondingly led to an increase in mediator reduction (Fig. 4-16). Notably, this is consistent with earlier findings, where the reduction rate of the mutant plateaued at a mediator concentration of 1 mM, even when higher mediator concentrations were tested (Fig. 4-13C) and suggests that the TonB complex is important to reach higher extracellular electron transfer rates in *P. putida.*

Passive diffusion is driven by concentration gradients, making diffusion through porins inherently bidirectional. As a result, porins can facilitate both the import and export of molecules (H. Nikaido, 1994). However, while porins allow for bidirectional movement, they exhibit selectivity based on the size and charge of the molecules. Negatively charged residues lining the porin channel can repel negatively charged molecules, hindering their passage. Studies have shown that more negatively charged molecules are less favored for diffusion through porins (Acosta-Gutiérrez, Bodrenko, & Ceccarelli, 2021). The mediator ferricyanide undergoes reduction in the periplasm, changing its charge from -3 to -4. There are no reports on the influence of the TonB complex on diffusion through porins, however, it is tempting to speculate that changes in charge may impact diffusion kinetics in the efflux direction from the periplasm. If the increased negative charge impairs efflux through porins, the TonB complex may play a role in this process. Consequently, in the absence of the TonB complex, the rate of efflux could remain limited even with porin overexpression, as the impaired mediator efflux would negate any potential benefit from increased porin activity.

Regarding mediator efflux, the transcriptome data revealed upregulated genes associated with RND efflux systems, particularly *oprJ*, which is part of the MexCD-oprJ RND efflux system (log2-FC 4.53) (Supplementary, Table 6-7). An influence of TonB on efflux systems such as MexAB-oprM and MexCD-oprJ has been reported in *P. aeruginosa*, where the deletion of TonB increased antibiotic susceptibility, indicating

compromised efflux pump activity (Zhao et al., 1998). Similar, TonB has been found to be involved in the activity of RND efflux pumps, such as the MtrC-MtrD-MtrE system in *Neisseria gonorrhoeae* (Rouquette-Loughlin, Stojiljkovic, Hrobowski, Balthazar Jacqueline, & Shafer William, 2002), and the MacA2B2 ATP-binding cassette (ABC) macrolide efflux pump in *Aeromonas hydrophila* (Dong et al., 2021). The involvement of an RND efflux pump in *P. aeruginosa* in the secretion of phenazines, a class of natural mediators, has been documented previously (Sakhtah et al., 2016). These findings suggest that the TonB complex in *P. putida* may play a dual role in mediating TBDR-dependent periplasmic uptake as well as facilitating the efflux of mediators across the outer membrane. Hinting towards the involvement of efflux systems in periplasmic mediator export, *P. putida* KT2440 carrying an empty plasmid (used as control) demonstrated improved bio-electrochemical performance (Yu, et al., 2018). This could be related to the presence of antibiotics in the medium, potentially triggering the expression of efflux pumps that facilitate membrane transport. However, further investigations are required to confirm the role of efflux systems and the TonB complex in mediator efflux.

Next, the performance of the KT/234 strain was compared to that of the KT/234-oprF strain in the bio-electrochemical system (Fig. 4-17). Immediately after inoculation, the KT/234-oprF strain generated a significantly higher current output reaching up to 1.0 mA, within just one hour of bio-electrochemical cultivation. This value was more than twice as high as that of the KT/234 strain (0.44 mA). Notably, the glucose consumption rate of KT/234-oprF nearly doubled (0.089 mM/h compared to 0.048 mM/h), resulting in a higher current peak of 2.83 mA, compared to 1.93 mA for KT/234. This suggests that higher periplasmic mediator turnover, associated with OprF overexpression, increased the extracellular transfer and glucose oxidation rates. However, the increased glucose consumption rate of KT/234-oprF was accompanied by a 3.5-fold higher accumulation of gluconate (0.051 mM/h compared to 0.015 mM/h of KT/234), the process now

appeared to be limited by other factors. Following the maximum peak current, gluconate was completely re-consumed with 2KG emerging as the primary product by the end of the fermentation. In the KT/234 strain, glucose consumption, 2KG production, and gluconate formation/re-consumption occurred simultaneously. In contrast, the KT/234-oprF strain first fully consumed glucose up to the initial current peak (86 hours), accompanied by significant gluconate accumulation. After glucose was fully depleted, the strain converted gluconate into 2KG at a higher rate, yielding a second current peak at 131 hours. The increased turnover of the mediator driven by porin overexpression enhanced electron transfer and glucose consumption. However, the formed gluconate could not be further converted to the same extent. The oxidized form of the mediator was available throughout the fermentation (Supplementary, Fig. 6-8), pointing to other limiting factors, linked to the electron-generating reactions, i.e. the conversion of glucose to gluconate, mediated by glucose dehydrogenase (Gcd), downstream conversion of gluconate to 2KG by gluconate dehydrogenase (Gad), and electron transfer catalyzed by cytochrome-c reductase, the proposed mediator interaction site (Lai, et al., 2020).

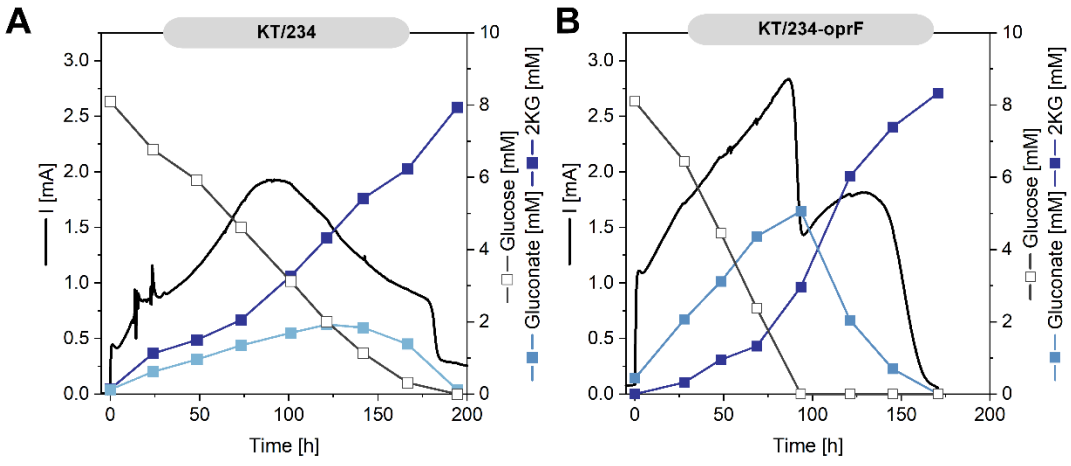


**Figure 4-17: Effect of overexpression of porin OprF on the bio-electrochemical performance of *P. putida* KT2440 using [Fe(CN)$_6$] as the mediator.** The data represent the produced current (mA) and the concentrations of glucose, gluconate, and 2-ketogluconate for KT/234 (A) and KT/234-oprF (B).

An inspection of the biochemical details of those reactions revealed that they differ in terms of co-factor usage. Gcd is dependent on PQQ, while Gad requires FAD. The re-oxidation of the two cofactors occurs at different levels in the electron transport chain. $PQQH_2$ transfers its electrons to ubiquinone, whereas $FADH_2$ is re-oxidized by the succinate dehydrogenase complex, with electrons subsequently transferred to ubiquinone. Eventually, the ubiquinol pool preferentially accepts electrons from $PQQH_2$ rather than from the succinate dehydrogenase complex. However, there is currently no research available to support this hypothesis.

Generally, the periplasmic oxidation pathway to gluconate (and 2KG) provides an ecological advantage for the cell. It enables the conversion of sugar substrates into their corresponding sugar acid forms, which cannot be utilized by competing microbes that rely solely on the EMP pathway (Volke, et al., 2023). Moreover, as a Gram-negative bacterium with an outer and an inner membrane, *P. putida* relies on the porin OprB for glucose uptake, whose uptake is dependent on the concentration gradient between the external environment and the periplasm. By converting glucose directly into gluconate, *P. putida* enhances its ability to capture more glucose, thereby increasing its competitive advantage (Thomas, 2017). This likely contributes to the favorable kinetics of the initial reaction from glucose to gluconate.

Based on these findings, further optimization of the bio-electrochemical performance of *P. putida* should aim at optimizing the balance between enhanced passive diffusion through OprF, active transport by the TonB-ExbBD complex, both in influx and efflux direction, in combination with fine-tuned reaction kinetics of the major electron-producing pathways from glucose to gluconate and 2KG by Gcd and Gad. Studies have shown that overexpressing Gcd enhances the bio-electrochemical performance of *P. putida* (Yu, et al., 2018). This work further demonstrated that deletion of genes involved in acetate production increases bio-electrochemical conversion (Fig. 4-9). Integrating these

findings could lead to a deeper understanding of the limiting reactions of extracellular electron transfer, ultimately enhancing the bio-electrochemical performance of *P. putida*. Other strategies for enhancing transmembrane transport include the artificial permeabilization of the membrane through the addition of agents like branched polyethyleneimine (Soh, Lee, & Mitchell, 2020) and cetyltrimethylammonium bromide (CTAB) (Gemünde, et al., 2024; J. Wu et al., 2022). While externally added permeabilization agents can increase cell permeability, they can present several potential drawbacks that may compromise cell viability over the long process time needed: These include potential disruption of membrane integrity, interference with cellular processes, and the possible induction of cellular stress responses. Furthermore, due to their possible toxicity, the use of these agents in large-scale applications necessitates careful handling and disposal to prevent environmental contamination. Consequently, more targeted mediator transport strategies, such as the overexpression of porins, that enhance efficiency while minimizing negative impacts are desirable.

# 5 Conclusion and Outlook

The main objective of this work was to gain a deeper understanding of the anaerobic, electrogenic phenotype of *P. putida* KT2440 under bio-electrochemical conditions during glucose oxidation. The research aimed to identify previously uncharacterized metabolic reactions and pathways active under these conditions, as well as to investigate the mechanisms of mediator transport to advance our understanding of extracellular electron transfer between cell, mediator, and anode. This work highlights the exceptional metabolic versatility of *P. putida* for anaerobic, non-growth production of the industrially relevant 2-ketogluconate (2KG) and provides a strong foundation to apply *P. putida* in bio-electrochemical biotransformations.

The first part of this work presents the first comprehensive systems biology analysis of the electrogenic phenotype of *P. putida* KT2440, integrating transcriptomic, proteomic, metabolomic and $^{13}C$ enrichment data. As shown, it uncovered key adaptation mechanisms of *P. putida* under anoxic-electrogenic conditions, including the activation of protein and lipid catabolism, acetate production, and the generation of gluconate and 2KG for energy and reducing power. Under bio-electrochemical conditions, *P. putida* significantly reduced its energy consumption, likely in response to lower ATP content. This adaptation involved global resource reallocation, affecting transcriptional expression, protein abundance, and metabolite levels, with a notable shutdown of the energy-intensive flagellar machinery and silencing of the translation apparatus. These major adjustments enabled the cells to maintain a stable energy charge and sustain substantial metabolic activity over several weeks. Building on these findings, mutants, affected in acetate production, were created, showing significantly improved 2KG production in terms of titer, yield, and productivity compared to the wild type. To compensate for the reduced energy supply from decreased acetate production, the periplasmic 2KG pathway was reinforced, making these mutants highly promising for enhanced 2KG production under anoxic-electrogenic conditions. 2KG is a product of

industrial value with applications in the pharmaceutical, cosmetic, and food sectors (K. Li et al., 2016). Industrially, microbial fermentation has proven to be the most efficient method for producing 2KG, compared to enzymatic or chemical synthesis, utilizing *Gluconobacter*, *Klebsiella,* and *Pseudomonas* as potential genera (L. Sun et al., 2020). Additionally, in the bio-electrochemical systems *P. putida* can convert sugars, other than glucose, into their respective (keto)sugar acids for instance galactonic acid and L-arabonic acid, both of which are commercially attractive (Mehtiö, et al., 2016; Werpy, Holladay, & White, 2004). Future strain optimization efforts could focus on eliminating multiple acetate production pathways to further improve the bio-electrochemical yields of this (keto)sugar acids.

The non-growth anoxic-electrogenic mode deepens our understanding of the interplay between glucose phosphorylation and its oxidation into gluconate and 2KG (Volke, et al., 2023). Under balanced growth conditions, only a small fraction of glucose is fully oxidized to 2KG, with approximately 90% of the carbon flux bypassing this pathway (Kohlstedt & Wittmann, 2019; Nikel, et al., 2015). However, under stress or nutrient-limiting conditions, slowly growing cells secrete higher levels of gluconate and 2KG (Volke, et al., 2023). In the anoxic-electrogenic mode, cells predominantly convert glucose into 2KG, achieving up to 96% conversion. This near-exclusive 2KG formation in non-growth conditions was also noted in later stages of fed-batch processes using lignin-based aromatics (Kohlstedt et al., 2022), suggesting that this is the cell's ultimate metabolic mode when growth is no longer feasible. The periplasmic glucose oxidation pathway enables cells to partially decouple ATP formation from NADH generation (Ebert, et al., 2011), striking a balance between protein investment for glucose mineralization and energy yield.

The efficiency of mediated electron transfer is directly linked to the cycling of mediators between microbes and electrodes, making it crucial to understand the underlying transport mechanisms, which remain largely unexplored (Gemünde, et al., 2022).

Understanding and improving the mediator transport mechanism not only allows to maximize process efficiency, but also opens the possibility to decrease the amount of employed mediator, which pose potential environmental risks (Lai, et al., 2020) and are challenging to remove during downstream processing (Fruehauf, Enzmann, Harnisch, Ulber, & Holtmann, 2020). Current research on the recycling or removal of mediators is limited, but potential strategies may include filtration or chromatography-based approaches. Investigating these methods will be important for upscaling, especially concerning economic feasibility (Gemünde, et al., 2022).

In this study, we demonstrated that the TonB-ExbBD complex, commonly found in Gram-negative bacteria, plays a significant role in transmembrane mediator transport in *P. putida*, with varying specificity for different metal complex mediators. Additionally, we identified diffusion through porins as another key mediator transport mechanism. Notably, the presence of TonB was essential for enhancing the mediator reduction rate through the overexpression of the general porin OprF, suggesting a dual role for TonB in both the uptake and efflux of periplasmic mediators. The wild type overexpressing OrpF showed a significant increase in glucose consumption rate and electron transfer. The accumulation of gluconate in this strain, however, suggested that further fine tuning of the key electron-producing and electron-transfer pathways, and mediator uptake is required. Moreover, at higher rates, the engineered mutant Δ*aldBI* Δ*aldBII*, designed to reduce acetate formation, revealed potential bottlenecks in the electrogenic process that extend beyond metabolic engineering. The bioreactor design likely needs to be optimized to further improve the process performance.

Electro-fermentation, the type of bio-electrochemical process employed here, typically operates at lower current densities compared to other microbial electrochemical technologies. This characteristic allows for its potential integration into existing bioprocesses using relatively small surface area electrodes (Virdis et al., 2022). A promising initial step toward industrial application is the development of conversion kits,

designed to upgrade conventional commercial bioreactors into bio-electroreactors (Rosa, Hunger, Zschernitz, Strehlitz, & Harnisch, 2019). While this represents an important advancement, this technology remains in its early stages, and further research and development are essential to enable large-scale implementation. A key foundation for this will be a deeper understanding of electrogenic metabolism and the microbe-electrode interactions that drive the system's efficiency and scalability.

Taken together, this work provides new insights collectively open new avenues for optimizing *P. putida* KT2440 for bio-electrochemical applications, emphasizing the potential of non-growth anoxic-electrogenic conditions to enhance both product yield and efficiency.

# 6 Supplementary

**Table 6-1.** List of primers used for genetic engineering in this work. The overhangs for Gibson assembly and enzyme restrictions (pSEVA234-oprF) are underlined. RBS in bold.

| Name | Sequence (5'→3') | Application |
|---|---|---|
| PP_5266_UP_fwd | GAATTCGAGCTCGGTACCCGAAACC GAAGTAATTACCAAGAC | Amplification of upstream region for deletion of *PP_5266* |
| PP_5266_UP_rev | TGCGAATGGCCGCAACCCTTGGGGC CTCCTGAAACAT | Amplification of upstream region for deletion of *PP_5266* |
| PP_5266_DW_fwd | CGGATGTTTCAGGAGGCCCCAAGGG TTGCGGCCATTCG | Amplification of downstream region for deletion of *PP_5266* |
| PP_5266_DW_rev | GTCGACTCTAGAGGATCCCCCATTG CCCCAGCGGTGATG | Amplification of downstream region for deletion of *PP_5266* |
| acsA-I_UP_fwd | GGTATTGCCGGGAAGGGTTACAGCC TTGCCGACGAAA | Amplification of upstream region for deletion of *acsA-I* |
| acsA-I_UP_rev | TGAATTCGAGCTCGGTACCCCCATC ACGCGGTATTCGAGA | Amplification of upstream region for deletion of *acsA-I* |
| acsA-I_DW_fwd | GTCGACTCTAGAGGATCCCCGGTAA CAGCTGCCCGATATG | Amplification of downstream region for deletion *acsA-I* |
| acsA-I_DW_rev | TTCGTCGGCAAGGCTGTAACCCTTC CCGGCAATACC | Amplification of downstream region for deletion *acsA-I* |
| acsA-II_UP_fwd | GCCAGATTTGCGGCCGCCGGGGCG GGTGGTCCTGCTCTT | Amplification of upstream region for deletion of *acsA-II* |
| acsA-II_UP_rev | TGAATTCGAGCTCGGTACCCTGCGC GCTAAAGGCCTCAAC | Amplification of upstream region for deletion of *acsA-II* |
| acsA-II_DW_fwd | GTCGACTCTAGAGGATCCCCCATTA TCCGTAGGACGAGCCG | Amplification of downstream region for deletion *acsA-II* |
| acsA-II_DW_rev | CAAGAGCAGGACCACCCGCCCGG CGGCCGCAAATCTG | Amplification of downstream region for deletion *acsA-II* |
| aldB-I_UP_fwd | GCGAAGAAGGCGACGCGGTGGTGT GTCTCCTTGGTATTGT | Amplification of upstream region for deletion of *aldB-I* |
| aldB-I_UP_rev | TGAATTCGAGCTCGGTACCCCTGGT GCAGGCTGTTCATTT | Amplification of upstream region for deletion of *aldB-I* |
| aldB-I_DW_fwd | GTCGACTCTAGAGGATCCCCCGACG ACAGTTCGGCCAGCG | Amplification of downstream region for deletion *aldB-I* |
| aldB-I_DW_rev | ACAATACCAAGGAGACACACCACCG CGTCGCCTTCTTCG | Amplification of downstream region for deletion *aldB-I* |
| aldB-II_UP_fwd | GGTATTGCCGGGAAGGGTTACAGCC TTGCCGACGAAA | Amplification of upstream region for deletion of *aldB-II* |
| aldB-II_UP_rev | TGAATTCGAGCTCGGTACCCCCATC ACGCGGTATTCGAGA | Amplification of upstream region for deletion of *aldB-II* |
| aldB-II_DW_fwd | GTCGACTCTAGAGGATCCCCGGTAA CAGCTGCCCGATATG | Amplification of downstream region for deletion *aldB-II* |

| | | |
|---|---|---|
| aldB-II_DW_rev | TTCGTCGGCAAGGCTGTAACCCTTC CCGGCAATACC | Amplification of downstream region for deletion *aldB-II* |
| scpC_UP_fwd | GTCGACTCTAGAGGATCCCCGGTCC TGGCCTTCATCATG | Amplification of upstream region for deletion of *scpC* |
| scpC_UP_rev | CGTTCCGTACCACATCCGGAGGATT GTTATCTCGGGCTACTG | Amplification of upstream region for deletion of *scpC* |
| Δ*exbBD* Δ*tonB*_UP_fwd | GTCGACTCTAGAGGATCCCCCTGCT TGAGACGAACAGCAG | Amplification of upstream region for deletion Δ*exbBD* Δ*tonB* |
| Δ*exbBD* Δ*tonB* _UP_rev | TTGTGACAGAAGCAAAAGTCGCTGG CCGGACCTGATGAA | Amplification of upstream region for deletion Δ*exbBD* Δ*tonB* |
| Δ*exbBD* Δ*tonB* _DW_fwd | TTCATCAGGTCCGGCCAGCGACTTT TGCTTCTGTCACAA | Amplification of downstream region for deletion Δ*exbBD* Δ*tonB* |
| Δ*exbBD* Δ*tonB* _DW_-rev | TGAATTCGAGCTCGGTACCCGTTGC GCAGCTTTTCACG | Amplification of downstream region for deletion Δ*exbBD* Δ*tonB* |
| Δ*PP_1446*_UP_fwd | GGTCGACTCTAGAGGATCCCCACCA ATCAGGCTGGCCT | Amplification of upstream region for deletion Δ*PP_1446* |
| Δ*PP_1446* _UP_rev | CGATCTTCGTCGCTTGTGGTGGGGA TGGGGCGTTCCTTG | Amplification of upstream region for deletion Δ*PP_1446* |
| Δ*PP_1446* _DW_fwd | CCAAGGAACGCCCCATCCCCACCAC AAGCGACGAAGATCG | Amplification of downstream region for deletion Δ*PP_1446* |
| Δ*PP_1446*_DW_-rev | TGAATTCGAGCTCGGTACCCGTCAG CTGGAATTCGGTGTC | Amplification of downstream region for deletion Δ*PP_1446* |
| Δ*PP_3325* _UP_rev | ATGCATGATGGTTCCTCGGTGTAAA GTCTCCGTTTTTCACG | Amplification of upstream region for deletion Δ*PP_3325* |
| Δ*PP_3325* -TS1-rev | GAATTCGAGCTCGGTACCCTGGGCA GAACCTGATGTTC | Amplification of upstream region for deletion Δ*PP_3325* |
| Δ*PP_3325* _DW_fwd | GTCGACTCTAGAGGATCCCCCCTGC ACTTCCAGCGTCTTGC | Amplification of downstream region for deletion Δ*PP_3325* |
| Δ*PP_3325*_DW_-rev | GTGAAAAACGGAGACTTTACACCGA GGAACCATCATGCAT | Amplification of downstream region for deletion Δ*PP_3325* |
| pSEVA234-oprF_fwd | TAAGCA*GGATCC***AGGAGGAAAAAC** **AT**ATGAAACTGAAAAACACCTTGG | Amplification of *oprF* (*PP_2089*) for insertion into pSEVA234 |
| pSEVA234-oprF_rev | TAAGCA*TCTAGA*TTACTTGGCCTGG GCTTCTA | Amplification of *oprF* (*PP_2089*) for insertion into pSEVA234 |

**Table 6-2**: Mean values of uncorrected and corrected values (n=4) of glucose and product concentrations from bio-electrochemical fermentation of *P. putida* KT2440, which were used to estimate the carbon balance, yields and specific production rates of 2-ketogluconate, acetate, and cumulative acid production over time as shown in Fig. 4-1 and discussed in Results and Discussion chapter 4.1.1.

| **Time** | **Glucose** | **2KG** | **Gluconate** | **Acetate** | **Pyruvate** | **Succinate** | **Lactate** |
|---|---|---|---|---|---|---|---|
| h | mM | mM | mM | mM | mM | mM | mM |
| | | | **Uncorrected** | | | | |
| 0 | 8.21 | 0.00 | 0.08 | 0.00 | 0.00 | 0.00 | 0.01 |
| 23.03 | 7.52 | 0.24 | 0.76 | 0.12 | 0.06 | 0.53 | 0.27 |
| 47.67 | 6.74 | 0.43 | 0.80 | 0.21 | 0.12 | 0.59 | 0.30 |
| 72.78 | 6.39 | 0.88 | 0.80 | 0.54 | 0.21 | 0.69 | 0.28 |
| 99.97 | 5.44 | 1.68 | 1.09 | 0.87 | 0.33 | 0.68 | 0.21 |
| 125.73 | 4.87 | 2.75 | 1.26 | 1.15 | 0.39 | 0.63 | 0.13 |
| 147.5 | 3.52 | 4.05 | 1.08 | 1.38 | 0.36 | 0.55 | 0.12 |
| 197.28 | 2.91 | 5.90 | 0.97 | 1.71 | 0.20 | 0.28 | 0.11 |
| 240.75 | 2.08 | 6.57 | 0.49 | 2.11 | 0.23 | 0.29 | 0.10 |
| 290.03 | 1.72 | 7.30 | 0.00 | 2.51 | 0.22 | 0.13 | 0.07 |
| 335.98 | 0.98 | 7.55 | 0.00 | 2.77 | 0.16 | 0.00 | 0.04 |
| 383.45 | 0.18 | 7.94 | 0.00 | 3.04 | 0.15 | 0.00 | 0.01 |
| | | | **Corrected** | | | | |
| h | mM | mM | mM | mM | mM | mM | mM |
| 0 | 8.21 | 0.00 | 0.08 | 0.00 | 0.00 | 0.00 | 0.01 |
| 23.03 | 7.47 | 0.24 | 0.75 | 0.12 | 0.05 | 0.52 | 0.27 |
| 47.67 | 6.65 | 0.43 | 0.79 | 0.2 | 0.11 | 0.58 | 0.29 |
| 72.78 | 6.26 | 0.86 | 0.96 | 0.53 | 0.21 | 0.67 | 0.27 |
| 99.97 | 5.28 | 1.63 | 1.06 | 0.85 | 0.32 | 0.66 | 0.21 |
| 125.73 | 4.70 | 2.65 | 1.22 | 1.11 | 0.38 | 0.61 | 0.13 |
| 147.5 | 3.37 | 3.88 | 1.03 | 1.32 | 0.34 | 0.53 | 0.12 |
| 197.28 | 2.75 | 5.57 | 0.92 | 1.62 | 0.19 | 0.26 | 0.10 |
| 240.75 | 2.07 | 6.13 | 0.46 | 1.97 | 0.21 | 0.21 | 0.10 |
| 290.03 | 1.58 | 6.5 | 0.00 | 2.3 | 0.2 | 0.12 | 0.07 |
| 335.98 | 0.89 | 7.03 | 0.00 | 2.51 | 0.14 | 0.00 | 0.04 |
| 383.45 | 0.08 | 7.12 | 0.00 | 2.71 | 0.13 | 0.00 | 0.01 |

**Table 6-3**: Fatty acid composition of *P. putida* KT2440 (30 mg cell dry weight) analyzed at the start of the process (0 h) and after 100 hour of bio-electrochemical cultivation. Analysis was conducted by DSMZ Services (Leibniz Institute DSMZ - Deutsche Sammlung von Mikroorganismen und Zellkulturen GmbH, Braunschweig, Germany).

| **Fatty acid** | **0 h** | **100 h** |
|---|---|---|
| 10:0 3OH | 2.0 | 1.6 |
| 12:0 | 4.4 | 6.2 |
| 12:0 2OH | 1.0 | 1.4 |
| 12:1 3OH w7c | 0.2 | 0.1 |
| 12:0 3OH | 1.6 | 2.1 |
| 14:1 w7c | 0.2 | 0.1 |
| 14:1 w5c | - | 0.1 |
| 14:0 | 0.3 | 0.3 |
| 16:1 w7c | **30.6** | **7.0** |
| 16:1 w7t | **2.3** | **14.8** |
| 16:0 | 30.2 | 32.9 |
| 17:0 cyclo w7c | 0.3 | 0.8 |
| 18:1 w7c | **25.7** | **12.6** |
| 18:1 w7t | **-** | **17.8** |
| 18:1 w5c | 0.1 | |
| 18:0 | 1.1 | 2.1 |
| Sum n:0 | 36.0 | 41.5 |
| Sum n:0 OH | 4.6 | 5.1 |
| Sum n:1 *cis* | **56.8** | **19.9** |
| *Sum n:0 cyclo* | 0.3 | 0.8 |
| Sum n:1 *trans* | **2.3** | **32.6** |
| Degree of Saturation | 40.6 | 46.7 |
| Average carbon chain length | 16.1 | 16.2 |

**Table 6-4:** Impact of anoxic-electrochemical conditions on the expression of genes related to assembly of the flagellum in *P. putida* KT2440. The data reflect differences between process start (0 h) and 24 hour incubation in the bio-electrochemical system. Statistically non-significant differences are shown in red (Benjamini-Hochberg FDR > 0.05). Log2FC values are color-coded as follows: < -2 in dark blue, < -1 in light blue, > 1 in light yellow, and > 2 in bright yellow.

| Gene name | Locus tag | log2FC | $p_{corr}$-value |
|---|---|---|---|
| *fliE* | PP_4370 | -0.99 | 1.00E-02 |
| *fliF* | PP_4369 | -0.01 | 2.55E-02 |
| *fliG* | PP_4368 | -1.07 | 1.97E-03 |
| *fliH* | PP_4367 | -0.09 | 0.20 |
| *fliI* | PP_4366 | -0.76 | 0.22 |
| *fliJ* | PP_4365 | 0.26 | 0.10 |
| *fliK* | PP_4361 | -0.85 | 0.13 |
| *fliL* | PP_4359 | -0.29 | 8.95E-05 |
| | PP_5209 | -1.95 | 7.54E-06 |
| *fliM* | PP_4358 | -0.14 | 4.17E-03 |
| *fliN* | PP_4357 | -0.01 | 1.74E-02 |
| *fliO* | PP_4356 | 0.98 | 3.97E-03 |
| *fliP* | PP_4355 | 0.76 | 0.19 |
| *fliQ* | PP_4354 | 0.20 | 1.42E-02 |
| *flhB* | PP_4352 | 1.71 | 6.77E-05 |
| *flgA* | PP_4394 | -0.80 | 1.49E-02 |
| *flgB* | PP_4391 | -2.41 | 5.41E-05 |
| *flgC* | PP_4390 | -3.14 | 5.65E-05 |
| *flgD* | PP_4389 | -2.78 | 4.26E-06 |
| *flgE* | PP_4388 | -2.77 | 2.30E-05 |
| *flgF* | PP_4386 | -1.75 | 7.05E-05 |
| *flgG* | PP_4385 | -1.62 | 1.29E-04 |
| *flgH* | PP_4384 | -2.02 | 3.21E-05 |
| *flgI* | PP_4383 | -1.03 | 6.85E-03 |
| *flgJ* | PP_4382 | -1.28 | 2.26E-03 |
| *flgK* | PP_4381 | -1.10 | 0.17 |
| *flgL* | PP_4380 | -2.04 | 2.21E-03 |
| | PP_1087 | -1.39 | 4.80E-03 |
| *fliC* | PP_4378 | -1.60 | 9.61E-03 |
| *fliD* | PP_4376 | -3.01 | 2.90E-06 |
| *fliS* | PP_4375 | -2.74 | 3.68E-05 |
| *fliT* | PP_4374 | -2.64 | 5.31E-06 |
| *motA* | PP_4905 | -0.56 | 8.55E-02 |
| | PP_4335 | -0.41 | 0.17 |
| *flgM* | PP_4395 | -1.40 | 2.41E-02 |
| | PP_4396 | -1.40 | 0.10 |
| *fliY* | PP_0227 | -1.08 | 2.35E-02 |
| | PP_5157 | 0.94 | 3.80E-03 |
| *fleQ* | PP_4373 | -0.66 | 6.62E-03 |
| *rpoN* | PP_0952 | -0.49 | 0.17 |
| *atoC* | PP_4371 | -0.09 | 0.15 |
| *fliA* | PP_4341 | -0.89 | 4.40E-02 |

**Table 6-5:** Impact of anoxic-electrochemical conditions on the expression of genes, related to central carbon metabolism, in *P. putida* KT2440. The data reflect differences between process start (0 h) and 24 hour incubation in the bio-electrochemical system. Statistically non-significant $p_{corr}$-values (Benjamini-Hochberg FDR > 0.05) are highlighted in bold and italic. Log2FC values are color-coded as follows: < -2 in dark blue, < -1 in light blue, > 1 in light yellow, and > 2 in bright yellow.

| Metabolic pathway | Gene name | Locus tag | log2FC | $p_{corr}$-value |
|---|---|---|---|---|
| **Glucose uptake** | *oprB-I* | PP_1019 | -1.41 | ***1.75E-01*** |
| | *oprB-II* | PP_1445 | 0.86 | 4.45E-02 |
| | *oprB-III* | PP_3570 | 2.73 | 3.05E-05 |
| | *gtsA* | PP_1015 | -1.80 | 1.90E-02 |
| | *gtsB* | PP_1016 | -0.26 | 5.45E-02 |
| | *gtsC* | PP_1017 | -0.49 | ***3.37E-01*** |
| | *gtsD* | PP_1018 | -0.10 | ***8.95E-01*** |
| | *glk* | PP_1011 | 0.15 | ***6.01E-01*** |
| **Gluconate / 2-Ketogluconate formation / uptake** | *gcd* | PP_1444 | -1.44 | 3.01E-03 |
| | *gnl* | PP_1170 | 1.88 | 1.65E-04 |
| | *gadA / gdh* | PP_3382 | 2.51 | 2.43E-04 |
| | *gadB / gdh* | PP_3383 | 1.87 | 1.86E-04 |
| | *gadC / gdh* | PP_3384 | 1.05 | 1.97E-04 |
| | *gad / gdh* | PP_3623 | -1.48 | 6.14E-03 |
| | *gad / gdh* | PP_4232 | 2.94 | 8.33E-06 |
| | *gnuK* | PP_3416 | -0.48 | ***2.60E-01*** |
| | *gntT* | PP_3417 | 0.19 | ***5.56E-01*** |
| | *kguT* | PP_3377 | 0.39 | ***7.34E-02*** |
| | *kguK* | PP_3378 | 1.39 | ***2.43E-01*** |
| **ED pathway** | *edd* | PP_1010 | 3.58 | 3.61E-07 |
| | *eda* | PP_1024 | -0.80 | ***2.27E-01*** |
| **Pentose phosphate pathway** | *zwf-I* | PP_1022 | -0.95 | ***5.71E-02*** |
| | *zwf-II* | PP_4042 | -0.77 | 4.60E-02 |
| | *zwf* | PP_5351 | 0.68 | 3.15E-02 |
| | *pgl* | PP_1023 | -0.81 | ***1.46E-01*** |
| | *rpe* | PP_0415 | 1.88 | 1.69E-03 |
| | *gnd* | PP_4043 | -0.39 | ***3.28E-01*** |
| | *tktA* | PP_4965 | 1.25 | 2.35E-03 |
| | | PP_5367 | 1.10 | ***2.42E-01*** |
| | *tal* | PP_2168 | -1.30 | 5.20E-04 |
| | *rpiA* | PP_5150 | -0.08 | ***1.43E-01*** |
| **EMP pathway** | *pgi-1* | PP_1808 | -0.51 | 2.67E-02 |
| | *pgi-2* | PP_4701 | -0.23 | ***6.04E-01*** |
| | *fbp* | PP_5040 | -0.73 | 1.61E-02 |
| | *fda* | PP_4960 | -0.36 | 3.39E-02 |
| | | PP_2037 | 3.97 | 2.08E-03 |
| | | PP_2871 | 3.20 | 4.09E-06 |
| | | PP_3224 | 4.32 | 7.65E-06 |
| | *tpiA* | PP_4715 | -0.09 | 2.92E-02 |
| | *gap-I / gapA* | PP_1009 | 1.62 | 1.81E-02 |
| | *gap-II / gapB* | PP_2149 | 0.92 | ***3.13E-01*** |
| | | PP_0665 | 3.29 | 2.89E-06 |
| | | PP_3443 | -0.90 | 2.52E-02 |
| | *pgk* | PP_4963 | 0.88 | ***1.59E-01*** |
| | *pgm* | PP_3578 | 0.46 | ***2.40E-01*** |
| | | PP_2243 | 3.19 | 2.44E-06 |

| | | | | |
|---|---|---|---|---|
| | | PP_3923 | 1.58 | 3.56E-07 |
| | | PP_4450 | 0.01 | 3.89E-04 |
| | *pykA* | PP_1362 | -0.87 | 4.10E-02 |
| | *pykF* | PP_4301 | 4.01 | 1.14E-06 |
| | *ppsA* | PP_2082 | -0.22 | ***3.14E-01*** |
| | | PP_2081 | -0.01 | 7.48E-03 |
| **Pyruvate dehydrogenase** | *acoA* | PP_0555 | 2.98 | 1.78E-06 |
| | *acoB* | PP_0554 | 4.01 | 2.75E-06 |
| | *acoC* | PP_0553 | 3.52 | 7.83E-05 |
| | *aceF* | PP_0338 | 3.29 | 4.42E-06 |
| | *aceE* | PP_0339 | 1.15 | ***2.55E-01*** |
| **Citric acid cycle** | *gltA* | PP_4194 | 1.25 | 2.88E-02 |
| | *acnAI* | PP_2112 | -0.18 | ***1.89E-01*** |
| | *acnB* | PP_2339 | 0.74 | 5.31E-03 |
| | *acnAII* | PP_2336 | 0.25 | 1.10E-02 |
| | *icd* | PP_4011 | -2.55 | 1.09E-03 |
| | *idh* | PP_4012 | 2.23 | 2.26E-02 |
| | *aceK* | PP_4565 | 0.41 | 3.77E-03 |
| | *sdhA* | PP_4191 | -0.18 | ***7.92E-01*** |
| | *sdhB* | PP_4190 | -0.04 | ***5.87E-01*** |
| | *sdhD* | PP_4192 | -0.85 | 1.09E-02 |
| | *sdhC* | PP_4193 | -0.47 | 3.02E-02 |
| | *sucD* | PP_4185 | -0.44 | ***6.36E-01*** |
| | *sucC* | PP_4186 | -0.17 | ***8.58E-01*** |
| | *sucA* | PP_4189 | 0.64 | ***5.43E-01*** |
| | *sucB* | PP_4188 | 1.09 | ***3.25E-01*** |
| | *lpdG* | PP_4187 | 1.07 | ***3.37E-01*** |
| | *fumC-I* | PP_0944 | 3.43 | 1.86E-02 |
| | *fumC-II* | PP_1755 | -1.33 | 2.85E-02 |
| | | PP_0897 | 2.28 | 1.51E-03 |
| | | PP_2652 | 0.38 | ***9.11E-02*** |
| | *mdh* | PP_0654 | -0.99 | 4.69E-03 |
| | *mqo-I* | PP_0751 | 1.58 | 7.89E-03 |
| | *mqo-II* | PP_1251 | 2.84 | 4.64E-03 |
| | *mqo-III* | PP_2925 | -1.26 | 2.40E-03 |
| | | PP_3591 | -0.59 | 2.79E-02 |
| **Glyoxylate shunt** | *aceA* | PP_4116 | 3.15 | 6.84E-05 |
| | *glcB* | PP_0356 | 1.71 | 7.03E-03 |
| **Anaplerosis / Gluconeogenesis** | *ppc* | PP_1505 | 1.78 | 1.31E-03 |
| | *pycB* | PP_5346 | 2.6 | 1.01E-03 |
| | *pycA* | PP_5347 | 2.47 | 8.18E-05 |
| | *maeB* | PP_5085 | 2.06 | ***5.63E-01*** |
| **Acetate formation** | *acsA-I* | PP_4487 | 2.16 | 1.69E-02 |
| | *acsA-II* | PP_4702 | 0.91 | ***2.03E-01*** |
| | *aldB-I* | PP_0545 | 1.27 | ***1.55E-01*** |
| | *aldB-II* | PP_2680 | 2.81 | 1.08E-02 |
| | *scpC* | PP_0154 | 2.93 | 2.04E-05 |
| | | PP_5266 | 2.26 | 7.53E-05 |
| **Lactate formation** | *lldD* | PP_4736 | 2.22 | 1.37E-03 |
| **C4-dicarboxylate transporter** | *dctA-I* | PP_1188 | 2.21 | 7.39E-04 |
| | *dctA-II* | PP_2056 | 2.00 | ***6.76E-02*** |
| | *dctA-III* | PP_2255 | -0.85 | ***1.82E-01*** |
| **Acetate symporter** | *actP-I* | PP_1743 | 2.64 | 2.78E-03 |

| | | | |
|---|---|---|---|
| *actP-II* | PP_2797 | 1.42 | 1.09E-02 |
| *actP-III* | PP_3272 | 4.06 | 5.27E-07 |

**Table 6-6:** Impact of anoxic-electrochemical conditions on the expression of genes and protein abundance, related to fatty acid metabolism in *P. putida* KT2440. The data reflect differences between process start (0 h) and 24 hour incubation in the bio-electrochemical system. Non-significant differences are shown in red (Benjamini-Hochberg FDR >0.05). Log2FC values are color-coded as follows: < -2 in dark blue, < -1 in light blue, > 1 in light yellow, and > 2 in bright yellow.

| Metabolic pathway | Gene name | Locus Tag | Log2FC Transcriptome | Log2FC Proteome |
|---|---|---|---|---|
| **Fatty acid de novo synthesis** | *accA* | PP_1607 | -1.59 | 0.42 |
| | *accB* | PP_0559 | -1.84 | |
| | *accC* | PP_0558 | -0.73 | 0.74 |
| | *atoB* | PP_3123 | -2.32 | |
| | *fabB* | PP_4175 | -0.38 | |
| | *fabF* | PP_1916 | 1.69 | 0.8 |
| | *fabD* | PP_1913 | 0.1 | -2.05 |
| | *fabG* | PP_1914 | -0.94 | |
| | *fabZ* | PP_1602 | 0.16 | 1.1 |
| | *fabA* | PP_4174 | -1.06 | |
| | *aacS* | PP_3071 | 0.52 | |
| | *acpP* | PP_1915 | -0.45 | -2.59 |
| | *fabH* | PP_4379 | -0.46 | |
| **ß-oxidation** | *fadA* | PP_2051 | 2.30 | |
| | *fadB* | PP_2136 | 1.31 | |
| | *fadBA* | PP_2214 | -0.81 | |
| | *fadE* | PP_1893 | -0.53 | |
| | *fadD-I* | PP_4549 | 0.65 | |
| | *fadD-II* | PP_4550 | -0.40 | |
| | *yqeF* | PP_4636 | -1.15 | |
| | *acd* | PP_2216 | -1.89 | |
| | *paaF* | PP_3284 | 4.38 | |
| | *paaH* | PP_3282 | 4.43 | -0.37 |
| | *pcaF-I* | PP_1377 | 4.46 | |
| | *pcaF-II* | PP_2137 | 0.91 | |
| | *bktB* | PP_3754 | -0.23 | |
| **Methylcitrate cycle** | *mmgF* | PP_2334 | -2.04 | |
| | *prpC* | PP_2335 | -1.47 | |
| | *acnA-II* | PP_2336 | 0.25 | |
| | *prpF* | PP_2337 | 0.44 | |
| | *prpD* | PP_2338 | 0.37 | |
| | *cti* | PP_2376 | 2.15 | |

**Table 6-7**. Impact of anoxic-electrochemical conditions on the expression of genes localized on the outer membrane ($p_{corr}$ value <0.05) in *P. putida* KT2440. The data reflect differences between process start (0 h) and 24 hour incubation in the bio-electrochemical system. TonB complex (*exbBD, tonB*) related genes are marked with ● , RND efflux protein genes are marked with ● , porins and porin-like protein genes are marked with ● , and hypothetical protein genes are marked with ● . Log2FC values are color-coded as follows: < -2 in dark blue, < -1 in light blue, > 1 in light yellow, and > 2 in bright yellow.

| | Locus Tag | Gene name | $p_{corr}$ value | Log2FC | Product Name (Uniprot) |
|---|---|---|---|---|---|
| | PP_2408 | *czcC-II* | 4.4E-07 | 4.80 | cobalt-zinc-cadmium resistance protein |
| | PP_1046 | *xcpQ* | 3.1E-06 | 4.78 | type II secretion pathway protein XcpQ |
| ● | PP_4755 | | 7.5E-07 | 4.72 | ferrichrome-iron receptor |
| | PP_1284 | *algE* | 4.4E-07 | 4.69 | alginate production protein AlgE |
| | PP_3069 | | 4.1E-07 | 4.63 | outer membrane autotransporter |
| | PP_1044 | *uxpA* | 4.8E-07 | 4.62 | lipoprotein UxpA |
| ● | PP_5385 | *czcC* | 8.1E-07 | 4.62 | CzcC family metal RND transporter outer membrane protein |
| ● | PP_0037 | *oprP* | 4.2E-07 | 4.60 | porin P |
| ● | PP_2590 | | 1.9E-06 | 4.58 | ferric siderophore receptor |
| ● | PP_3390 | | 8.9E-07 | 4.58 | porin |
| ● | PP_1173 | *galP-I* | 6.5E-07 | 4.54 | porin-like protein |
| ● | PP_2819 | *oprJ* | 3.9E-07 | 4.53 | outer membrane protein OprJ |
| ● | PP_2420 | | 1.8E-06 | 4.50 | ferric siderophore receptor |
| ● | PP_4613 | *fecA* | 5.1E-06 | 4.49 | outer membrane ferric citrate porin |
| ● | PP_2193 | | 7.2E-07 | 4.49 | ferric siderophore receptor |
| ● | PP_3340 | | 6.1E-07 | 4.48 | TonB-dependent receptor |
| ● | PP_0046 | *opdT-I* | 3.8E-06 | 4.34 | tyrosine-specific outer membrane porin D |
| ● | PP_2517 | *galP* | 3.0E-06 | 4.33 | porin-like protein |
| | PP_1889 | *fimD* | 4.8E-06 | 4.32 | type I pili subunit FimD |
| ● | PP_2058 | | 1.4E-05 | 4.31 | porin |
| ● | PP_0669 | | 1.0E-06 | 4.30 | ferric siderophore receptor |
| ● | PP_2042 | | 3.6E-07 | 4.28 | hypothetical protein |
| ● | PP_2702 | | 8.0E-06 | 4.27 | porin |
| | PP_2069 | | 1.1E-05 | 4.26 | multidrug MFS transporter outer membrane protein |
| ● | PP_0861 | | 4.0E-06 | 4.25 | outer membrane ferric siderophore receptor |
| | PP_1263 | | 1.1E-05 | 4.24 | fusaric acid resistance protein |
| ● | PP_4211 | *ompQ* | 2.0E-06 | 4.18 | outer membrane pyoverdine efflux protein |
| ● | PP_3084 | | 7.5E-06 | 4.16 | ferric siderophore receptor |
| ● | PP_0350 | | 9.7E-07 | 4.14 | ferrichrome-iron receptor |
| ● | PP_3427 | *oprN* | 7.3E-07 | 4.04 | multidrug RND transporter outer membrane protein OprN |
| ● | PP_3200 | | 2.4E-05 | 4.03 | hypothetical protein |
| | PP_2638 | | 2.4E-06 | 4.00 | cellulose synthase operon protein C |
| | PP_2204 | *copB-I* | 4.4E-06 | 3.99 | copper resistance protein B |
| ● | PP_0267 | | 1.7E-06 | 3.94 | ferric siderophore receptor |
| ● | PP_3450 | | 1.7E-06 | 3.93 | TPR repeat-containing protein |
| | PP_0045 | *czcC-I* | 6.5E-07 | 3.92 | cobalt-zinc-cadmium resistance protein |
| | PP_3373 | *bamA-II* | 1.6E-05 | 3.90 | outer membrane protein assembly factor |
| | PP_3478 | | 1.4E-06 | 3.90 | secretion protein |
| ● | PP_2242 | *fepA* | 4.8E-06 | 3.89 | ferric enterobactin transport system outer membrane subunit |

| | | | | | |
|---|---|---|---|---|---|
| | PP_1450 | | 1.4E-06 | 3.75 | TPS family activation/secretion protein |
| | PP_4971 | | 2.0E-05 | 3.67 | outer membrane-bound lytic murein transglycolase A |
| | PP_0867 | | 2.4E-04 | 3.67 | FecA-like outer membrane receptor |
| | PP_4544 | | 4.7E-06 | 3.63 | hypothetical protein |
| | PP_1880 | | 2.1E-06 | 3.59 | outer membrane autotransporter |
| | PP_3299 | | 9.4E-07 | 3.57 | lipoprotein |
| | PP_3612 | | 8.4E-06 | 3.56 | TonB-dependent receptor |
| | PP_3271 | *phaK* | 3.2E-06 | 3.52 | phenylacetic acid-specific porin |
| | PP_3464 | | 3.9E-05 | 3.45 | hypothetical protein |
| | PP_0179 | | 1.4E-06 | 3.41 | putative efflux transporter |
| | PP_3764 | *opdN* | 1.4E-03 | 3.36 | outer membrane porin D |
| | PP_4291 | | 3.1E-05 | 3.29 | hypothetical protein |
| | PP_1847 | | 7.5E-06 | 3.28 | TonB-dependent ferric siderophore receptor |
| | PP_3939 | *nicP-II* | 1.6E-06 | 3.25 | porin-like protein |
| | PP_0160 | | 2.6E-05 | 3.12 | ferrioxamine receptor |
| | PP_1006 | | 1.2E-05 | 3.11 | heme receptor |
| | PP_0272 | | 3.0E-05 | 3.04 | ferric siderophore receptor |
| | PP_4217 | *fpvA* | 1.5E-02 | 2.97 | TonB-dependent outer membrane ferripyoverdine receptor FpvA |
| | PP_2662 | | 1.2E-05 | 2.97 | hypothetical protein |
| | PP_3575 | | 2.1E-04 | 2.95 | ferric siderophore receptor |
| | PP_3330 | | 1.4E-04 | 2.92 | ferric siderophore receptor |
| | PP_3155 | | 2.1E-05 | 2.92 | ferric siderophore receptor |
| | PP_0535 | | 2.0E-05 | 2.84 | ferric siderophore receptor |
| | PP_3570 | *oprB-III* | 3.0E-05 | 2.73 | carbohydrate-selective porin |
| | PP_3325 | | 1.7E-03 | 2.67 | ferric siderophore receptor |
| | PP_4137 | | 8.5E-06 | 2.67 | outer membrane siderophore receptor |
| | PP_5250 | *opdB* | 1.9E-05 | 2.60 | proline-specific outer membrane porin D |
| | PP_3656 | | 1.4E-05 | 2.56 | aromatic compound-specific porin |
| | PP_1446 | | 2.0E-02 | 2.44 | TonB-dependent receptor |
| | PP_3630 | *opdT-II* | 2.6E-04 | 2.38 | tyrosine-specific outer membrane porin D |
| | PP_0573 | | 6.3E-05 | 2.38 | hypothetical protein |
| | PP_4606 | | 9.0E-05 | 2.31 | ferric siderophore receptor |
| | PP_1449 | | 5.5E-04 | 2.29 | hypothetical protein |
| | PP_3582 | | 1.9E-05 | 2.25 | RND transporter outer membrane protein |
| | PP_4145 | *mltD* | 2.5E-05 | 2.14 | membrane-bound lytic murein transglycosylase D |
| | PP_4514 | | 1.7E-04 | 2.09 | alpha/beta hydrolase superfamily esterase |
| | PP_3397 | | 1.7E-05 | 1.97 | hypothetical protein |
| | PP_1061 | | 8.4E-05 | 1.95 | ATP-dependent DNA helicase |
| | PP_1445 | *oprB-II* | 2.3E-04 | 1.90 | carbohydrate-selective porin |
| | PP_1577 | | 1.3E-04 | 1.90 | lambda family tail tape meausure protein |
| | PP_0418 | *estP* | 1.7E-03 | 1.88 | esterase EstP |
| | PP_4032 | | 3.3E-04 | 1.87 | lipoprotein Blc |
| | PP_1502 | | 1.1E-03 | 1.75 | OmpA family protein |
| | PP_4057 | | 1.0E-02 | 1.74 | membrane protein |
| | PP_3168 | *nicP-I* | 4.0E-03 | 1.73 | porin-like protein |
| | PP_1384 | *ttgC* | 1.6E-03 | 1.70 | efflux pump outer membrane protein TtgC |
| | PP_0504 | *oprG* | 1.1E-05 | 1.68 | outer membrane protein OprG |
| | PP_4989 | *pilJ* | 5.8E-05 | 1.68 | twitching motility protein PilJ |

| | | | | | |
|---|---|---|---|---|---|
| | PP_1798 | | 7.0E-04 | 1.66 | outer membrane efflux protein |
| | PP_0799 | *opdC* | 1.5E-05 | 1.61 | histidine-specific outer membrane porin D |
| | PP_1599 | *bamA-I* | 1.6E-04 | 1.58 | outer membrane protein assembly factor |
| | PP_2754 | | 1.7E-04 | 1.54 | OprD family outer membrane porin |
| | PP_2892 | | 1.0E-04 | 1.50 | hypothetical protein |
| | PP_1579 | | 5.5E-03 | 1.40 | hypothetical protein |
| | PP_1887 | | 1.6E-02 | 1.37 | hypothetical protein |
| | PP_1273 | | 1.0E-03 | 1.29 | multidrug MFS transporter outer membrane protein |
| | PP_1419 | *opdH* | 7.2E-03 | 1.11 | tricarboxylate-specific outer membrane porin |
| | PP_0913 | | 3.5E-02 | 1.07 | hypothetical protein |
| | PP_5308 | *tonB* | 1.1E-02 | 0.97 | TonB energy transducing system subunit TonB |
| | PP_5057 | | 2.8E-04 | 0.93 | M23/M37 family peptidase |
| | PP_0678 | | 1.9E-02 | 0.93 | hypothetical protein |
| | PP_0525 | | 1.9E-03 | 0.84 | B12 family TonB-dependent receptor |
| | PP_1383 | *galP-II* | 4.5E-04 | 0.81 | porin-like protein |
| | PP_2558 | | 2.3E-02 | 0.73 | outer membrane efflux protein |
| | PP_4171 | | 3.6E-03 | 0.72 | hypothetical protein |
| | PP_0715 | | 1.5E-02 | 0.65 | outer membrane efflux protein |
| | PP_0773 | *yiaD* | 3.0E-02 | 0.49 | OmpA/MotB domain-containing protein |
| | PP_5037 | | 3.6E-02 | 0.48 | lipocalin family lipoprotein |
| | PP_0938 | | 1.1E-04 | 0.43 | hypothetical protein |
| | PP_3852 | | 2.7E-03 | 0.26 | BNR domain-containing protein |
| | PP_0805 | | 2.8E-02 | 0.19 | outer membrane efflux protein |
| | PP_4669 | | 2.0E-02 | -0.19 | OmpA family protein |
| | PP_5379 | *copB-II* | 3.1E-02 | -0.37 | copper resistance protein B |
| | PP_5307 | *exbD* | 1.1E-02 | -0.46 | TonB-gated outer membrane transporter gating inner membrane protein |
| | PP_5306 | *exbB* | 5.4E-03 | -0.55 | biopolymer transport protein ExbB |
| | PP_0577 | | 9.6E-03 | -0.58 | hypothetical protein |
| | PP_4303 | | 4.5E-03 | -0.88 | hypothetical protein |
| | PP_5080 | *pilQ* | 9.5E-04 | -0.99 | type IV pili biogenesis protein |
| | PP_0192 | *fkl* | 5.1E-04 | -1.01 | FKBP-type peptidyl-prolyl *cis-trans* isomerase |
| | PP_0851 | *pilF* | 2.3E-04 | -1.05 | type IV pili biogenesis protein PilF |
| | PP_0765 | | 1.7E-02 | -1.13 | hypothetical protein |
| | PP_4293 | | 8.2E-05 | -1.14 | hypothetical protein |
| | PP_2089 | *oprF* | 4.3E-02 | -1.15 | porin F |
| | PP_4465 | | 7.0E-03 | -1.20 | porin |
| | PP_4923 | | 1.4E-02 | -1.24 | outer membrane efflux protein |
| | PP_1689 | | 2.5E-02 | -1.33 | long-chain fatty acid transporter |
| | PP_1131 | *slyB* | 1.9E-04 | -1.35 | outer membrane lipoprotein |
| | PP_1087 | | 4.8E-03 | -1.39 | OmpA family outer membrane protein |
| | PP_0329 | | 4.2E-04 | -1.43 | hypothetical protein |
| | PP_4704 | | 6.8E-05 | -1.43 | hypothetical protein |
| | PP_1122 | | 8.8E-05 | -1.60 | OmpA family protein |
| | PP_1019 | *oprB-I* | 4.9E-02 | -1.72 | carbohydrate-selective porin |
| | PP_1622 | | 1.4E-05 | -1.88 | M23B subfamily metallopeptidase |
| | PP_0883 | *opdP* | 6.6E-03 | -1.94 | glycine-glutamate dipeptide porin |
| | PP_4384 | *flgH* | 3.2E-05 | -2.02 | flagellar L-ring protein |

| | | | | | |
|---|---|---|---|---|---|
| | PP_2163 | *vacJ* | 7.2E-06 | -2.22 | lipoprotein VacJ |
| | PP_1206 | *oprD* | 8.9E-04 | -2.29 | basic amino acid specific porin OprD |
| | PP_3214 | | 3.8E-07 | -3.19 | hypothetical protein |

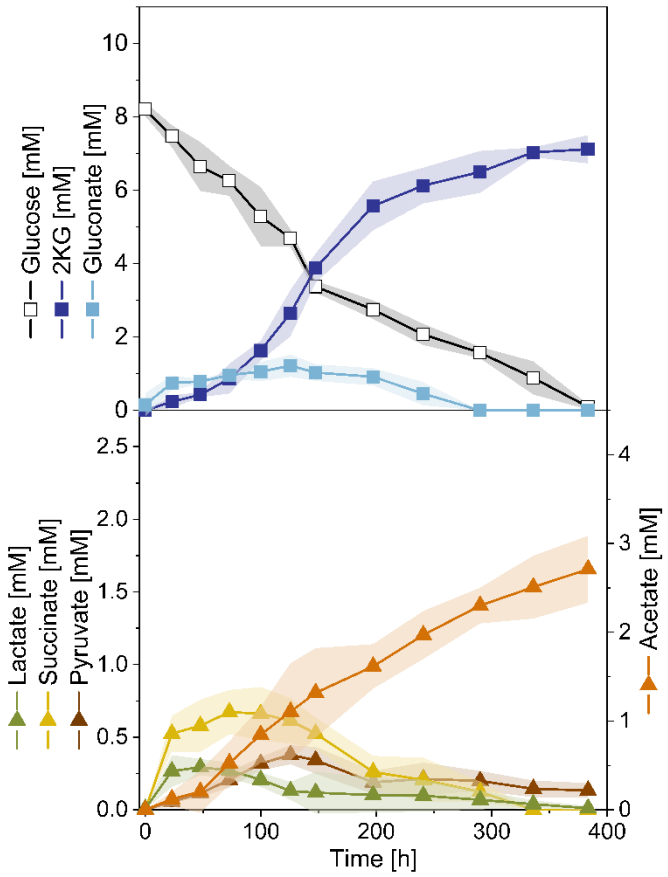


**Figure 6-1: Bio-electrochemical cultivation of *P. putida* KT2440 on glucose.** The data comprise water evaporation-corrected (0.09 mL $h^{-1}$) concentrations of glucose (mM), gluconate (mM), and 2-ketogluconate (mM), lactate (mM), succinate (mM), pyruvate (mM), and acetate (mM) (Supplementary, Table 6-2). The uncorrected values are shown in Fig. 4-1. (n=4).

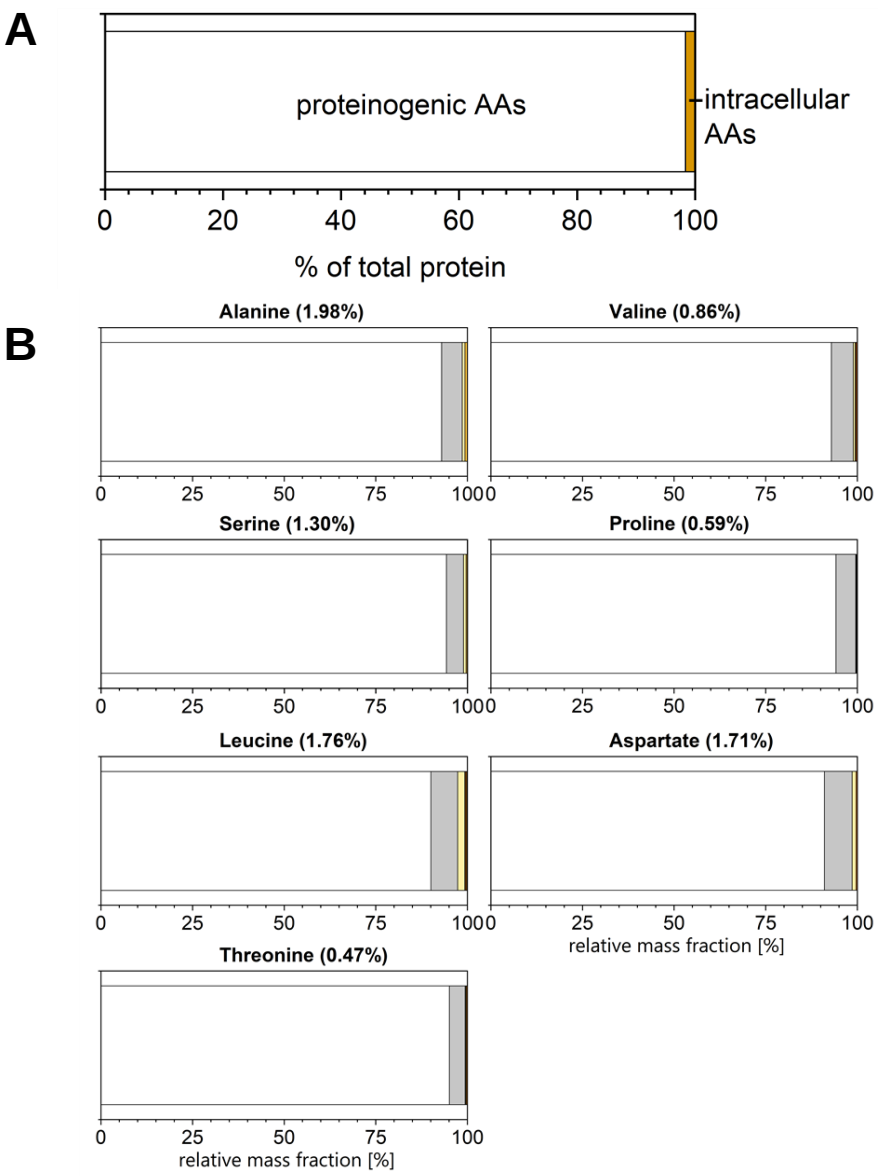


**Figure 6-2: Summed fraction labelling (SFL) of amino acids derived from hydrolyzed *P. putida* KT2440 cells, after 100 h incubation on [$^{13}C_6$] glucose in the bio-electrochemical system.** In addition, the share of protein-bound (98.4%) and free intracellular amino acids (1.6%) is shown (A). The calculation was based on a cellular protein content of 0.553 g $g^{-1}$ (van Duuren et al., 2013), and estimated levels of intracellular amino acids in *P. putida* (Bolten, et al., 2007). The SFL data of selected proteiongenic amio acids are given below (B).

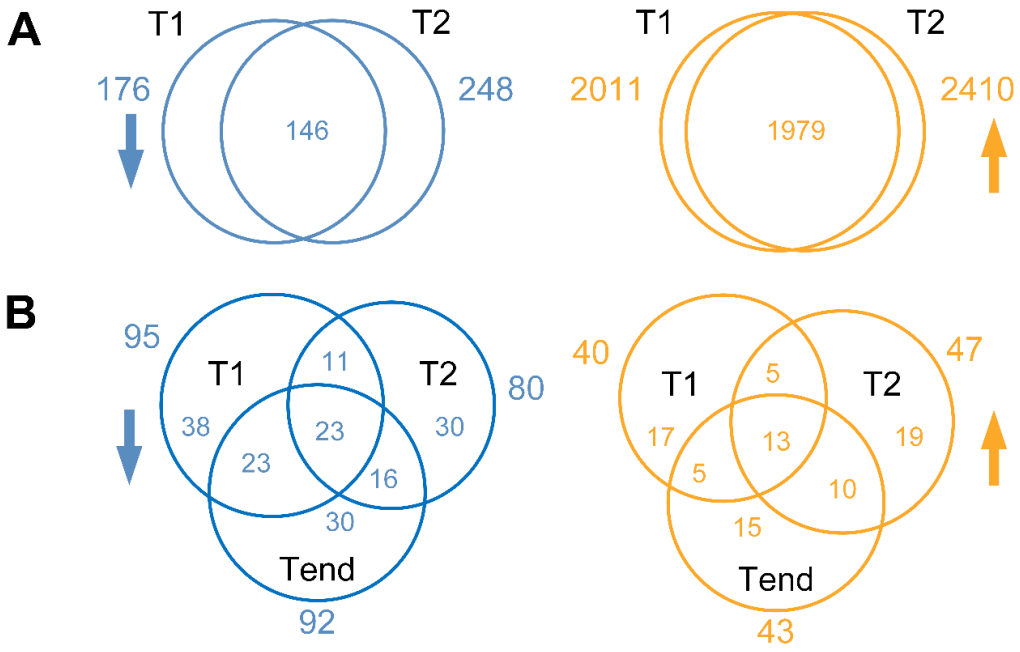


**Figure 6-3: Venn diagramms depicting the impact of anoxic-electrochemical conditions on gene expression and protein abundance in *P. putida* KT2440.** Significantly down- (blue, log2FC < -2) and upregulated (yellow, log2FC > 2) genes at T1 (24 h) and T2 (100h) compared to T0 (pre-culture) (A). Significantly lower (blue, log2FC < -1) and higher (yellow, log2FC > 1) abundant proteins at T1 (24 h), T2 (100h) and Tend (380h) compared to T0 (pre-culture) (B).

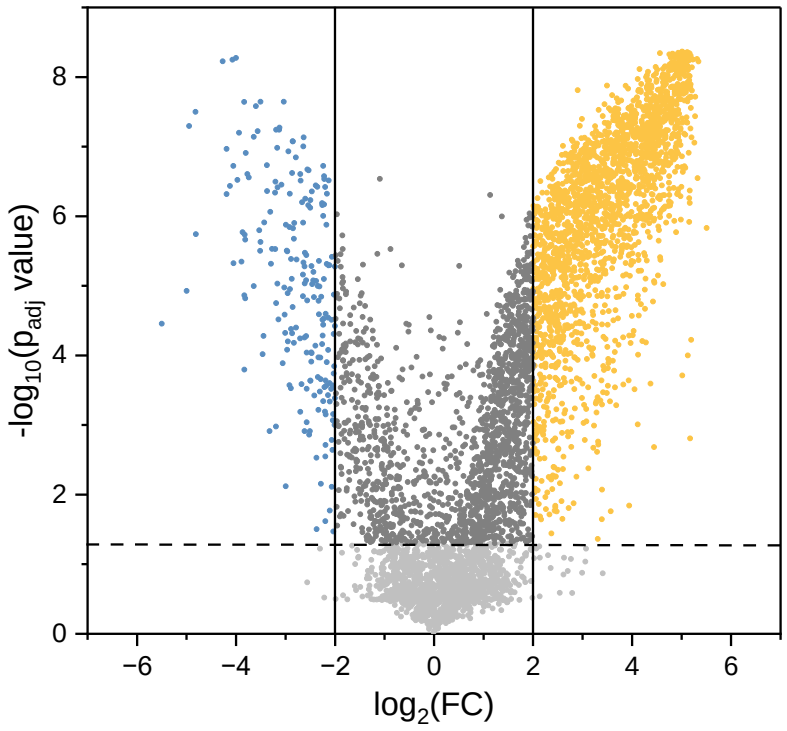


**Figure 6-4: Transcriptomic changes during bio-electrochemical fermentation of *P. putida* KT2440 on glucose.** Volcano plot showing global transcriptomic differences between 0 h (T0) and 100 h (T2) of bio-electrochemical cultivation. Significantly downregulated genes (log2FC < -2) are highlighted in blue, and significantly upregulated genes (log2FC > 2) are highlighted in yellow.

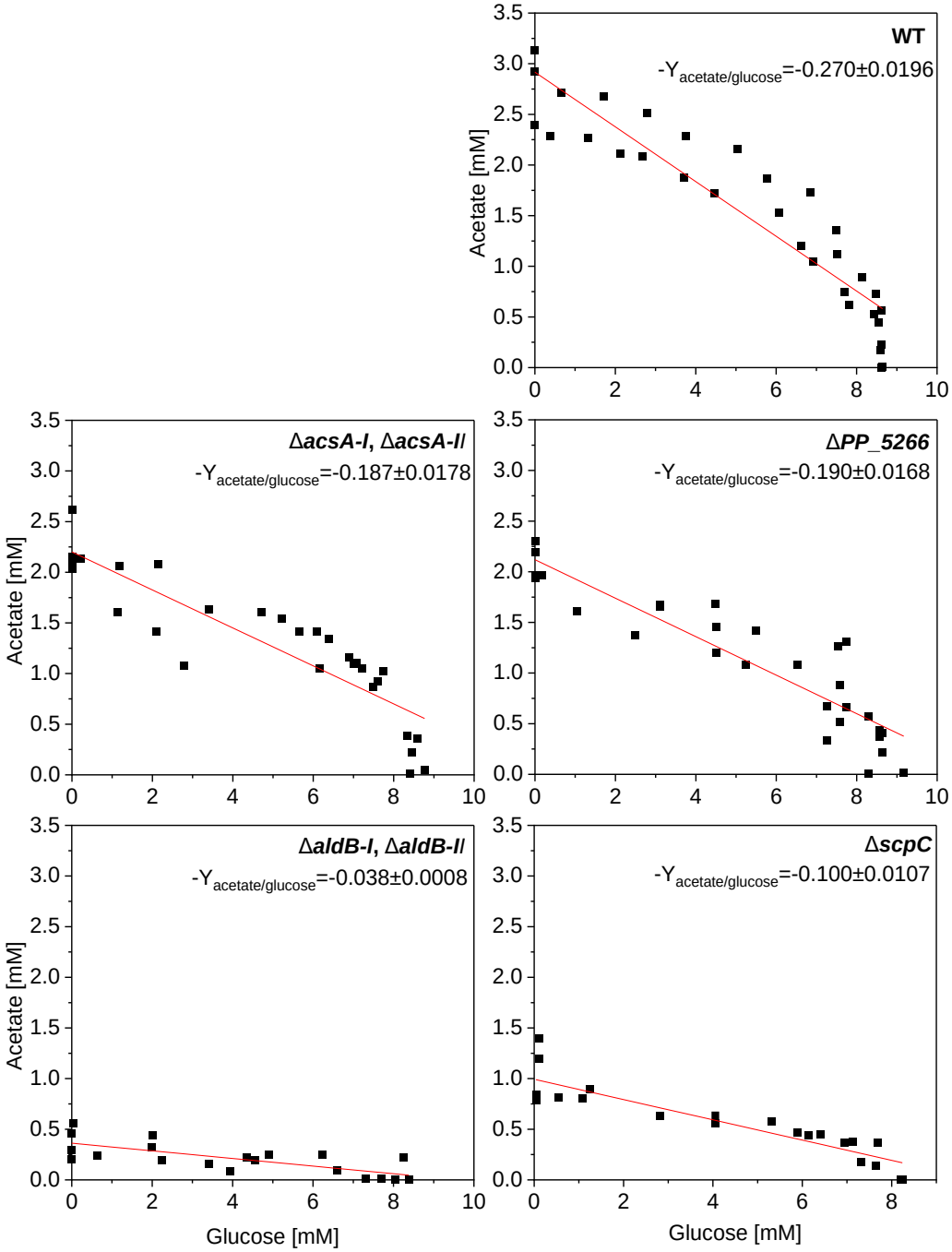


**Figure 6-5:** Regression analysis for determination of yield coefficients for *P. putida* KT2440, and acetate formation mutants Δ*acsA-I* Δ*acsA II*, Δ*PP5266*, Δ*aldB-I* Δ*aldB-II*, and Δs*cpC* during bio-electrochemical cultivation.

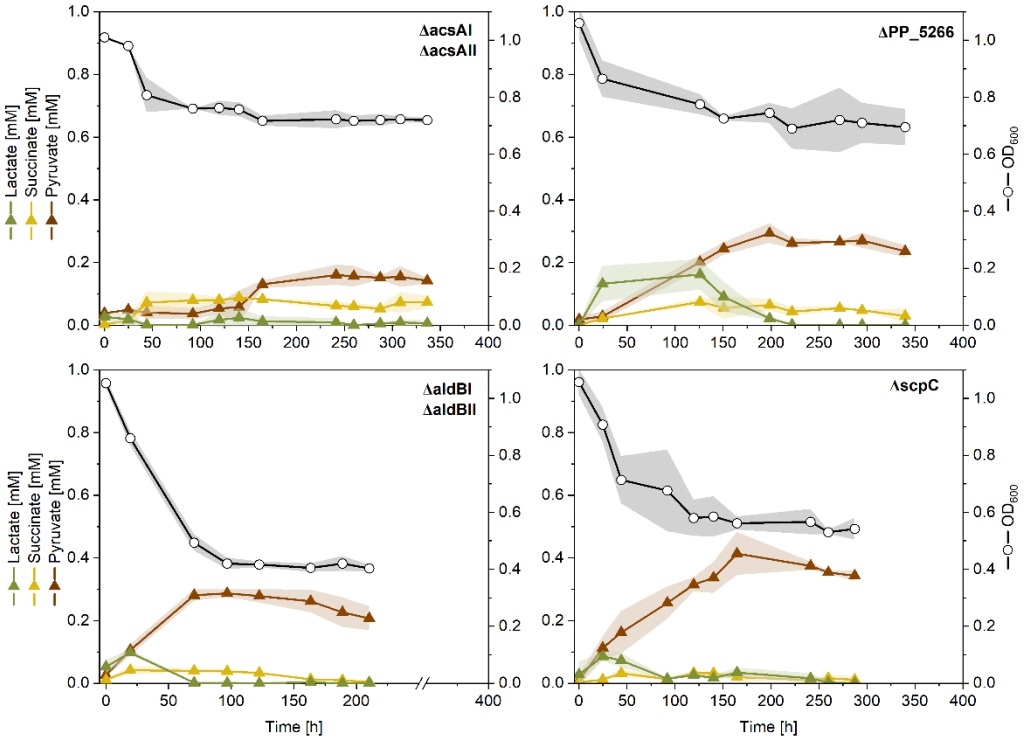


**Figure 6-6: Impact of acetate production during bio-electrochemical fermentation on glucose of acetate deletion mutants.** Fermentation profiles of deletion mutants, each lacking one of the four acetate biosynthetic routes. The data represent cell concentration ($OD_{600}$), and concentrations of lactate (mM), succinate (mM), and pyruvate (mM). (n=4)

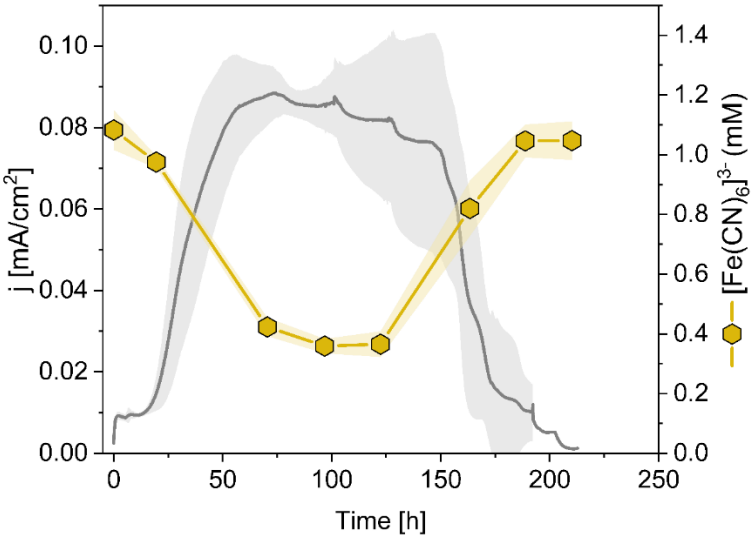


**Figure 6-7: Bio-electrochemical run of *P. putida* Δ*aldBI* Δ*aldBII* on glucose**. The data represent the current density (mA/cm$^2$) and the concentrations of the oxidized mediator ($[Fe(CN)_6]^{3-}$) [mM]. (n=4)

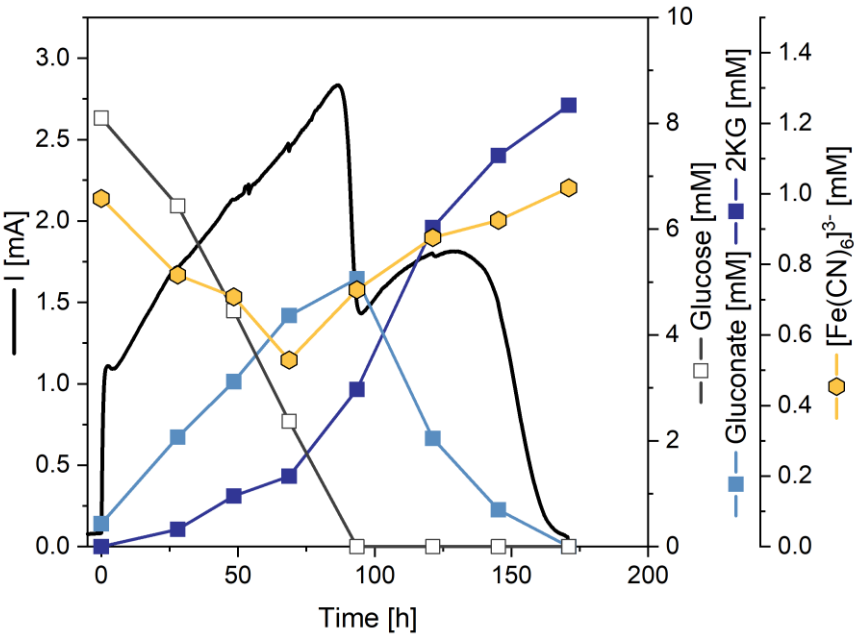


**Figure 6-8: Bio-electrochemical fermentation of *P. putida* pSEVA234-oprF on glucose**. The data comprise the time profiles of current (mA), concentrations of glucose (mM), gluconate (mM), and 2-ketogluconate (mM), and $[Fe(CN)_6]^{3-}$ (mM).

# 7 References


Acosta-Gutiérrez, S., Bodrenko, I. V., & Ceccarelli, M. (2021). The Influence of Permeability through Bacterial Porins in Whole-Cell Compound Accumulation. *Antibiotics, 10*(6).

Adler, P., Bolten, C. J., Dohnt, K., Hansen, C. E., & Wittmann, C. (2013). Core fluxome and metafluxome of lactic acid bacteria under simulated cocoa pulp fermentation conditions. *Applied and environmental microbiology, 79*(18), 5670-5681.

Akkaya, Ö., Pérez-Pantoja, D. R., Calles, B., Nikel, P. I., & de Lorenzo, V. (2018). The Metabolic Redox Regime of *Pseudomonas putida* Tunes Its Evolvability toward Novel Xenobiotic Substrates. *mBio, 9*(4), e01512-01518.

Ankenbauer, A., Schäfer, R. A., Viegas, S. C., Pobre, V., Voß, B., Arraiano, C. M., et al. (2020). *Pseudomonas putida* KT2440 is naturally endowed to withstand industrial-scale stress conditions. *Microbial biotechnology, 13*(4), 1145-1161.

Askitosari, T. D., Berger, C., Tiso, T., Harnisch, F., Blank, L. M., & Rosenbaum, M. A. (2020). Coupling an Electroactive *Pseudomonas putida* KT2440 with Bioelectrochemical Rhamnolipid Production. *Microorganisms, 8*(12).

Atkinson, D. E. (1968). The energy charge of the adenylate pool as a regulatory parameter. Interaction with feedback modifiers. *Biochemistry, 7*(11), 4030-4034.

Batlle-Vilanova, P., Ganigué, R., Ramió-Pujol, S., Bañeras, L., Jiménez, G., Hidalgo, M., et al. (2017). Microbial electrosynthesis of butyrate from carbon dioxide: Production and extraction. *Bioelectrochemistry, 117*, 57-64.

Becker, J., Kuhl, M., Kohlstedt, M., Starck, S., & Wittmann, C. (2018). Metabolic engineering of *Corynebacterium glutamicum* for the production of *cis, cis*-muconic acid from lignin. *Microbial Cell Factories, 17*(1), 115.

Becker, J., Reinefeld, J., Stellmacher, R., Schäfer, R., Lange, A., Meyer, H., et al. (2013). Systems-wide analysis and engineering of metabolic pathway fluxes in bio-succinate producing *Basfia succiniciproducens*. *Biotechnol Bioeng, 110*(11), 3013-3023.

Beckers, V., Poblete-Castro, I., Tomasch, J., & Wittmann, C. (2016). Integrated analysis of gene expression and metabolic fluxes in PHA-producing *Pseudomonas putida* grown on glycerol. *Microbial cell factories, 15*(1), 73.

Beganovic, S., Rückert-Reed, C., Sucipto, H., Shu, W., Gläser, L., Patschkowski, T., et al. (2023). Systems biology of industrial oxytetracycline production in *Streptomyces rimosus*: the secrets of a mutagenized hyperproducer. *Microbial cell factories, 22*(1), 222.

Belda, E., van Heck, R. G. A., José Lopez-Sanchez, M., Cruveiller, S., Barbe, V., Fraser, C., et al. (2016). The revisited genome of *Pseudomonas putida* KT2440 enlightens its value as a robust metabolic chassis. *Environmental microbiology, 18*(10), 3403-3424.

Benjamini, Y., & Hochberg, Y. (1995). Controlling the False Discovery Rate: A Practical and Powerful Approach to Multiple Testing. *Journal of the Royal Statistical Society: Series B (Methodological), 57*(1), 289-300.

Berger, A., Dohnt, K., Tielen, P., Jahn, D., Becker, J., & Wittmann, C. (2014). Robustness and Plasticity of Metabolic Pathway Flux among Uropathogenic Isolates of *Pseudomonas aeruginosa*. *PloS One, 9*(4), e88368.

Bergkessel, M., Basta, D. W., & Newman, D. K. (2016). The physiology of growth arrest: uniting molecular and environmental microbiology. *Nature Reviews Microbiology, 14*(9), 549-562.

Bitter, W., Tommassen, J., & Weisbeek, P. J. (1993). Identification and characterization of the *exbB*, *exbD* and *tonB* genes of *Pseudomonas putida* WCS358: their involvement in ferric-pseudobactin transport. *Mol Microbiol, 7*(1), 117-130.

Boas, J. V., Oliveira, V. B., Simões, M., & Pinto, A. M. F. R. (2022). Review on microbial fuel cells applications, developments and costs. *Journal of Environmental Management, 307*, 114525.

Boël, G., Smith, P. C., Ning, W., Englander, M. T., Chen, B., Hashem, Y., et al. (2014). The ABC-F protein EttA gates ribosome entry into the translation elongation cycle. *Nat Struct Mol Biol, 21*(2), 143-151.

Bolam, D. N., & van den Berg, B. (2018). TonB-dependent transport by the gut microbiota: novel aspects of an old problem. *Curr Opin Struct Biol, 51*, 35-43.

Bolten, C. J., Kiefer, P., Letisse, F., Portais, J. C., & Wittmann, C. (2007). Sampling for metabolome analysis of microorganisms. *Anal Chem, 79*(10), 3843-3849.

Bonneau, A., Roche, B., & Schalk, I. J. (2020). Iron acquisition in *Pseudomonas aeruginosa* by the siderophore pyoverdine: an intricate interacting network including periplasmic and membrane proteins. *Scientific Reports, 10*(1), 120.

Borrero-de Acuña, J. M., Gutierrez-Urrutia, I., Hidalgo-Dumont, C., Aravena-Carrasco, C., Orellana-Saez, M., Palominos-Gonzalez, N., et al. (2021). Channelling carbon flux through the meta-cleavage route for improved poly(3-hydroxyalkanoate) production from benzoate and lignin-based aromatics in *Pseudomonas putida* H. *Microbial biotechnology, 14*(6), 2385-2402.

Borrero-de Acuña, J. M., Rohde, M., Saldias, C., & Poblete-Castro, I. (2021). Fed-Batch mcl-Polyhydroxyalkanoates Production in *Pseudomonas putida* KT2440 and ΔphaZ Mutant on Biodiesel-Derived Crude Glycerol. *Frontiers in Bioengineering and Biotechnology, 9*(642023).

Bosire, E. M., Blank, L. M., & Rosenbaum, M. A. (2016). Strain- and Substrate-Dependent Redox Mediator and Electricity Production by *Pseudomonas aeruginosa*. *Applied and environmental microbiology, 82*(16), 5026-5038.

Brandenberg, O. F., Schubert, O. T., & Kruglyak, L. (2022). Towards synthetic PETtrophy: Engineering *Pseudomonas putida* for concurrent polyethylene terephthalate (PET) monomer metabolism and PET hydrolase expression. *Microbial cell factories, 21*(1), 119.

Bruinsma, L., Martin-Pascual, M., Kurnia, K., Tack, M., Hendriks, S., van Kranenburg, R., et al. (2023). Increasing cellular fitness and product yields in *Pseudomonas putida* through an engineered phosphoketolase shunt. *Microbial cell factories, 22*(1), 14.

Bujdoš, D., Popelářová, B., Volke, D. C., Nikel, P. I., Sonnenschein, N., & Dvořák, P. (2023). Engineering of *Pseudomonas putida* for accelerated co-utilization of glucose and cellobiose yields aerobic overproduction of pyruvate explained by an upgraded metabolic model. *Metabolic Engineering, 75*, 29-46.

Burgos, A. E., Belchior, J. C., & Sinisterra, R. D. (2002). Controlled release of rhodium (II) carboxylates and their association complexes with cyclodextrins from hydroxyapatite matrix. *Biomaterials, 23*(12), 2519-2526.

Butler, J. E., Kaufmann, F., Coppi, M. V., Núñez, C., & Lovley, D. R. (2004). MacA, a diheme c-type cytochrome involved in Fe(III) reduction by *Geobacter sulfurreducens*. *Journal of bacteriology, 186*(12), 4042-4045.

Carlson, C. A., & Ingraham, J. L. (1983). Comparison of denitrification by *Pseudomonas stutzeri*, *Pseudomonas aeruginosa*, and *Paracoccus denitrificans*. *Applied and environmental microbiology, 45*(4), 1247-1253.

Chen-Guang, L., Jin-Cheng, Q., & Yen-Han, L. (2017). Fermentation and Redox Potential. In A. F. Jozala (Ed.), *Fermentation Processes*: IntechOpen.

Chen, X., Jiang, S., Zheng, Z., Pan, L., & Luo, S. (2012). Effects of culture redox potential on succinic acid production by *Corynebacterium crenatum* under anaerobic conditions. *Process Biochemistry, 47*(8), 1250-1255.

Childers, S. E., Ciufo, S., & Lovley, D. R. (2002). *Geobacter metallireducens* accesses insoluble Fe(iii) oxide by chemotaxis. *Nature, 416*(6882), 767-769.

Chukwubuikem, A., Berger, C., Mady, A., & Rosenbaum, M. (2021). Role of phenazine-enzyme physiology for current generation in a bioelectrochemical system. *Microbial biotechnology, 14*.

Clifford, E. R., Bradley, R. W., Wey, L. T., Lawrence, J. M., Chen, X., Howe, C. J., et al. (2021). Phenazines as model low-midpoint potential electron shuttles for photosynthetic bioelectrochemical systems. *Chem Sci, 12*(9), 3328-3338.

Cook, T. B., Rand, J. M., Nurani, W., Courtney, D. K., Liu, S. A., & Pfleger, B. F. (2018). Genetic tools for reliable gene expression and recombineering in *Pseudomonas putida*. *Journal of industrial microbiology & biotechnology, 45*(7), 517-527.

Cornelis, P., & Bodilis, J. (2009). A survey of TonB-dependent receptors in fluorescent pseudomonads. *Environmental Microbiology Reports, 1*(4), 256-262.

Cornelis, P., & Matthijs, S. (2002). Diversity of siderophore-mediated iron uptake systems in fluorescent pseudomonads: not only pyoverdines. *Environmental microbiology, 4*(12), 787-798.

Crousilles, A., Dolan, S. K., Brear, P., Chirgadze, D. Y., & Welch, M. (2018). Gluconeogenic precursor availability regulates flux through the glyoxylate shunt in *Pseudomonas aeruginosa*. *Journal of Biological Chemistry, 293*(37), 14260-14269.

Culviner, P. H., Guegler, C. K., & Laub, M. T. (2020). A Simple, Cost-Effective, and Robust Method for rRNA Depletion in RNA-Sequencing Studies. *mBio, 11*(2), 10.1128/mbio.00010-00020.

Davies, K. J., Lloyd, D., & Boddy, L. (1989). The effect of oxygen on denitrification in *Paracoccus denitrificans* and *Pseudomonas aeruginosa*. *J Gen Microbiol, 135*(9), 2445-2451.

de Lorenzo, V., Pérez-Pantoja, D., & Nikel, P. I. (2024). *Pseudomonas putida* KT2440: the long journey of a soil-dweller to become a synthetic biology chassis. *Journal of bacteriology, 206*(7), e00136-00124.

de Lorenzo, V., & Timmis, K. N. (1994). Analysis and construction of stable phenotypes in gram-negative bacteria with Tn5- and Tn10-derived minitransposons. *Methods Enzymol, 235*, 386-405.

De Vrieze, J., Arends, J. B. A., Verbeeck, K., Gildemyn, S., & Rabaey, K. (2018). Interfacing anaerobic digestion with (bio)electrochemical systems: Potentials and challenges. *Water Research, 146*, 244-255.

del Castillo, T., Ramos, J. L., Rodríguez-Herva, J. J., Fuhrer, T., Sauer, U., & Duque, E. (2007). Convergent peripheral pathways catalyze initial glucose catabolism in *Pseudomonas putida*: genomic and flux analysis. *Journal of bacteriology, 189*(14), 5142-5152.

Demling, P., Ankenbauer, A., Klein, B., Noack, S., Tiso, T., Takors, R., et al. (2021). *Pseudomonas putida* KT2440 endures temporary oxygen limitations. *Biotechnology and Bioengineering, 118*(12), 4735-4750.

Dietrich, D., Jovanovic-Gasovic, S., Cao, P., Kohlstedt, M., & Wittmann, C. (2023). Refactoring the architecture of a polyketide gene cluster enhances docosahexaenoic acid production in *Yarrowia lipolytica* through improved expression and genetic stability. *Microbial cell factories, 22*(1), 023-02209.

Dolan, S. K., Kohlstedt, M., Trigg, S., Vallejo Ramirez, P., Kaminski, C. F., Wittmann, C., et al. (2020). Contextual Flexibility in *Pseudomonas aeruginosa* Central Carbon Metabolism during Growth in Single Carbon Sources. *mBio, 11*(2), e02684-02619.

Dolan, S. K., Wijaya, A., Kohlstedt, M., Gläser, L., Brear, P., Silva-Rocha, R., et al. (2022). Systems-Wide Dissection of Organic Acid Assimilation in *Pseudomonas aeruginosa* Reveals a Novel Path To Underground Metabolism. *mBio, 13*(6), e02541-02522.

Dong, Y., Li, Q., Geng, J., Cao, Q., Zhao, D., Jiang, M., et al. (2021). The TonB system in *Aeromonas hydrophila* NJ-35 is essential for MacA2B2 efflux pump-mediated macrolide resistance. *Veterinary Research, 52*(1), 63.

Dos Santos, V. A. P. M., Heim, S., Moore, E. R. B., Strätz, M., & Timmis, K. N. (2004). Insights into the genomic basis of niche specificity of *Pseudomonas putida* KT2440. *Environmental microbiology, 6*(12), 1264-1286.

Dowling, D. N., Pipke, R., & Dwyer, D. F. (1993). A DNA module encoding bph genes for the degradation of polychlorinated biphenyls (PCBs). *FEMS Microbiol Lett, 113*(2), 149-154.

Dvořák, P., Burýšková, B., Popelářová, B., Ebert, B. E., Botka, T., Bujdoš, D., et al. (2024). Synthetically-primed adaptation of *Pseudomonas putida* to a non-native substrate D-xylose. *Nature Communications, 15*(1), 2666.

Ebert, B. E., Kurth, F., Grund, M., Blank, L. M., & Schmid, A. (2011). Response of *Pseudomonas putida* KT2440 to increased NADH and ATP demand. *Applied and environmental microbiology, 77*(18), 6597-6605.

Espinosa-Urgel, M., Kolter, R., & Ramos, J. L. (2002). Root colonization by *Pseudomonas putida*: love at first sight. *Microbiology, 148*(Pt 2), 341-343.

Espinosa-Urgel, M., Salido, A., & Ramos, J. L. (2000). Genetic analysis of functions involved in adhesion of *Pseudomonas putida* to seeds. *Journal of bacteriology, 182*(9), 2363-2369.

Firer-Sherwood, M., Pulcu, G. S., & Elliott, S. J. (2008). Electrochemical interrogations of the Mtr cytochromes from *Shewanella*: opening a potential window. *J Biol Inorg Chem, 13*(6), 849-854.

Franden, M. A., Jayakody, L. N., Li, W.-J., Wagner, N. J., Cleveland, N. S., Michener, W. E., et al. (2018). Engineering *Pseudomonas putida* KT2440 for efficient ethylene glycol utilization. *Metabolic Engineering, 48*, 197-207.

Fruehauf, H. M., Enzmann, F., Harnisch, F., Ulber, R., & Holtmann, D. (2020). Microbial Electrosynthesis-An Inventory on Technology Readiness Level and Performance of Different Process Variants. *Biotechnol J, 15*(10), 31.

Fujita, M., Mori, K., Hara, H., Hishiyama, S., Kamimura, N., & Masai, E. (2019). A TonB-dependent receptor constitutes the outer membrane transport system for a lignin-derived aromatic compound. *Communications Biology, 2*(1), 432.

García-Angulo, V. A. (2017). Overlapping riboflavin supply pathways in bacteria. *Critical Reviews in Microbiology, 43*(2), 196-209.

Gemünde, A., Lai, B., Pause, L., Krömer, J., & Holtmann, D. (2022). Redox Mediators in Microbial Electrochemical Systems. *ChemElectroChem, 9*(13), e202200216.

Gemünde, A., Ruppert, N.-L., & Holtmann, D. (2024). Unraveling the Electron Transfer in *Cupriavidus necator* – Insights Into Mediator Reduction Mechanics. *ChemElectroChem, 11*(14), e202400273.

Gibson, D. G., Young, L., Chuang, R. Y., Venter, J. C., Hutchison, C. A., 3rd, & Smith, H. O. (2009). Enzymatic assembly of DNA molecules up to several hundred kilobases. *Nature Methods, 6*(5), 343-345.

Gläser, L., Kuhl, M., Jovanovic, S., Fritz, M., Vögeli, B., Erb, T. J., et al. (2020). A common approach for absolute quantification of short chain CoA thioesters in prokaryotic and eukaryotic microbes. *Microbial cell factories, 19*(1), 160.

Godoy, P., Ramos-González, M.-I., & Ramos, J. L. (2004). *Pseudomonas putida* mutants in the *exbBexbDtonB* gene cluster are hypersensitive to environmental and chemical stressors. *Environmental microbiology, 6*(6), 605-610.

Godoy, P., Ramos-González, M. I., & Ramos, J. L. (2001). Involvement of the TonB system in tolerance to solvents and drugs in *Pseudomonas putida* DOT-T1E. *Journal of bacteriology, 183*(18), 5285-5292.

Gorby, Y. A., Yanina, S., McLean, J. S., Rosso, K. M., Moyles, D., Dohnalkova, A., et al. (2006). Electrically conductive bacterial nanowires produced by *Shewanella oneidensis* strain MR-1 and other microorganisms. *Proceedings of the National Academy of Sciences of the United States of America, 103*(30), 11358-11363.

Hancock, R. E., & Wong, P. G. (1984). Compounds which increase the permeability of the *Pseudomonas aeruginosa* outer membrane. *Antimicrob Agents Chemother, 26*(1), 48-52.

Hannon, J., Bakker, A., Lynd, L., & Wyman, C. E. (2007). Comparing the scale-up of anaerobic and aerobic processes *Annual Meeting of the American Institute of Chemical Engineers*. Salt Lake City.

Härtig, C., Loffhagen, N., & Harms, H. (2005). Formation of *trans* fatty acids is not involved in growth-linked membrane adaptation of *Pseudomonas putida*. *Applied and environmental microbiology, 71*(4), 1915-1922.

Hartney, S. L., Mazurier, S., Kidarsa, T. A., Quecine, M. C., Lemanceau, P., & Loper, J. E. (2011). TonB-dependent outer-membrane proteins and siderophore utilization in *Pseudomonas fluorescens* Pf-5. *BioMetals, 24*(2), 193-213.

Heipieper, H. J., & de Bont, J. A. (1994). Adaptation of *Pseudomonas putida* S12 to ethanol and toluene at the level of fatty acid composition of membranes. *Applied and environmental microbiology, 60*(12), 4440-4444.

Heipieper, H. J., Meinhardt, F., & Segura, A. (2003). The *cis-trans* isomerase of unsaturated fatty acids in *Pseudomonas* and *Vibrio*: biochemistry, molecular biology and physiological function of a unique stress adaptive mechanism. *FEMS Microbiol Lett, 229*(1), 1-7.

Helander, I. M., & Mattila-Sandholm, T. (2000). Fluorometric assessment of Gram-negative bacterial permeabilization. *Journal of Applied Microbiology, 88*(2), 213-219.

Hernandez, C. A., & Osma, J. F. (2020). Microbial Electrochemical Systems: Deriving Future Trends From Historical Perspectives and Characterization Strategies. *Frontiers in Environmental Science, 8*(44).

Hintermayer, S., Yu, S., Krömer, J. O., & Weuster-Botz, D. (2016). Anodic respiration of *Pseudomonas putida* KT2440 in a stirred-tank bioreactor. *Biochemical Engineering Journal, 115*, 1-13.

IUPAC. (1997). *The IUPAC Gold Book* (2nd ed.). Oxford: Blackwell Scientific Publications.

Jones, S., White, J., Aden, A., Werpy, T., Petersen, G., Bozell, J., et al. (2004). Top Value Added Chemicals From Biomass. Volume I - Results of Screening for Potential Candidates From Sugars and Synthesis Gas. *U.S. D. o. Energy*, 1-76.

Jovanovic Gasovic, S., Dietrich, D., Gläser, L., Cao, P., Kohlstedt, M., & Wittmann, C. (2023). Multi-omics view of recombinant *Yarrowia lipolytica*: Enhanced ketogenic amino acid catabolism increases polyketide-synthase-driven docosahexaenoic production to high selectivity at the gram scale. *Metab Eng, 80*, 45-65.

Kadier, A., Simayi, Y., Abdeshahian, P., Azman, N. F., Chandrasekhar, K., & Kalil, M. S. (2016). A comprehensive review of microbial electrolysis cells (MEC) reactor designs and configurations for sustainable hydrogen gas production. *Alexandria Engineering Journal, 55*(1), 427-443.

Kampers, L. F. C., Koehorst, J. J., van Heck, R. J. A., Suarez-Diez, M., Stams, A. J. M., & Schaap, P. J. (2021). A metabolic and physiological design study of *Pseudomonas putida* KT2440 capable of anaerobic respiration. *BMC Microbiology, 21*(1), 9.

Kampers, L. F. C., Volkers, R. J. M., & Martins Dos Santos, V. A. P. (2019). *Pseudomonas putida* KT2440 is HV1 certified, not GRAS. *12*(5), 845-848.

Kastner, J. R., Eiteman, M. A., & Lee, S. A. (2003). Effect of redox potential on stationary-phase xylitol fermentations using *Candida tropicalis*. *Applied microbiology and biotechnology, 63*(1), 96-100.

Kiil, K., Binnewies, T. T., Willenbrock, H., Hansen, S. K., Yang, L., Jelsbak, L., et al. (2008). Comparative Genomics of *Pseudomonas Pseudomonas* (pp. 1-24).

Kim, C., Kim, M. Y., Michie, I., Jeon, B. H., Premier, G. C., Park, S., et al. (2017). Anodic electro-fermentation of 3-hydroxypropionic acid from glycerol by recombinant *Klebsiella pneumoniae* L17 in a bioelectrochemical system. *Biotechnology for biofuels, 10*(199), 017-0886.

Kim, H. J., Park, H. S., Hyun, M. S., Chang, I. S., Kim, M., & Kim, B. H. (2002). A mediator-less microbial fuel cell using a metal reducing bacterium, *Shewanella putrefaciens*. *Enzyme and Microbial Technology, 30*(2), 145-152.

Klebba, P. E., Newton, S. M. C., Six, D. A., Kumar, A., Yang, T., Nairn, B. L., et al. (2021). Iron Acquisition Systems of Gram-negative Bacterial Pathogens Define TonB-Dependent Pathways to Novel Antibiotics. *Chem Rev, 121*(9), 5193-5239.

Kohlstedt, M., Starck, S., Barton, N., Stolzenberger, J., Selzer, M., Mehlmann, K., et al. (2018). From lignin to nylon: Cascaded chemical and biochemical conversion using metabolically engineered *Pseudomonas putida*. *Metabolic Engineering, 47*, 279-293.

Kohlstedt, M., Weimer, A., Weiland, F., Stolzenberger, J., Selzer, M., Sanz, M., et al. (2022). Biobased PET from lignin using an engineered *cis*, *cis*-muconate-producing *Pseudomonas putida* strain with superior robustness, energy and redox properties. *Metabolic Engineering, 72*, 337-352.

Kohlstedt, M., & Wittmann, C. (2019). GC-MS-based $^{13}C$ metabolic flux analysis resolves the parallel and cyclic glucose metabolism of *Pseudomonas putida* KT2440 and *Pseudomonas aeruginosa* PAO1. *Metab Eng, 54*, 35-53.

Kotloski, N., J., & Gralnick, J., A. (2013). Flavin Electron Shuttles Dominate Extracellular Electron Transfer by *Shewanella oneidensis*. *mBio, 4*(1), 10.1128/mbio.00553-00512.

Kracke, F., & Krömer, J. O. (2014). Identifying target processes for microbial electrosynthesis by elementary mode analysis. *BMC Bioinformatics, 15*(1), 014-0410.

Kracke, F., Lai, B., Yu, S., & Krömer, J. O. (2018). Balancing cellular redox metabolism in microbial electrosynthesis and electro fermentation – A chance for metabolic engineering. *Metabolic Engineering, 45*, 109-120.

Lai, B., Bernhardt, P. V., & Krömer, J. O. (2020). Cytochrome c Reductase is a Key Enzyme Involved in the Extracellular Electron Transfer Pathway towards Transition Metal Complexes in *Pseudomonas Putida*. *ChemSusChem, 13*(19), 5308-5317.

Lai, B., Nguyen, A. V., & Krömer, J. O. (2019). Characterizing the Anoxic Phenotype of *Pseudomonas putida* Using a Bioelectrochemical System. *Methods and protocols, 2*(2), 26.

Lai, B., Yu, S., Bernhardt, P. V., Rabaey, K., Virdis, B., & Krömer, J. O. (2016). Anoxic metabolism and biochemical production in *Pseudomonas putida* F1 driven by a bioelectrochemical system. *Biotechnology for biofuels, 9*, 39-39.

Lange, A., Becker, J., Schulze, D., Cahoreau, E., Portais, J. C., Haefner, S., et al. (2017). Bio-based succinate from sucrose: High-resolution $^{13}C$ metabolic flux analysis and metabolic engineering of the rumen bacterium *Basfia succiniciproducens*. *Metabolic Engineering, 44*, 198-212.

Lessie, T. G., & Phibbs, P. V. (1984). ALTERNATIVE PATHWAYS OF CARBOHYDRATE UTILIZATION IN PSEUDOMONADS. *Annual Review of Microbiology, 38*(Volume 38), 359-388.

Li, J., Jiang, M., Chen, K.-Q., Ye, Q., Shang, L.-A., Wei, P., et al. (2010). Effect of redox potential regulation on succinic acid production by *Actinobacillus succinogenes*. *Bioprocess and Biosystems Engineering, 33*(8), 911-920.

Li, K., Mao, X., Liu, L., Lin, J., Sun, M., Wei, D., et al. (2016). Overexpression of membrane-bound gluconate-2-dehydrogenase to enhance the production of 2-keto-d-gluconic acid by *Gluconobacter oxydans*. *Microbial cell factories, 15*(1), 121.

Liu, H., Chen, Z., Cui, J.-Q., Ntakirutimana, S., Xu, T., Liu, Z.-H., et al. (2024). Funneling lignin hydrolysates into β-ketoadipic acid by engineered *Pseudomonas putida* KT2440. *Industrial Crops and Products, 218*, 118956.

Liu, H., Grot, S., & Logan, B. E. (2005). Electrochemically Assisted Microbial Production of Hydrogen from Acetate. *Environmental Science & Technology, 39*(11), 4317-4320.

Loeschcke, A., & Thies, S. (2015). *Pseudomonas putida*-a versatile host for the production of natural products. *Applied microbiology and biotechnology, 99*(15), 6197-6214.

Loffhagen, N., Härtig, C., & Babel, W. (1995). Fatty acid patterns of *Acinetobacter calcoaceticus* 69-V indicate sensitivity against xenobiotics. *Applied microbiology and biotechnology, 44*(3), 526-531.

Logan, B. E., Call, D., Cheng, S., Hamelers, H. V. M., Sleutels, T. H. J. A., Jeremiasse, A. W., et al. (2008). Microbial Electrolysis Cells for High Yield Hydrogen Gas Production from Organic Matter. *Environmental Science & Technology, 42*(23), 8630-8640.

Loh, B., Grant, C., & Hancock, R. E. (1984). Use of the fluorescent probe 1-N-phenylnaphthylamine to study the interactions of aminoglycoside antibiotics with the outer membrane of *Pseudomonas aeruginosa*. *Antimicrob Agents Chemother, 26*(4), 546-551.

Lovley, D. R. (1993). Dissimilatory metal reduction. *Annu Rev Microbiol, 47*, 263-290.

Lovley, D. R. (2008). The microbe electric: conversion of organic matter to electricity. *Current opinion in biotechnology, 19*(6), 564-571.

Löwe, H., Schmauder, L., Hobmeier, K., Kremling, A., & Pflüger-Grau, K. (2017). Metabolic engineering to expand the substrate spectrum of *Pseudomonas putida* toward sucrose. *MicrobiologyOpen, 6*(4), e00473.

Luscher, A., Moynié, L., Auguste, P. S., Bumann, D., Mazza, L., Pletzer, D., et al. (2018). TonB-Dependent Receptor Repertoire of *Pseudomonas aeruginosa* for Uptake of Siderophore-Drug Conjugates. *Antimicrob Agents Chemother, 62*(6), 00097-00018.

Malvankar, N. S., & Lovley, D. R. (2012). Microbial Nanowires: A New Paradigm for Biological Electron Transfer and Bioelectronics. *ChemSusChem, 5*(6), 1039-1046.

Marini, J. L., & Saxena, S. S. (2017).

Marsili, E., Baron, D. B., Shikhare, I. D., Coursolle, D., Gralnick, J. A., & Bond, D. R. (2008). *Shewanella* secretes flavins that mediate extracellular electron transfer. *Proceedings of the National Academy of Sciences of the United States of America, 105*(10), 3968-3973.

Martínez-García, E., & de Lorenzo, V. (2011). Engineering multiple genomic deletions in Gram-negative bacteria: analysis of the multi-resistant antibiotic profile of *Pseudomonas putida* KT2440. *Environmental microbiology, 13*(10), 2702-2716.

Martinez-Garcia, E., Fraile, S., Rodriguez-Espeso, D., Vecchietti, D., Bertoni, G., & de Lorenzo, V. (2020). The naked cell: emerging properties of a surfome-streamlined *Pseudomonas putida* strain. *bioRxiv*, 2020.2005.2017.100628.

Martínez-García, E., Nikel, P. I., Aparicio, T., & de Lorenzo, V. (2014). *Pseudomonas* 2.0: genetic upgrading of *P. putida* KT2440 as an enhanced host for heterologous gene expression. *Microbial cell factories, 13*, 159-159.

Matilla, M. A., & Krell, T. (2018). Plant Growth Promotion and Biocontrol Mediated by Plant-Associated Bacteria. In D. Egamberdieva & P. Ahmad (Eds.), *Plant Microbiome: Stress Response* (pp. 45-80). Singapore: Springer Singapore.

Matilla, M. A., Ramos, J. L., Bakker, P. A. H. M., Doornbos, R., Badri, D. V., Vivanco, J. M., et al. (2010). *Pseudomonas putida* KT2440 causes induced systemic resistance and changes in Arabidopsis root exudation. *Environmental Microbiology Reports, 2*(3), 381-388.

McAnulty, M. J., & Wood, T. K. (2014). YeeO from *Escherichia coli* exports flavins. *Bioengineered, 5*(6), 386-392.

Mehtiö, T., Toivari, M., Wiebe, M. G., Harlin, A., Penttilä, M., & Koivula, A. (2016). Production and applications of carbohydrate-derived sugar acids as generic biobased chemicals. *Crit Rev Biotechnol, 36*(5), 904-916.

Millard, P., Enjalbert, B., Uttenweiler-Joseph, S., Portais, J. C., & Létisse, F. (2021). Control and regulation of acetate overflow in *Escherichia coli*. *Elife, 15*(10), 63661.

Molina, L., La Rosa, R., Nogales, J., & Rojo, F. (2019). Influence of the Crc global regulator on substrate uptake rates and the distribution of metabolic fluxes in *Pseudomonas putida* KT2440 growing in a complete medium. *Environmental microbiology, 21*(11), 4446-4459.

Moscoviz, R., Toledo-Alarcón, J., Trably, E., & Bernet, N. (2016). Electro-Fermentation: How To Drive Fermentation Using Electrochemical Systems. *Trends in Biotechnology, 34*(11), 856-865.

Nadal-Rey, G., McClure, D. D., Kavanagh, J. M., Cassells, B., Cornelissen, S., Fletcher, D. F., et al. (2022). Computational fluid dynamics modelling of hydrodynamics, mixing and oxygen transfer in industrial bioreactors with Newtonian broths. *Biochemical Engineering Journal, 177*, 108265.

Nakazawa, T. (2002). Travels of a *Pseudomonas*, from Japan around the world. *Environmental microbiology, 4*(12), 782-786.

Nakazawa, T., & Yokota, T. (1973). Benzoate metabolism in *Pseudomonas putida*(*arvilla*) mt-2: demonstration of two benzoate pathways. *Journal of bacteriology, 115*(1), 262-267.

Nelson, K. E., Weinel, C., Paulsen, I. T., Dodson, R. J., Hilbert, H., Martins dos Santos, V. A. P., et al. (2002). Complete genome sequence and comparative analysis of the metabolically versatile *Pseudomonas putida* KT2440. *Environmental microbiology, 4*(12), 799-808.

Nguyen, A. V., Lai, B., Adrian, L., & Krömer, J. O. (2021). The anoxic electrode-driven fructose catabolism of *Pseudomonas putida* KT2440. *Microbial biotechnology*.

Nielsen, J., Tillegreen, C. B., & Petranovic, D. (2022). Innovation trends in industrial biotechnology. *Trends in Biotechnology, 40*(10), 1160-1172.

Niessen, J., Schröder, U., Harnisch, F., & Scholz, F. (2005). Gaining electricity from in situ oxidation of hydrogen produced by fermentative cellulose degradation. *Letters in Applied Microbiology, 41*(3), 286-290.

Nikaido, H. (1989). Outer membrane barrier as a mechanism of antimicrobial resistance. *Antimicrob Agents Chemother, 33*(11), 1831-1836.

Nikaido, H. (1994). Porins and specific diffusion channels in bacterial outer membranes. *The Journal of biological chemistry, 269*(6), 3905-3908.

Nikaido, H. (2003). Molecular Basis of Bacterial Outer Membrane Permeability Revisited. *Microbiology and Molecular Biology Reviews, 67*(4), 593-656.

Nikel, P. I., Chavarría, M., Danchin, A., & de Lorenzo, V. (2016). From dirt to industrial applications: *Pseudomonas putida* as a Synthetic Biology chassis for hosting harsh biochemical reactions. *Current Opinion in Chemical Biology, 34*, 20-29.

Nikel, P. I., Chavarria, M., Fuhrer, T., Sauer, U., & de Lorenzo, V. (2015). *Pseudomonas putida* KT2440 Strain Metabolizes Glucose through a Cycle Formed by Enzymes of the Entner-Doudoroff, Embden-Meyerhof-Parnas, and Pentose Phosphate Pathways. *The Journal of biological chemistry, 290*(43), 25920-25932.

Nikel, P. I., & de Lorenzo, V. (2013). Engineering an anaerobic metabolic regime in *Pseudomonas putida* KT2440 for the anoxic biodegradation of 1,3-dichloroprop-1-ene. *Metab Eng, 15*, 98-112.

Nikel, P. I., & de Lorenzo, V. (2018). *Pseudomonas putida* as a functional chassis for industrial biocatalysis: From native biochemistry to trans-metabolism. *Metabolic Engineering, 50*, 142-155.

Nikel, P. I., Fuhrer, T., Chavarría, M., Sánchez-Pascuala, A., Sauer, U., & de Lorenzo, V. (2021). Reconfiguration of metabolic fluxes in *Pseudomonas putida* as a response to sub-lethal oxidative stress. *The ISME Journal*.

Nikel, P. I., Martínez-García, E., & de Lorenzo, V. (2014). Biotechnological domestication of pseudomonads using synthetic biology. *Nat Rev Microbiol, 12*(5), 368-379.

Nogales, J., Mueller, J., Gudmundsson, S., Canalejo, F. J., Duque, E., Monk, J., et al. (2020). High-quality genome-scale metabolic modelling of *Pseudomonas putida* highlights its broad metabolic capabilities. *Environmental microbiology, 22*(1), 255-269.

Noinaj, N., Guillier, M., Barnard, T. J., & Buchanan, S. K. (2010). TonB-dependent transporters: regulation, structure, and function. *Annu Rev Microbiol, 64*, 43-60.

Okuyama, H., Sasaki, S., Higashi, S., & Murata, N. (1990). A *trans*-unsaturated fatty acid in a psychrophilic bacterium, *Vibrio* sp. strain ABE-1. *Journal of bacteriology, 172*(6), 3515-3518.

Olavarria, K., Marone, M. P., da Costa Oliveira, H., Roncallo, J. C., da Costa Vasconcelos, F. N., da Silva, L. F., et al. (2015). Quantifying NAD(P)H production in the upper Entner–Doudoroff pathway from *Pseudomonas putida* KT2440. *FEBS Open Bio, 5*(1), 908-915.

Pappenberger, G., & Hohmann, H. P. (2014). Industrial production of L-ascorbic Acid (vitamin C) and D-isoascorbic acid. *Adv Biochem Eng Biotechnol, 143*, 143-188.

Pause, L., Weimer, A., Wirth, N. T., Nguyen, A. V., Lenz, C., Kohlstedt, M., et al. (2023). Anaerobic glucose uptake in *Pseudomonas putida* KT2440 in a bioelectrochemical system. *Microbial biotechnology, 17*, e14375.

Pedrotta, V., & Witholt, B. (1999). Isolation and characterization of the *cis*-*trans*-unsaturated fatty acid isomerase of *Pseudomonas oleovorans* GPo12. *Journal of bacteriology, 181*(10), 3256-3261.

Pei, J., Zhou, Q., Jing, Q., Li, L., Dai, C., Li, H., et al. (2011). The mechanism for regulating ethanol fermentation by redox levels in *Thermoanaerobacter ethanolicus*. *Metab Eng, 13*(2), 186-193.

Poblete-Castro, I., Becker, J., Dohnt, K., dos Santos, V. M., & Wittmann, C. (2012). Industrial biotechnology of *Pseudomonas putida* and related species. *Applied microbiology and biotechnology, 93*(6), 2279-2290.

Poblete-Castro, I., Binger, D., Oehlert, R., & Rohde, M. (2014). Comparison of mcl-Poly(3-hydroxyalkanoates) synthesis by different *Pseudomonas putida* strains from crude glycerol: citrate accumulates at high titer under PHA-producing conditions. *BMC Biotechnology, 14*(1), 962.

Poole, K., Zhao, Q., Neshat, S., Heinrichs, D. E., & Dean, C. R. (1996). The *Pseudomonas aeruginosa tonB* gene encodes a novel TonB protein. *Microbiology, 142*(6), 1449-1458.

Potter, M. C., & Waller, A. D. (1911). Electrical effects accompanying the decomposition of organic compounds. *Proceedings of the Royal Society of London. Series B, Containing Papers of a Biological Character, 84*(571), 260-276.

Prévoteau, A., Carvajal-Arroyo, J. M., Ganigué, R., & Rabaey, K. (2020). Microbial electrosynthesis from $CO_2$: forever a promise? *Current opinion in biotechnology, 62*, 48-57.

Puchałka, J., Oberhardt, M. A., Godinho, M., Bielecka, A., Regenhardt, D., Timmis, K. N., et al. (2008). Genome-scale reconstruction and analysis of the *Pseudomonas putida* KT2440 metabolic network facilitates applications in biotechnology. *PLoS computational biology, 4*(10), e1000210-e1000210.

Rabaey, K., Boon, N., Höfte, M., & Verstraete, W. (2005). Microbial phenazine production enhances electron transfer in biofuel cells. *Environmental Science & Technology, 39*(9), 3401-3408.

Rabaey, K., Rodríguez, J., Blackall, L. L., Keller, J., Gross, P., Batstone, D., et al. (2007). Microbial ecology meets electrochemistry: electricity-driven and driving communities. *The ISME Journal, 1*(1), 9-18.

Reva, O. N., Weinel, C., Weinel, M., Böhm, K., Stjepandic, D., Hoheisel, J. D., et al. (2006). Functional genomics of stress response in *Pseudomonas putida* KT2440. *Journal of bacteriology, 188*(11), 4079-4092.

Rohles, C. M., Glaser, L., Kohlstedt, M., Giesselmann, G., Pearson, S., del Campo, A., et al. (2018). A bio-based route to the carbon-5 chemical glutaric acid and to bionylon-6,5 using metabolically engineered *Corynebacterium glutamicum*. *Green Chemistry, 20*(20), 4662-4674.

Rosa, L., Hunger, S., Zschernitz, T., Strehlitz, B., & Harnisch, F. (2019). Integrating Electrochemistry Into Bioreactors: Effect of the Upgrade Kit on Mass Transfer, Mixing Time and Sterilizability. *Frontiers in Energy Research, 7*.

Rosenow, C., Saxena, R. M., Durst, M., & Gingeras, T. R. (2001). Prokaryotic RNA preparation methods useful for high density array analysis: comparison of two approaches. *Nucleic acids research, 29*(22), e112-e112.

Rouquette-Loughlin, C., Stojiljkovic, I., Hrobowski, T., Balthazar Jacqueline, T., & Shafer William, M. (2002). Inducible, but Not Constitutive, Resistance of *Gonococci* to Hydrophobic Agents Due to the MtrC-MtrD-MtrE Efflux Pump Requires TonB-ExbB-ExbD Proteins. *Antimicrobial Agents and Chemotherapy, 46*(2), 561-565.

Rozendal, R. A., Hamelers, H. V. M., Euverink, G. J. W., Metz, S. J., & Buisman, C. J. N. (2006). Principle and perspectives of hydrogen production through biocatalyzed electrolysis. *International Journal of Hydrogen Energy, 31*(12), 1632-1640.

Sakhtah, H., Koyama, L., Zhang, Y., Morales, D. K., Fields, B. L., Price-Whelan, A., et al. (2016). The *Pseudomonas aeruginosa* efflux pump MexGHI-OpmD transports a natural phenazine that controls gene expression and biofilm development. *Proceedings of the National Academy of Sciences of the United States of America, 113*(25), 6.

Sambrook, J., Fritsch, E. F., & Maniatis, T. (1989). *Molecular cloning: a laboratory manual*: Cold spring harbor laboratory press.

Sánchez-Pascuala, A., Fernández-Cabezón, L., de Lorenzo, V., & Nikel, P. I. (2019). Functional implementation of a linear glycolysis for sugar catabolism in *Pseudomonas putida*. *Metabolic Engineering, 54*, 200-211.

Sasnow, S. S., Wei, H., & Aristilde, L. (2016). Bypasses in intracellular glucose metabolism in iron-limited *Pseudomonas putida*. *MicrobiologyOpen, 5*(1), 3-20.

Schmitz, S., Nies, S., Wierckx, N., Blank, L. M., & Rosenbaum, M. A. (2015). Engineering mediator-based electroactivity in the obligate aerobic bacterium *Pseudomonas putida* KT2440. *Frontiers in microbiology, 6*(284).

Schröder, U. (2011). Discover the possibilities: microbial bioelectrochemical systems and the revival of a 100-year–old discovery. *Journal of Solid State Electrochemistry, 15*(7), 1481-1486.

Sciarria, T. P., Batlle-Vilanova, P., Colombo, B., Scaglia, B., Balaguer, M. D., Colprim, J., et al. (2018). Bio-electrorecycling of carbon dioxide into bioplastics. *Green Chemistry, 20*(17), 4058-4066.

Scott, K., & Yu, E. H. (2015). *Microbial Electrochemical and Fuel Cells: Fundamentals and Applications*: Elsevier Science.

Seidel, K., Kühnert, J., & Adrian, L. (2018). The Complexome of *Dehalococcoides mccartyi* Reveals Its Organohalide Respiration-Complex Is Modular. *Frontiers in microbiology, 9*(1130).

Short, K. A., King, R. J., Seidler, R. J., & Olsen, R. H. (1992). Biodegradation of phenoxyacetic acid in soil by *Pseudomonas putida* PP0301(pR0103), a constitutive degrader of 2,4-dichlorophenoxyacetate. *Mol Ecol, 1*(2), 89-94.

Silva-Rocha, R., Martínez-García, E., Calles, B., Chavarría, M., Arce Rodríguez, A., De las Heras, A., et al. (2012). The Standard European Vector Architecture (SEVA): A coherent platform for the analysis and deployment of complex prokaryotic phenotypes. *Nucleic acids research, 41*.

Soh, S. M., Lee, D.-G., & Mitchell, R. J. (2020). Enhanced microbial fuel cell (MFC) power outputs through Membrane Permeabilization using a branched polyethyleneimine. *Biosensors and Bioelectronics, 170*, 112623.

Sohn, S. B., Kim, T. Y., Park, J. M., & Lee, S. Y. (2010). In silico genome-scale metabolic analysis of *Pseudomonas putida* KT2440 for polyhydroxyalkanoate synthesis, degradation of aromatics and anaerobic survival. *Biotechnol J, 5*(7), 739-750.

Son, J., Lim, S. H., Kim, Y. J., Lim, H. J., Lee, J. Y., Jeong, S., et al. (2023). Customized valorization of waste streams by *Pseudomonas putida*: State-of-the-art, challenges, and future trends. *Bioresource technology, 371*, 128607.

Steen, A., Utkur, F. O., Borrero-de Acuna, J. M., Bunk, B., Roselius, L., Buhler, B., et al. (2013). Construction and characterization of nitrate and nitrite respiring *Pseudomonas putida* KT2440 strains for anoxic biotechnical applications. *Journal of biotechnology, 163*(2), 155-165.

Stegmüller, J., Rodríguez Estévez, M., Shu, W., Gläser, L., Myronovskyi, M., Rückert-Reed, C., et al. (2024). Systems metabolic engineering of the primary and secondary metabolism of *Streptomyces albidoflavus* enhances production of the reverse antibiotic nybomycin against multi-resistant *Staphylococcus aureus*. *Metab Eng, 81*, 123-143.

Stouthamer, A. H., & Bettenhaussen, C. (1973). Utilization of energy for growth and maintenance in continuous and batch cultures of microorganisms: A reevaluation of the method for the determination of ATP production by measuring molar growth yields. *Biochimica et Biophysica Acta (BBA) - Reviews on Bioenergetics, 301*(1), 53-70.

Sun, L., Wang, D. M., Sun, W. J., Cui, F. J., Gong, J. S., Zhang, X. M., et al. (2020). Two-Stage Semi-Continuous 2-Keto-Gluconic Acid (2KGA) Production by *Pseudomonas plecoglossicida* JUIM01 From Rice Starch Hydrolyzate. *Frontiers in Bioengineering and Biotechnology, 8*(120).

Sun, Y., Kokko, M., & Vassilev, I. (2023). Anode-assisted electro-fermentation with *Bacillus subtilis* under oxygen-limited conditions. *Biotechnology for Biofuels and Bioproducts, 16*(1), 6.

Tempest, D. W., & Neijssel, O. M. (1984). The status of YATP and maintenance energy as biologically interpretable phenomena. *Annual Review of Microbiology, 38*(Volume 38), 459-513.

Thomas, G. H. (2017). On the pull: periplasmic trapping of sugars before transport. *Mol Microbiol, 104*(6), 883-888.

Thormann, K. M., Saville, R. M., Shukla, S., Pelletier, D. A., & Spormann, A. M. (2004). Initial Phases of Biofilm Formation in *Shewanella oneidensis* MR-1. *Journal of bacteriology, 186*(23), 8096-8104.

Timmis, K. N. (2002). *Pseudomonas putida*: a cosmopolitan opportunist par excellence. *Environmental microbiology, 4*(12), 779-781.

Tokic, M., Hatzimanikatis, V., & Miskovic, L. (2020). Large-scale kinetic metabolic models of *Pseudomonas putida* KT2440 for consistent design of metabolic engineering strategies. *Biotechnology for biofuels, 13*(1), 33.

Träuble, H., & Overath, P. (1973). The structure of *Escherichia coli* membranes studied by fluorescence measurements of lipid phase transitions. *Biochim Biophys Acta, 307*(3), 491-512.

Trösch, R., & Willmund, F. (2019). The conserved theme of ribosome hibernation: from bacteria to chloroplasts of plants. *Biological Chemistry, 400*(7), 879-893.

Trunk, K., Benkert, B., Quäck, N., Münch, R., Scheer, M., Garbe, J., et al. (2010). Anaerobic adaptation in *Pseudomonas aeruginosa*: definition of the Anr and Dnr regulons. *Environmental microbiology, 12*(6), 1719-1733.

Tyanova, S., Temu, T., Sinitcyn, P., Carlson, A., Hein, M. Y., Geiger, T., et al. (2016). The Perseus computational platform for comprehensive analysis of (prote)omics data. *Nature Methods, 13*(9), 731-740.

Ugidos, A., Morales, G., Rial, E., Williams, H. D., & Rojo, F. (2008). The coordinate regulation of multiple terminal oxidases by the *Pseudomonas putida* ANR global regulator. *Environmental microbiology, 10*(7), 1690-1702.

van Duuren, J. B. J. H., Puchałka, J., Mars, A. E., Bücker, R., Eggink, G., Wittmann, C., et al. (2013). Reconciling in vivo and in silico key biological parameters of *Pseudomonas putida* KT2440 during growth on glucose under carbon-limited condition. *BMC Biotechnology, 13*(1), 93.

van Winden, W. A., Wittmann, C., Heinzle, E., & Heijnen, J. J. (2002). Correcting mass isotopomer distributions for naturally occurring isotopes. *Biotechnol Bioeng, 80*(4), 477-479.

Vander Wauven, C., Piérard, A., Kley-Raymann, M., & Haas, D. (1984). *Pseudomonas aeruginosa* mutants affected in anaerobic growth on arginine: evidence for a four-gene cluster encoding the arginine deiminase pathway. *Journal of bacteriology, 160*(3), 928-934.

Vardon, D. R., Franden, M. A., Johnson, C. W., Karp, E. M., Guarnieri, M. T., Linger, J. G., et al. (2015). Adipic acid production from lignin. *Energy & Environmental Science, 8*(2), 617-628.

Vassilev, I., Averesch, N. J. H., Ledezma, P., & Kokko, M. (2021). Anodic electro-fermentation: Empowering anaerobic production processes via anodic respiration. *Biotechnology advances, 48*, 107728.

Vassilev, I., Gießelmann, G., Schwechheimer, S. K., Wittmann, C., Virdis, B., & Krömer, J. O. (2018). Anodic electro-fermentation: Anaerobic production of L-Lysine by recombinant *Corynebacterium glutamicum*. *Biotechnology and Bioengineering, 115*(6), 1499-1508.

Vassilev, I., Hernandez, P. A., Batlle-Vilanova, P., Freguia, S., Krömer, J. O., Keller, J., et al. (2018). Microbial Electrosynthesis of Isobutyric, Butyric, Caproic Acids, and Corresponding Alcohols from Carbon Dioxide. *ACS Sustainable Chemistry & Engineering, 6*(7), 8485-8493.

Virdis, B., Hoelzle, R. D., Marchetti, A., Boto, S. T., Rosenbaum, M. A., Blasco-Gómez, R., et al. (2022). Electro-fermentation: Sustainable bioproductions steered by electricity. *Biotechnology advances, 59*, 107950.

Vogeleer, P., & Létisse, F. (2022). Dynamic Metabolic Response to (p)ppGpp Accumulation in *Pseudomonas putida*. *Frontiers in microbiology, 13*(872749).

Volke, D. C., Gurdo, N., Milanesi, R., & Nikel, P. I. (2023). Time-resolved, deuterium-based fluxomics uncovers the hierarchy and dynamics of sugar processing by *Pseudomonas putida*. *Metabolic Engineering, 79*, 159-172.

Volke, D. C., Martino, R. A., Kozaeva, E., Smania, A. M., & Nikel, P. I. (2022). Modular (de)construction of complex bacterial phenotypes by CRISPR/nCas9-assisted, multiplex cytidine base-editing. *Nature Communications, 13*(1), 3026.

von Wallbrunn, A., Richnow, H. H., Neumann, G., Meinhardt, F., & Heipieper, H. J. (2003). Mechanism of *cis-trans* Isomerization of Unsaturated Fatty Acids in *Pseudomonas putida*. *Journal of bacteriology, 185*(5), 1730-1733.

Wehrs, M., Tanjore, D., Eng, T., Lievense, J., Pray, T. R., & Mukhopadhyay, A. (2019). Engineering Robust Production Microbes for Large-Scale Cultivation. *Trends in Microbiology, 27*(6), 524-537.

Weimer, A., Kohlstedt, M., Volke, D. C., Nikel, P. I., & Wittmann, C. (2020). Industrial biotechnology of *Pseudomonas putida*: advances and prospects. *Applied microbiology and biotechnology, 104*(18), 7745-7766.

Weimer, A., Pause, L., Ries, F., Kohlstedt, M., Adrian, L., Krömer, J., et al. (2024). Systems biology of electrogenic *Pseudomonas putida* - multi-omics insights and metabolic engineering for enhanced 2-ketogluconate production. *Microbial cell factories, 23*(1), 246.

Werpy, T. A., Holladay, J. E., & White, J. F. (2004). *Top Value Added Chemicals From Biomass: I. Results of Screening for Potential Candidates from Sugars and Synthesis Gas*. United States.

White, D., Drummond, J., James, T., & Fuqua, C. (2011). *The physiologyand biochemistry of prokaryotes* (4th edition ed.). New York: Oxford University Press.

Wilson, D. N., & Nierhaus, K. H. (2007). The Weird and Wonderful World of Bacterial Ribosome Regulation. *Critical Reviews in Biochemistry and Molecular Biology, 42*(3), 187-219.

Winsor, G. L., Griffiths, E. J., Lo, R., Dhillon, B. K., Shay, J. A., & Brinkman, F. S. (2016). Enhanced annotations and features for comparing thousands of *Pseudomonas* genomes in the Pseudomonas genome database. *Nucleic acids research, 44*(D1), 17.

Wirth, N. T., Kozaeva, E., & Nikel, P. I. (2020). Accelerated genome engineering of *Pseudomonas putida* by I-SceI—mediated recombination and CRISPR-Cas9 counterselection. *Microbial biotechnology, 13*(1), 233-249.

Wittmann, C. (2002). Metabolic Flux Analysis Using Mass Spectrometry *Tools and Applications of Biochemical Engineering Science* (pp. 39-64). Berlin, Heidelberg: Springer Berlin Heidelberg.

Wittmann, C. (2007). Fluxome analysis using GC-MS. *Microbial Cell Factories, 6*, 6.

Wittmann, C., Hans, M., & Heinzle, E. (2002). In vivo analysis of intracellular amino acid labelings by GC/MS. *Anal Biochem, 307*(2), 379-382.

Wittmann, C., & Heinzle, E. (2005). Metabolic Activity Profiling by $^{13}C$ Tracer Experiments and Mass Spectrometry in *Corynebacterium glutamicum*. In J.-L. Barredo (Ed.), *Microbial Processes and Products* (pp. 191-204). Totowa, NJ: Humana Press.

Wittmann, C., Kiefer, P., & Zelder, O. (2004). Metabolic fluxes in *Corynebacterium glutamicum* during lysine production with sucrose as carbon source. *Applied and environmental microbiology, 70*(12), 7277-7287.

Wittmann, C., Weber, J., Betiku, E., Krömer, J., Böhm, D., & Rinas, U. (2007). Response of fluxome and metabolome to temperature-induced recombinant protein synthesis in *Escherichia coli*. *Journal of biotechnology, 132*(4), 375-384.

Wolfe, A. J. (2005). The acetate switch. *Microbiol Mol Biol Rev, 69*(1), 12-50.

Wordofa, G. G., Kristensen, M., Schrübbers, L., McCloskey, D., Forster, J., & Schneider, K. (2017). Quantifying the Metabolome of *Pseudomonas taiwanensis* VLB120: Evaluation of Hot and Cold Combined Quenching/Extraction Approaches. *Analytical Chemistry, 89*(17), 8738-8747.

Wu, G., Yan, Q., Jones, J. A., Tang, Y. J., Fong, S. S., & Koffas, M. A. G. (2016). Metabolic Burden: Cornerstones in Synthetic Biology and Metabolic Engineering Applications. *Trends in Biotechnology, 34*(8), 652-664.

Wu, J., Li, Y., Chen, X., Li, N., He, W., Feng, Y., et al. (2022). Improved membrane permeability with cetyltrimethylammonium bromide (CTAB) addition for enhanced bidirectional transport of substrate and electron shuttles. *Science of The Total Environment, 822*, 153443.

Yonei, S., Noda, A., Tachibana, A., & Akasaka, S. (1986). Mutagenic and cytotoxic effects of oxygen free radicals generated by methylviologen (paraquat) on *Escherichia coli* with different DNA-repair capacities. *Mutat Res, 163*(1), 15-22.

Yong, Y.-C., Yu, Y.-Y., Yang, Y., Liu, J., Wang, J.-Y., & Song, H. (2013). Enhancement of extracellular electron transfer and bioelectricity output by synthetic porin. *Biotechnology and Bioengineering, 110*(2), 408-416.

Yu, S., Lai, B., Plan, M. R., Hodson, M. P., Lestari, E. A., Song, H., et al. (2018). Improved performance of *Pseudomonas putida* in a bioelectrochemical system through overexpression of periplasmic glucose dehydrogenase. *Biotechnol Bioeng, 115*(1), 145-155.

Zakaria, B. S., & Dhar, B. R. (2019). Progress towards catalyzing electro-methanogenesis in anaerobic digestion process: Fundamentals, process optimization, design and scale-up considerations. *Bioresource technology, 289*, 121738.

Zhao, Q., Li, X. Z., Mistry, A., Srikumar, R., Zhang, L., Lomovskaya, O., et al. (1998). Influence of the TonB energy-coupling protein on efflux-mediated multidrug resistance in *Pseudomonas aeruginosa*. *Antimicrob Agents Chemother, 42*(9), 2225-2231.